Influence of Molecular Geometry and Chain Conformation on Properties of Polyelectrolyte Multilayers

Nicole Suzan Zacharia

Bachelor of Science, Materials Science and Engineering
Bachelor of Science, Mathematics
Massachusetts Institute of Technology, Cambridge, MA 2001

Submitted to the Department of Materials Science and Engineering
in fulfillment of the thesis requirement for the degree of

Doctor of Philosophy in Materials Science and Engineering
Massachusetts Institute of Technology
June 2007

Signature of Author: _____

Department of Materials Science and Engineering
April 20th, 2007

Certified by: _____

Paula T. Hammond
Bayer Chair Professor of Chemical Engineering
Thesis Advisor

Accepted by: _____

Samuel M. Allen
POSCO Professor of Physical Metallurgy
Chair, Departmental Committee on Graduate Students

The Influence of Molecular Geometry and Chain Conformation on Properties of Polyelectrolyte Multilayers

by

Nicole Suzan Zacharia

Submitted to the Department of Materials Science and Engineering
on April 20th, 2007, in partial fulfillment of the
requirements for the degree of Doctor of Philosophy in
Materials Science and Engineering

Abstract

The layer-by-layer (LbL) method of self-assembly is a versatile technique for fabricating thin polymer films. This thesis compares the properties of LbLfilms composed of different weak polycations. Slight perturbations in film assembly conditions can lead to large differences in film properties. Polyion bacisity and architecture are less understood variables. The polycations used are of similar chemical composition but different molecular geometries and basicity. Films studied were composed of poly(acrylic acid) (PAA) in combination with linear poly(ethylene imine) (LPEI), poly(allyl amine hydrochloride) (PAH), branched poly(ethylene imine) (BPEI), or poly(amidoamine) (PAMAM) dendrimer, generation four, amine surface. Various properties of these films are compared; including film thickness, chemical functional group availability, and film composition.

Carboxylic acid group ionization is found to increase with assembly pH, and PAA content is found to decrease. PAH, the most basic of the polycations, forms films that are the thinnest and the most ionized while PAMAM films have the most free free acid groups and form the thickest films.Permeability to chloroethyl ethyl sulfide vapor was seen to correlate with film ionization and therefore ionic crosslink density; diffusivity was highest in films that deposit in "loopy" layers and solubility was highest in films with the highest degree of ionization.

The diffusion of these polycations (specifically in the direction of film growth) is shown to be able to disrupt LbL heterostructures. A model system of a strong polycation (here poly(hexylviologen)) and PAA was used to show rejection of PXV in favor of a weak polycation, given that it was only partially charged.. Direct correlation between polycation charge density and ability to diffuse throughout bulk film was seen; polycations that are fully charged will simply adsorb to the surface while partially charged chains are mobile. Based on these observations, a strategy for creating compartmentalized heterostructures by inserting fully charged layer pairs was developed.

Two different drug delivery strategies were examined; encapsulation of block copolymer micelles in LbL structures and then electrochemically responsive films using Prussian Blue (PB) nanoparticles. Micelles are able to provide a hydrophobic environment within an LbL film, making these films useful for delivery of small molecules.

Thesis supervisor: Paula Hammond, Bayer Chair Professor of Chemical Engineering

Acknowledgements

During my years at MIT, many people have influenced and helped me in so many ways; from faculty to fellow students, to students of my own. To name them all here would be impossible. For any omission that I make here, I apologize, and I want to say that I am aware that whatever I have achieved at MIT has not been solely my own accomplishment, but the collective work of many others.

First and foremost I would like to thank my advisor Professor Paula Hammond for giving me the opportunity to work in her group, among other things. She has always been extremely understanding with me, through the long learning curve which I had to go through to be able to appreciate interesting research results, to the very slow rate at which I have published my findings, and to the rough patches I've had over the years. She has provided me a role model of how it is possible to be a woman in science and still maintain a family life and be respected by one's peers; and for that I have an enormous amount of respect.

I would also like to thank Professor Michael Rubner, who first introduced me to polymers and more specifically to layer by layer films many many years ago at the Wolf lecture during my freshman year. Here I am, ten years later, finishing my PhD and still studying layer by layer films. It's certainly not what I imagined when I signed up as a UROP in his lab. I have gained a lot from his group members and their research, as well as from their friendship and support.

Next I would like to acknowledge the coauthors of my papers, both published and in preparation: Dr. Dean DeLongchamp, Dr. Pil Yoo, Kevin Krogman, Kris Wood, Daniel Schmidt, Phuong Nguyen, Eric Verploegen, Jenny Lichter, and undergraduate students Miguel Modestino, Stacy Schroeder, Brian Adama, and Stefanie Wright. I would also like to mention that Dean served as a mentor to me during the first year that I worked in lab, and I feel that he was one of the instrumental people in shaping the course of my PhD research and I continue to appreciate his advice to this day. Other group members over the years have provided useful help in the form of both discussion and help with experiments; including (but not limited to) Kristoffer Stokes, Marianne Terrot, Jodie Lutkenhaus, Dr. Juhyun Park, Dr, Kris van Hege. Also I would like to thank Adam Nolte for help with mechanical testing (and many ideas!) and Taras Gorishnyy for help with ellipsometry. Cemal Akcaba who helped me with the nuts and bolts of writing and formatting this document, and Ylva Olsson who always made sure that I didn't lock myself away for too long while writing, and in the last stretches wasted hours of her time printing drafts of this document.

The biggest thank you of course goes to my family; my grandmother Ksenija and grandfather Vjekoslav, who have always delighted in my academic achievements, despite my inability to translate "polyelectrolyte multilayer" into Croatian. To my aunt Smilja who has provided my with a familial example of a success academic woman. To my brother Thomas, and most of all to my parents Suzana and Dubravko. Without them none of this would ever have happened; from their encouragement of my when I was little to their financial support through college, and for the love they have always given me.

This work made use of the Shared Experimental Facilities at MIT's Center for Materials Science and Engineering supported in part by the MRSEC program of the National Science Foundation under award number DMR 02-13282. This research was supported in part by the U.S. Army through the Institute for Soldier Nanotechnologies, under contract DAAD-19-02-D-0002 with the U.S. Army Research Office. The content does not necessarily reflect the position of the government, and no

official endorsement should be inferred. Part of this work is based upon research conducted at the Cornell High Energy Synchrotron Source (CHESS) that is supported by the National Science Foundation and the National Institutes of Health/National Institute of General Medical Sciences under award DMR-0225180.

Table of Contents

List of Figures

List of Tables

Chapter 1
Introduction

1.1 Introductory Remarks

Polymer thin films, from coatings to stand alone devices, are becoming increasingly relevant in today's world. As the fundamental understanding of soft materials increases and new technologies to control them down to the nanoscale are developed, the potential number of applications for polymer films is skyrocketing. Soft materials are often cheaper and easier to process than metals, ceramics, or semiconductors. As coatings they can be used to modify or functionalize surfaces, allowing for increased compatibility at biological interfaces or creating self-cleaning or anti-fogging coatings for textiles or windows. As devices, polymer films are being developed as drug delivery systems, fuel cells, batteries, solar cells, actuators, and light emitting diodes, to name a few. Responsive materials such as polymer hydrogels are being looked at for use as sensors, actuators, or thermometers.[1, 2] Polymer films already play an important role in processing semiconductors and as coatings for biomedical implants. The layer-by-layer (LbL) technique to assemble polyelectrolyte thin films is one method to reproducibly create thin films with a great deal of control over composition and film properties.[3]

This chapter serves to give a background on the LbL technique and the current understanding of the inner structure of these assemblies. This serves to provide a better understanding of the work presented in this thesis related to the influence of molecular geometry and chain conformation on the physical properties of polyelectrolyte multilayers. First, a general introduction to the layer-by-layer method of forming polyelectrolyte multilayers is given, including the different types of multilayers that can be formed. Internal organization in multilayers as currently understood is briefly explained. Dependence of multilayer properties on assembly conditions such as pH of polyion solution and deposition type (spraying, spin coating, dipping) is also discussed.

This thesis then examines multilayers constructed of different weak polycations in combination with polyacrylic acid. Four different amine functionalized polycations, of varying basicity and geometry are used throughout in order to determine how film properties may vary with these parameters. Basic film properties such as film thickness, composition and functional group availability are compared and then applications such as diffusion barriers and drug delivery systems

are considered. Diffusion of these polycations within bulk LbL film is found to be an important parameter that affects film structure.

1.2 Layer-by-Layer Polyelectrolyte Multilayers

1.2.1 Layer-by-Layer Technique

Since the early 1990's the layer-by-layer (LbL) method of depositing polyelectrolyte multilayers has received a great deal of attention.[3-5] These assemblies are based on the observation that oppositely charged polyelectrolytes will form strong complexes in solution, which are often insoluble. As the polymer chains complex with each other small counterions and water molecules are released, leading to entropic gain.[9] The next step was to direct the formation of these polyelectrolyte complexes onto substrates to form thin films, as introduced by Decher, et al.[3] Since then many studies have been performed to investigate their properties. In fact, the number of papers published relating to LbL deposition has increased exponentially over the years. LbL is a versatile technique, that when properly understood, can lead to extremely reproducible film thickness, swelling, and even phase separation. Substrates of nearly any geometry, such as microparticles[19] or the interior of membrane pores,[10] can be conformally coated, and many different components such as nanoparticles,[6] small multi-charged molecules,[7] and biomacromolecules[4] may be incorporated into LbL assemblies.

As described above, LbL deposition is the direction of strong complex formation between oppositely charged polyelectrolytes onto a substrate. This substrate can be of a wide range of materials, as long as there is either some native charge or a charge can be induced by a cleaning treatment such as plasma treatment.[8] The substrate is first exposed to a solution of oppositely charged polyion, which then begins to adsorb to that substrate. This adsorption is limited to one monolayer due to electrostatic repulsion between like charged molecules, and results not only in the neutralization of the substrate's charge, but to a reversal of charge at the film's surface.[17] The film is then rinsed to remove weakly adsorbed and entangled polymer chains, and then exposed to polyion solution of the opposite charge, where the surface charge is once again reversed due to adsorption of polyelectrolyte chains. This process can be repeated as many times as desired, in order to make films of any thickness. Low molecular weight chains cannot always be incorporated into LbL films, but once polymer molecular weight reaches a weight of the tens of thousands of grams per mol regular adsorption with little variation due to molecular weight occurs.[20]

When "dipping" a substrate with the standard computer controlled robot[8] into polyelectrolyte solutions, assembly of one layer pair will typically take 30 minutes. In order to speed this process,

alternate methods of assembly such as spin coating[15] and spraying[13, 14] have been developed. These methods result in films similar to those assembled by dipping, but with some differences in film properties such as thickness depending on the exact parameters of film assembly.

Slightly changing simple parameters, such as the ionic strength or pH of the polyion solutions, can drastically alter the architecture of electrostatically bound LbL films. Another parameter of interest is the length and number of rinsing steps in between polyion solutions, or even drying films between deposition steps. Chains can more readily rearrange if the film is hydrated. Also, if a dried film is exposed to a polyion solution, hydrophobic interactions may become more important.[23] Different "dipping" machines have been designed to hold substrates at different angles relative to the solutions, or even to rotate the substrate during deposition to cause more uniform film deposition.

Salt ions can act to shield charge along the polymer backbone, making fewer sites available for ionic bonding. The same is true for changing the pH of weak polyelectrolyte solutions; the charge density along the backbone will vary and change the distance between charges. This variation in charge density will change the chain conformations in solution, from fully stretched out to coiled, and will therefore affect the way that the chains adsorb onto the substrate. The result is that by using the same polyelectrolyte pair, films of vastly different thickness and ionic crosslink densities can be assembled. Figure 1-2 shows this for the example of poly(allyl amine) hydrochloride (PAH) and poly(acrylic acid) (PAA), which are both weak polyelectrolytes. In figure 1-2 (a) both polymers are assembled at pH values for which they are highly charged, resulting in the chains lying down in a stretched out conformation and creating a thin, "tightly" linked film. In figure 1-2 (b), both polymers are partially charged, resulting in thick, "loopy" structures due to the long average distance between ionic crosslinks. In figure 1-2 (c) PAH is highly charged while only a few of the PAA carboxylic acid

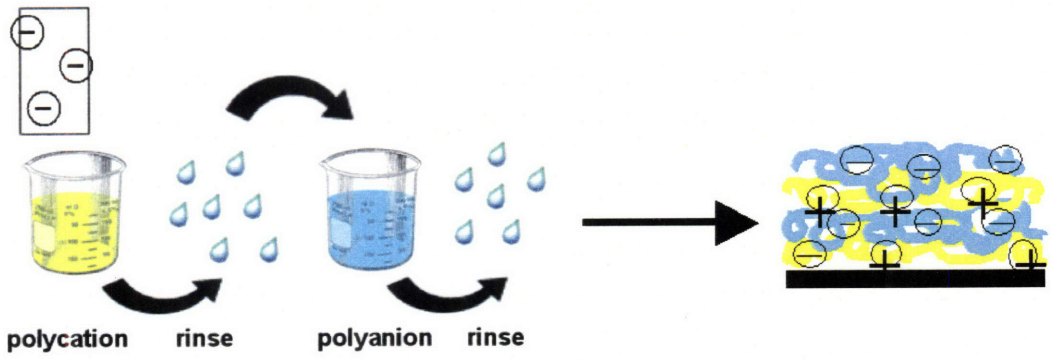

Figure 1-1: Schematic of LbL assembly process. Charged substrate is exposed first to one polyion, a rinse step, the oppositely charged polyion, and again a rinse. This is repeated until the desired film thickness is achieved.

functional groups are charged, leading to films of intermediate thickness in which there are many available carboxylic acid groups.

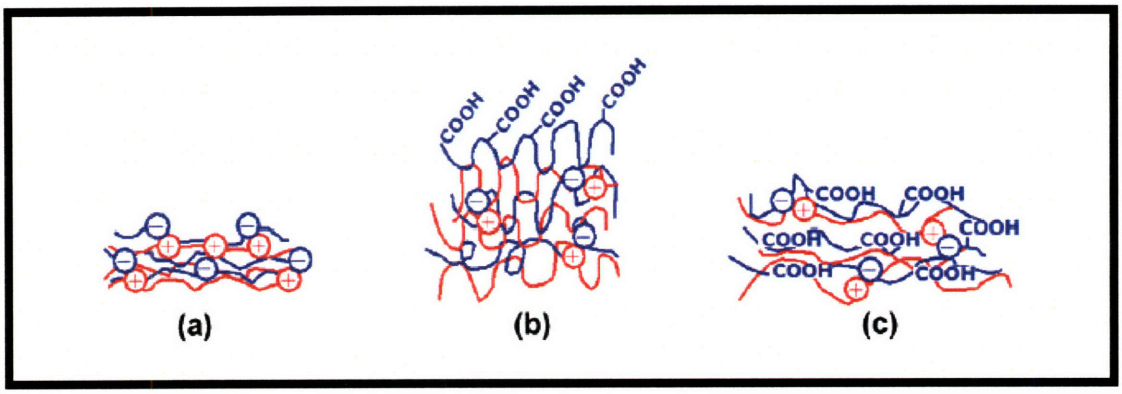

Figure 1-1: Different LbL architectures possible from the same polyelectrolyte pair. (a) both polymers highly charged (b) both polymers only partially charged and (c) PAH is fully charged but PAA is only partially charged.[22]

Although, as described above, the first reported LbL assemblies were held together by electrostatic forces, it has also been shown that hydrogen bonding[24-26, 28] can either participate in addition to electrostatic interactions or be the sole driving force for film formation. Other interactions such as van der Waals forces, charge transfer interactions,[33, 42, 43] multiple hydrogen bonding (such as in DNA), or even covalent linkages[27] may also be exploited to create films. Hydrophobic interactions can be exploited to adsorb neutral polymer chains onto hydrophobic surfaces.

Many LbL systems grow in a linear rate with respect to number of layer pairs after reaching a state steady growth regime. The initial 3-5 layer pairs, which are affected by polymer wetting of the substrate and other substrate properties, are usually extremely thin and show a non-linear growth. Often this is due to uneven coverage or "island" formation by the first layer pair or so. This general linearity of LbL growth gives the impression that LbL assembly is a process that takes place only at the film's surface. However, it is now widely accepted that in certain cases the entire bulk film participates in film assembly. In these cases nonlinear growth is observed for as many as 20 or 30 layer pairs and is related to extremely mobile chains being able to diffuse through the film. Small perturbations in assembly conditions or slight difference in the structure of the polyelectrolytes used can lead to enormous differences in the resulting film.

1.2.2 Internal Structure of LbL Films

Although we say that these films are assembled "layer-by-layer" it is not necessarily the case that they are well organized internally. Early studies using neutron scattering showed that instead of

being stratified, each "layer" actually overlaps with adjacent layers.[11, 12] The degree to which this happens depends on the mobility of the polymer chains as well as the strength of the complex formed.

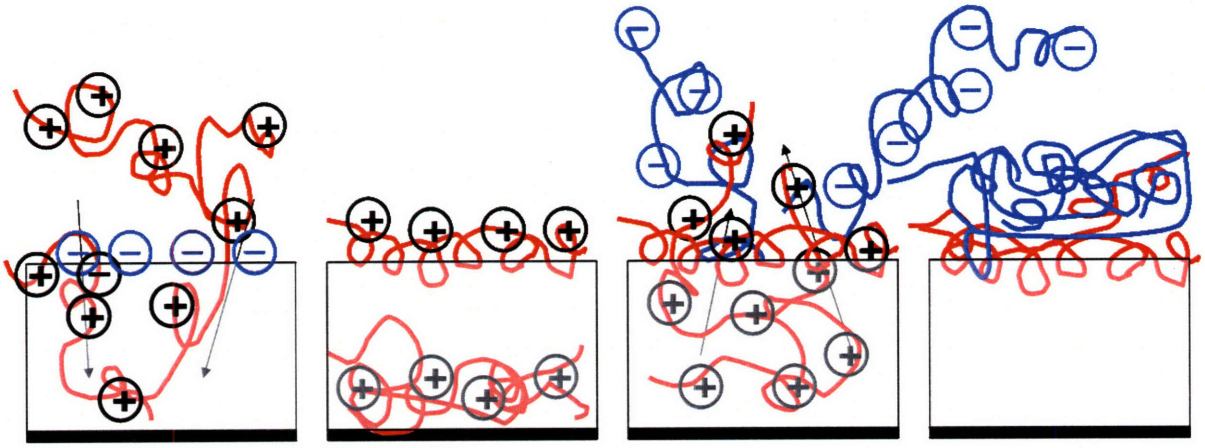

Figure 1-2: Schematic of how diffusion in LbL assemblies creates non-linear growth. (1) Polyanion diffuses into the film's bulk during assembly. (2) Charge reversal occurs at the film surface, and an excess of polcation remains within the film. (3) When exposed to polyanion, the excess polycation is attracted to the film surface, providing more material with which the polyanion can complex, and thus leading to more growth than would occur if complexation only took place with the surface of the film, resulting in (4) new film deposition thicker to single step adsorptions which previously took place.

Highly ionized chains which form many crosslinks and take an extended conformation in solution are less able to diffuse within the LbL structure, meaning that assemblies made from strong polyelectrolytes with little ionic shielding tend to be more stratified than those made using weak polyelectrolytes or strong ionic strength in the assembly solution. The hydrophobicity of the polymer's backbone will also affect the manner in which it adsorbs to the surface and its mobility within the solvated film during the assembly process.

Even though in every LbL assembly there is some degree of interpenetration between the layers, there are still some systems that are more ordered than others. Many typical LbL constructs grow linearly in thickness with layer number, as would be expected when the adsorption process is largely a surface phenomenon. However, there are some systems which grow superlinearly with number of layers. In these systems one or even both components has such a high degree of mobility within the bulk film that the mechanism for adsorption is changed. In these cases as polyion is being adsorbed to the film's surface, polyion is also diffusing into the bulk film. Then in the next adsorption step, this extra "reservoir" of material is attracted to the oppositely charged polymer at the surface, giving more material to complex with and meaning that layer is adsorbed than would have been expected.

The thicker the film the more pronounced this effect becomes, as more and more polyion can diffuse into the bulk of the film. The mobility of the polymer chain within the LbL film is related to chain geometry, conformation, hydrophilicity, and charge density along the chain's backbone.

Interdiffusion in LbL assemblies can be desirable in certain circumstances and to be avoided in others. Surface mobility of polymer chains has been shown to be able to create order on the surface layer of the film. Also, LbL assemblies with a strong degree of interdiffusion will be uniform throughout the bulk of the film. Sometimes, however, a stratified inner structure is desired, especially in the creation of devices such as batteries or films for the delivery of multiple drugs with a precise release profile. If this is the case, there are several strategies to compartmentalize the LbL films; using nanoparticles or tightly crosslinked layers (either chemically or ionically crosslinked). It has been shown that by assembling a film using a mixture of polyelectrolytes, the mode of growth (linear vs superlinear) can be changed.

1.2.3 Potential Applications of LbL Assemblies

Due to the versatility of the LbL technique; its ability to coat substrates of many geometries and type and to incorporate such a wide variety of molecules, these assemblies have shown promise in a number of applications.[12] LbL allows one to modify only the surface properties of a material, allowing the bulk to retain its original characteristics while rendering the surface superhydrophilic[45] or hydrophobic,[46] for example. Anti-reflection coatings[47] for windows or glasses are other applications. Other applications include devices ranging from electrochemical devices[16] such as fuel cells, batteries, catalysts, and sensors to organic electronics such as LEDs or luminescent devices[21] to biomedical devices such as use in drug delivery[44] or implant coatings to make materials more biocompatible. LbL can be used to modify textiles or surfaces that are not flat such as electrospun polymer mats or spherical particles.

As the applications of interest grow more complex, so will the desired thin film configuration. As mentioned above, the internal structure of LbL assemblies varies greatly depending on the nature of the polyelectrolytes used. In certain applications a uniform film may be desired, in others a stratified film might be needed. A greater understand of how the bulk LbL film participates during the assembly process and the conditions under which diffusion of polymer chains takes place is necessary; and with this understanding, strategies for controlling diffusion within the film structure may be developed.

1.3 Influence of Polyelectrolyte Properties on Adsorption and Incorporation into Multilayers

Studies of LbL films often explore the parameter space of assembly conditions; ionic strength or pH of the polyelectrolyte solutions, different deposition methods, or post assembly treatments such as exposure to different pH conditions or heat treatments. Another parameter to examine is the nature of the polyelectrolyte itself. Different strong and weak polyions are often been studied, including polypeptides and DNA. Block copolymers and branched chains are yet another class of molecules to look at.

The adsorption of single layers of polyelectrolytes has been thoroughly studied – from kinetics to the layer composition and thickness, both theoretically and experimentally.[18, 48, 49] Results from variation of both adsorption conditions, such as ionic strength for strong polyelectrolytes, solution pH in the case of weak polyelectrolytes, and changes in the polymers such as molecular weight or flexibility, may be found in the literature. Branching and various macromolecular architectures are less studied. Dendritic, star shaped, and hyperbranched polymers all have solution state properties different than linear molecules, and therefore different adsorption kinetics. Differently shaped molecules will differ in charge density, which is known to be an important factor in deposition onto a surface, and will entangle differently than linear chains. The structure of adsorbed monolayers of such polyelectrolytes will then most likely be different than those of their linear analogues.

A number of methods to immobilize dendrimers on surfaces have been investigated, including convalent linkage to SAMs,[29] complexation to metal ions on a surface,[31] making LB films[30] of dendrimers, and adsorption of charged dendrimers to hydrophilic surfaces[52] and uncharged dendrimers to surfaces such as gold.[32] Depending on the assembly conditions, these layers can be closely packed monolayers or aggregates on the surface due to the van der Waals interactions[53] between the cores. A closely packed monolayer of dendrimers will have a higher density of functional groups than a closely packed SAM.[32] There is also strong variation with generation as to the structure of the layer formed. Due to their high relative charge density they tend to complex strongly to charged surfaces and their spherical solution state conformation will flatten.

BPEI solution properties and adsorption have been studied because of its industrial applications, especially to stabilize colloidal solutions.[50, 51] Compared to LPEI some differences are seen due to the relative differences in charge density. Both LPEI and BPEI will rearrange their charge density when brought into proximity with a charged surface. The charged functional groups of BPEI are closer to each other than in the linear chains, and therefore the resulting charge density of the adsorbed

macromolecule is different. A greater understanding of how these differences affect monolayer and therefore multilayer structure is necessary.

Block copolymers of a number of different geometries, such as brushes, combs, and linear block copolymers may be used to create thin films of different properties. Phase segregation can be used to create micro and nanoscale structures within films, and using blocks that interact differently with the same solvent can create responsive thin films. Using block copolymers that form micelles in solution, it is possible to adsorb intact monolayers of micelles.[33, 34] When one or both of the blocks is a weak polyelectrolyte, this monolayer can be responsive to changes in ionic strength or pH, with micelles expanding and contracting.[35, 36] By adsorbing micelles onto a surface, the dissociation of micelles that occurs below the critical micelle concentration in solution can be avoided. One clear application for this type of thin film is the controlled release of some small molecule that can be incorporated into the micelle.

By integrating these types of polymers into LbL films, it should be possible to create more complex inner architectures than those previously reported. A few studies have already shown this to be possible,[22-26] stabilizing the films either by cross-linking or simply relying on electrostatic interactions. In this manner, hydrophobic small molecules that are otherwise difficult to incorporate into LbL assemblies can be encapsulated and integrated into the film's structure. In one case the micellar structure was used to design a nanoporous film.[26]

Charged micelles of block copolymers have been incorporated into multilayer films by several groups.[37-40, 54] Some of these micelles need to be stabilized through crosslinking prior to assembling in a LbL film,[37, 39] while others are directly incorporated into the film with no modifications.[39, 40] These films provide for the incorporation of hydrophobic environments in the LbL film, and therefore hydrophobic small molecules, for uses in drug delivery and optics.[41]

1.4 Thesis Scope

As LbL assemblies are studied in further depth, it has become more and more clear that the inner architecture of these films and general film properties are extremely sensitive to small perturbations in the method of film assembly. This includes method of deposition, dipping and rinsing times, and ionic strength and pH of polyion solutions. Different groups using similar methods of deposition, such as dipping but with different automated processes or by hand, or spin-coating or spraying under only slightly different conditions report extremely different (but reproducible) results. It has also been

observed that small changes in the structure of the selected polyelectrolytes can lead to significant differences in film properties.[33] Some polyelectrolytes are mobile within the film's bulk while others are not. The strength of interaction between pairs of polyelectrolytes also varies greatly and can cause difference in the resulting film. Many LbL studies focus on one or two model systems; while these studies have given us a great deal of general information about the LbL process, little work has been done to identify the affect of small changes in the actual polyelectrolytes used.

This thesis serves to probe the inner structure and properties of polyelectrolyte multilayers assembled with different polycations. More specifically, different amine containing weak polyelectrolytes are examined to see the role that their basicity, geometry, charge density, and hydrophilicity plays in the multilayers. Chapter 2 examines the basic film properties of these materials and how pH of assembly affect them; film formation, film ionization, and relative composition of polyanion and polycation. Chapter 3 describes an automated misting system that was developed to speed film deposition, and how these films differ and how they are similar to the dipped films.

In later chapters, applications relating to these properties are described. Chapter 3 also looks at organic vapor permeation of these films. Chapter 4 describes using PAMAM dendrimers as a platform for synthesizing metal nanoparticles in LbL assemblies. Chapter 5 looks at the mobility of LPEI and the challenge of creating well-defined heterostructured LbL assemblies. Chapters 6 and 7 look at using amine containing polyelectrolytes (a dendritic-linear block copolymer and then LPEI in combination with an inorganic nanoparticle) as a platform for drug delivery systems different than those previously reported in the literature. Chapter 6 looks at using PAMAM based micelles for encapsulation and release of drug in LbL assemblies. Chapter 7 describes work with Prussian Blue nanoparticles in films for drug delivery and the creation of freestanding LbL films. Chapter 8 summarizes the results and suggests possible directions for future work.

LbL assemblies are structures at non-equilibrium, and it is increasingly clear that the variables that can affect their properties are subtler than once thought, with small changes in assembly parameters causing large changes in the resulting films. As the complexity of desired film architectures increases, these parameters and their role in film formation need to be examined in further depth. The topics covered in this thesis serve as a beginning of a better understanding of how the structure of the polyelectrolytes used may change the properties of the LbL assembly.

Chapter 1 References

1. Zhang, Y.; Furyk, S.; Bergbreiter, D. E.; Cremer, P. S. *J. Amer. Chem Soc.* **2005**, *127*, 14505.
2. Mabeck, J. T.; Defranco, J. A.; Bernards, D. A.; Malliaras, G. G.; Hocdé, S.; Chase, C. J. *Appl. Phys. Lett.* **2005**, *87*, 013503.
3. Decher, G., Hong, J. D., Schmitt, J. *Thin Solid Films* **1992**, *210(1-2)*, 831-835.
4. Lvov, Y., Decher, G., Sukhorukov, G. *Macromolecules* **1993**, *26(20)*, 5396-5399.
5. Decher, G. *Science*, **1997**, *277(5330)*, 1232-1237.
6. Ostrander, J. W.; Mamedov, A. A.; Kotov, N. A. *J. Am. Chem. Soc.* **2001**, *123(6)*, 1101-1110.
7. Advincula, R. C.; Fells E.; Park, M. K. *Chem. Mater.* **2001**, *13(9)*, 2870-2878.
8. Lvov, Y., Haas, H.; Decher, G.; Moehwald, H.; Kalachev, A. *J. Phys. Chem.* **1993**, *97(49)*, 12835-12841.
9. Bucur, C. B.; Sui, Z.; Schlenoff, J. B. *J. Am. Chem. Soc.* **2006**, *128*, 13690-13691.
10. Lee, D.; Nolte, A. J.; Kunz, A. L.; Rubner, M. F.; Cohen, R. E. *J. Am. Chem. Soc.* **2006**, *128(26)*, 8521-8529.
11. Decher, G., Lvov, Y., Schmitt, J. *Thin Solid Films*, **1994**, *244(1-2)*, 772-777.
12. Bertrand, P., Jonas, A.; Laschewsky, A.; Legras, R. *Macromolecular Rapid Communications*, **2000**, *21(7)*, 319-348.
13. Lowman, G. M.; Tokuhisa, H.; Lutkenhaus, J. L.; P.T. Hammond *Langmuir* **2004**, *20*, 9791.
14. Schlenoff, J. B.; Dubas, S. T.; Farhat, T. *Langmuir* **2000**, *16*, 9968.
15. Cho, J.; Kim, S.; Char, K. *Kor J. Chem. Eng.* **2003**, *20(1)*, 174-179.
16. Hammond, P. T. Recent explorations in electrostatic multilayer thin film assembly. *Current Opinion in Colloid & Interface Science*, **1999**, *4(6)*, 430-442.
17. Schlenoff, J. B., Dubas, D. T. *Macromolecules* **2001**, *34(3)*, 592-598.
18. Schwarz, S.; Eichhorn, K. J.; Wischerhoff, E.; Laschewsky, A. *Colloids and Surfaces A – Physicochem. Eng. Aspects*, **1999**, *159(2-3)*, 491-501.
19. Okubo, T., Suda, M. *J. Colloid Interface Sci.*, **1999**, *213(2)*, 565-571.
20. Sui, Z.; Salloum, D.; Schlenoff, J. B. *Langmuir* **2003**, *19*, 2491-2495.
21. Clark, S. L., Handy, E. L.; Rubner, M. F.; Hammond, P. T. *Advanced Materials*, **1999**, *11(12)*, 1031-1035.
22. Mendelsohn, J. D.; Yang, S. Y.; Hiller, J.; Hochbaum, A. I.; Rubner, M. F. Rational deisgn of cytophilic and cytophobic polyelectrolyte multilayer thin films. *Biomacromolecules* **2003**, *4(1)*, 96-106.
23. Kotov, N. A. *Nanostructured Materials* **1999**, *285*, 797-801.
24. Stockton, W. B.; Rubner, M. F. *Macromolecules* **1997**, *30(9)*, 2717-2725.
25. Wang, L. Y.; Fu, Y.; Wang, Z.; Wang, Y.; Sun, C.; Fan, Y.; Zhang, X. *Macromol. Chem. Phys.* **1999**, *200(6)*, 1523-1527.
26. Sukhishvili, S. A.; Granick, S. *J. Am. Chem. Soc.* **2000**, *122(39)*, 9550-9551.
27. Yang, S. Y.; Rubner, M. F. *J. Am. Chem. Soc.* **2002**, *124(10)*, 2100-2101.
28. Sukhishvili, S. A.; Granick, S. *Macromolecules*, **2002**, *35(1)*, 301-310.
29. Wells, M.; Crooks, R. M. *J. Am. Chem. Soc.* **1996**, *118*, 3988.
30. Saville, P. M.; Reynolds, P. A.; White, J. W.; Hawker, C. J.; Fréchet, J. C. J.; Wooley, K. L.; Penfold, J.; Webster, J. R. P. *J. Phys. Chem.* **1995**, *99*, 8283.

31. Watanabe, S.; Regen, S. L.; *J. Am. Chem. Soc.* **1994,** *116*, 8855.
32. Tokuhisa, H.; Zhao, M.; Baker, L. A.; Phan, V. T.; Dermody, D. L.; Garcia, M. E.; Peez, R. F.; Crooks, R. M.; Mayer, T. M. *J. Am. Chem. Soc.* **1998**, *120*, 4492-4501.
33. Zhang, Y. J. and Cao, W. X.. *Langmuir*, **2001**, *17(16)*, 5021-5024.
34. Zhang, L. F.; Eisenberg, A. *Science* **1995,** 268, (5218), 1728-1731.
35. Webber, G. B.; Wanless, E. J.; Butun, V.; Armes, S. P.; Biggs, S. *Nano Letters* **2002,** 2, (11), 1307-1313.
36. Webber, G. B.; Wanless, E. J.; Armes, S. P.; Tang, Y. Q.; Li, Y. T.; Biggs, S. *Advanced Materials* **2004,** 16, (20), 1794-1798.
37. Emoto, K.; Iijima, M.; Nagasaki, Y.; Kataoka, K. *J. Am. Chem. Soc.* **2000,** 122, 2653-2654.
38. Emoto, K.; Nagasaki, Y.; Kataoka, K. *Langmuir* **2000,** 16, 5738-5742.
39. Ma, N.; Zhang, H.; Song, B.; Wang, Z.; Zhang, X. *Chemistry of Materials* **2005,** 17, (20), 5065-5069.
40. Ma, N.; Wang, Y.; Wang, Z.; Zhang, X. *Langmuir* **2006,** 22, (8), 3906-3909.
41. Cho, J., Hong, J., Char, K., Caruso, F. *J. Am. Chem. Soc.*, **2006**, 128.
42. Shimazaki, Y.; Mitsuishi, M.; Ito, S.; Yamamoto, M. *Langmuir*, **1997,** *13(6)*, 1385-1387.
43. Shimazaki, Y.; Misuishi, M.; Ito, S.; Yamamoto, M. *Langmuir*, **1998**, *14(10)*, 2768-2773.
44. Wood, K.C.; Chuang, H.F.; Batten, R.D.; Lynn, D.M.; Hammond, P.T. *Proc. Natl. Acad. Sci. USA* **2006**, *103*, 10207-10212.
45. Cebeci, F. C.; Wu, Z. Z.; Zhai, L.; Cohen, R. E.; Rubner, M. F. *Langmuir* **2006**, *22(6)*, 2856-2862.
46. Zhai, L.; Berg, M. C.; Cebeci, F. C.; Kim, Y.; Milwid, J. M.; Rubner, M. F.; Cohen, R. E. *Nano Lett.* **2006**, *6(6)*, 1213-1217.
47. Wu, Z. Z.; Walish, J.; Nolte, A. J.; Zhai, L.; Cohen, R. E.; Rubner, M. F. *Adv. Mater.* **2006**, *18(20)*, 2699.
48. Åkesson, T.; Woodward, C.; Jönsson, B. *J. Chem. Phys.* **1989**, *91*, 2461.
49. Wang, T. K.; Audebert, R. *J. Colloid Interface Sci.* **1987**, *199*, 459.
50. Claesson, P. M.; Paulson, O. E. H.; Blomberg, E.; Burns, N. L. *Coilloids Surfaces A: Physiochem. Eng. Aspects* **1997**, *223-224*, 341-353.
51. Schneider, M.; Brinkmann, M.; Möhwald, H. *Macromolecules* **2003**, *36*, 3510-3518.
52. Tsukruk, V. V.; Rinderspracher, F.; Bliznyuk, V. N. *Langmuir* **1997**, *13(8)*, 2171-2176.
53. Bliznyuk, V. N.; Rinderspracher, F. Tsukruk, V. V. *Polymer* **1998**, *39(21)*, 5249-5252.
54. Qi, B.; Tong, X.; Zhao, Y. *Macromolecules* **2006,** 39, (17), 5714-5719.

Chapter 2
Multilayers Containing Weak Polyelectrolytes with Amine Functional Groups

2.1 Introduction

The LbL process creates films that are kinetically trapped into non-equilibrium structures, meaning that small variations in the assembly parameters can lead to significant changes in film properties. Parameters such as dipping time,[1] solution concentration, rinsing conditions[3] and the use of drying steps have been extensively examined. Another key parameter, both for multilayers and the adsorption of polyelectrolyte monolayers, is the charge density of the polyelectrolytes.[2,3] This has been studied by varying ionic strength of strong polyelectrolyte solutions,[1,3,4] pH of weak polyelectrolyte solutions,[5,6] and by using copolymers of fixed composition[7-9] (and therefore charge density). Furthermore, even when the primary driving force for film assembly is electrostatic interactions, secondary forces such as hydrogen bonding[10] or hydrophobic interactions may participate in stabilizing the film structure.

Adsorption of weak polyelectrolytes is more complicated than the strong polyelectrolyte case for a number of reasons. At low degrees of ionization, the charged groups will electrostatically repel each other, while the neutral, hydrophobic chain segments will cluster together. This leads to the "pearl necklace" configuration; small spherical globules of non-charged polymer segments separated by charged segments. When oppositely charged weak polyelectrolytes come into close proximity of each other the localized changes in pH will cause the charge density on each chain to rearrange.[11,12] In the case of certain pairs of weak polyelectrolytes the acid-base interactions between oppositely charged groups can be even more favorable than simple ion pair formation. Within those acid-base interactions, primary amine groups are more basic than other amines and will therefore more strongly interact will acid groups.

Often when weak polyelectrolyte adsorption is studied, one system is used in order to reduce the number of competing parameters. However, as it is becoming more and more clear that things like molecular architecture can be important to film properties it is necessary to compare different polyelectrolyte systems.

In this study, four systems were examined for their assembly behavior, relative polymer composition, chemical functional group availability, and physical properties. The polyanion poly(acrylic acid) was assembled with four different polycations – poly(allyl amine hydrochloride) (PAH), linear and branched poly(ethylene imine) (LPEI and BPEI), and poly(amidoamine) dendrimer (PAMAM, G4, NH_2 surface), shown in figure 2-1. Films were assembled with solutions of both polyions at the same pH, ranging from pH 3 – pH 6. While these polycations are chemically similar in that they posses amine functional groups, they each have different molecular architectures or conformations over this pH range, which results in different properties of the LbL assemblies.

The two linear polycations used are PAH and LPEI, PAH has a hydrophobic backbone with pendant primary amine groups, and a pKa value near 8, while LPEI the amine containing anologue of poly(ethylene oxide), a very hydrophilic polymer with secondary amine functional groups and a pKa value of ~5.5. PAH is the stronger polybase, and is essentially fully charged over the pH assembly conditions used in this thesis, meaning that it takes a more extended conformation. LPEI is partially charged at the pH values of interest, and takes a more coiled conformation than the PAH. LPEI is also extremely well solvated, especially compared to PAH. For this reason, LPEI shows great mobility within LbL assemblies during film formation, while PAH does not. Hydrophobic interactions must always be considered when PAH is used to form multilayers.

The other two polycations are branched polymers, BPEI and PAMAM. BPEI is comprised of 50% secondary amine groups, 25% primary amine groups and 25% tertiary amine groups. It has a pKa of ~6.5,[15,16] making it a stronger polybase than LPEI, but weaker than PAH. Over the studied assembly pH range it is largely charged, but given its highly branched structure the conformation will be more akin to a pincushion than an extended chain. PAMAM dendrimer is an extremely monodisperse hyperbranched molecule (PDI = 1.0003 – 1.0005).[18] PAMAM's structure has a large number of chain ends in a small volume, giving arise to properties different than other polymers in terms of reactivity, intrinsic viscosity, solubility and miscibility.[19] PAMAM's surface is covered with primary amine groups, and the dendrimer's interior contains tertiary amine groups as well as amide linkages. As dendrimer generation increases, the dendrimer becomes more and more spherical, with a crowded surface and relatively large amounts of free volume in the core.

Theoretical models support a number of different interpretations of PAMAM's solution state conformation, but it is generally accepted that the dendritic arms have some degree of flexibility, until very high generation number, and that G4 PAMAM will be about 5 nm in diamter in its fully

extended state. Hydrogen bonding through the amide linkages stabilizes the PAMAM interior structure, and has also been observed intermolecularly in PAMAM salts.[2] The literature varies as to the pKa values for the primary and tertiary amine groups; 3.85 and 6.85 (for 1° and 3° groups, respectively) by Tomalia et al,[17] 6.85 and 10.29 by Diallo, et al,[22] 6.70 and 9.00 by Cakara,[21] et al, and 6.30 and 9.23 by Crooks, et al.[20] In this thesis the values from Tomalia's work were used. In this case the PAMAM dendrimer surface is charged over the entire range of assembly conditions, and the inner tertiary amine groups are largely neutral in the pH 5 and 6 cases, and partially charged at pH 3 and 4. We should therefore expect electrostatic repulsion of tertiary amine groups to cause the lower pH solution conformation of the dendrimer to be more fully extended. The FTIR spectra of cast PAMAM films at different pH can be seen in figure 2-2. There are no significant differences in the spectra over the pH range of 3 - 6. As expected, prominent features can be seen due to amide linkages (figure 2-2 (a) and (f)) as well as protonated primary amine groups (figure 2-2 (b) and (g)). In the pH 3 and pH 4 spectra a small feature at 2620 cm^{-1} (figure 2-2 (e)) may be attributed to protonated tertiary amine groups.

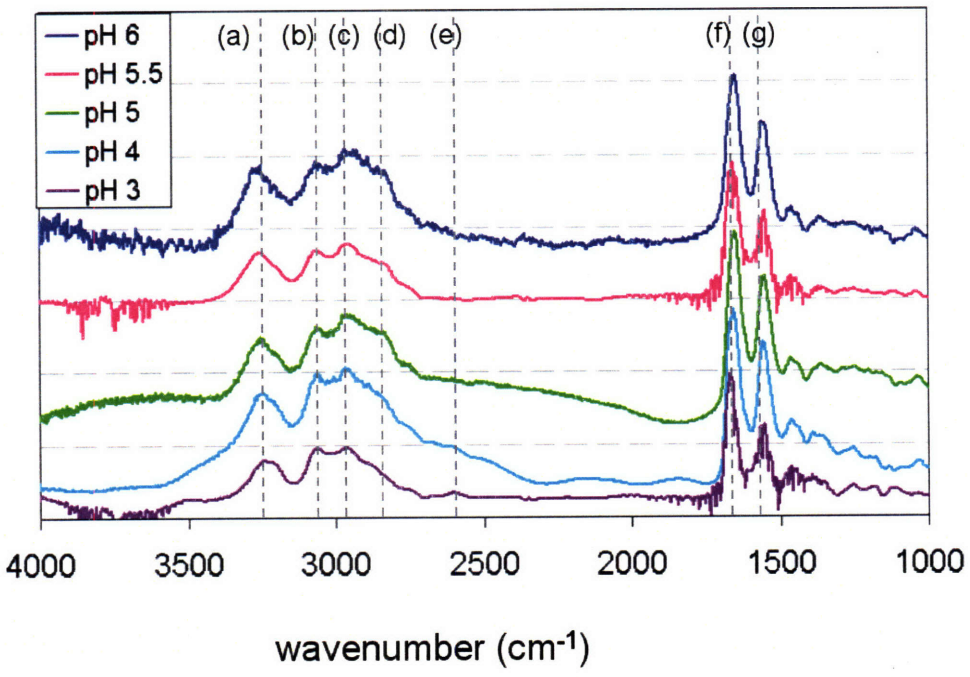

Figure 2-1: FTIR of cast PAMAM films at varying pH. Features at 3260 cm-1 (a) and 1650 cm-1 (f) are due to solid state amide linkages. The peak at 3070 cm-1 (b) is characteristic of charged primary amines and 1560 cm-1 (g) is an asymmetric –NH3+ deformation vibrations. The small shoulder at 2620 cm^{-1} (e), which appears in the pH 3 and 4 spectra, is due to protonated tertiary amine groups.

The peak at 2980 cm^{-1} (c) is characteristic of C-C binding in the dendrimer backbone, and the shoulder at 2850 cm^{-1} (d) is characteristic of N-H and O-H stretching, suggesting that there is some inter- and intramolecular hydrogen bonding may be present.

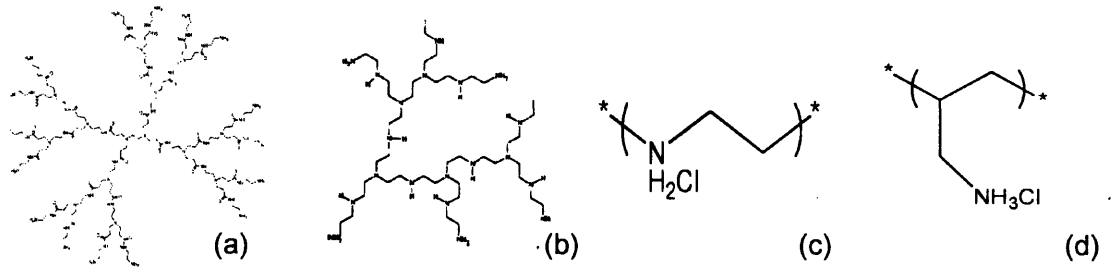

Figure 2-2: Structures of amine containing polycations used in this study – (a) PAMAM dendrimer, (b) BPEI, (c) LPEI, and (d) PAH.

2.2 Experimental Details

Materials: Linear and branched poly(ethylene imine) (LPEI, MW = 25,000, and BPEI, MW = 70,000), poly(acrylic acid) (PAA, MW = 90,000) were purchased from Polysciences. Poly(amido amine) dendrimer (PAMAM G4, NH_2 surface, 22 wt% in methanol) was purchased from Dendritech. Poly(allylamine hydrochloride) (PAH, MW = 70,000) was purchased from Sigma Aldrich. Polymer solutions were made using DI water at a concentration of 20 mmol with respect to the repeat unit, and adjusted to the required pH using HCl or NaOH. Si wafers were purchased from Silicon Quest All silicon was cleaned with methanol and Milli-Q water, followed by a five minute oxygen plasma etch (Harrick PCD 32G) to clean and hydroxylate the surface. Glass slides from VWR were cleaned by sonication for 10 minutes in each of a series of solvents; dichloromethane, acetone, methanol, and then DI water, and then exposed to 5 minutes of oxygen plasma etch. VWR poly(propylene) weigh boats were used for substrates for TGA samples.

LbL films were constructed as follows according to the alternate dipping method using an automated Carl Zeiss HMS Series Programmable Slide Stainer.[8] Briefly, pretreated substrates were submerged in a polycationic dipping solution for 10 minutes followed by a cascade rinse cycle consisting of three deionized water rinsing baths (30, 60, and 60 seconds, respectively). Substrates were then submerged in a polyanionic solution for 10 minutes followed by the same cascade rinsing

cycle, and the entire process was repeated as desired. Following deposition, films were immediately removed from the final rinsing bath and dried thoroughly under a stream of dry nitrogen gas.

Film thickness measurements were, made using a Tencor P10 profilometer by scoring the film with a razor blade and profiling the score. A tip force of 5 mg was used to avoid penetrating the film. Atomic Force Microscopy was conducted using a Digital Instruments Dimension 3100 in tapping mode at an amplitude set point of 0.8 V under dry conditions. Height and phase images were taken at scanning rates of approximately 1.5 Hz. TGA was performed using a TA Instruments model Q50. Samples were prepared by depositing 100 layer pairs of each polyelectrolyte pair on polypropylene substrate and then peeling the film off, in a manner as previously described by our group.[25] The samples were dried in a vacuum oven at 70°C for 30 minutes in order to remove loosely bound water. The samples were equilibrated at 30°C, raised to 115°C at a rate of 5°C per minute, held at 115°C for 30 minutes in order to remove any remaining water, then heated to 700°C at a rate of 5°C per minute.

FTIR measurements were performed using a Nicolet Magna 860 Fourier Transform Infra-Red Spectrometer with a DTGS detector. Samples were examined in transmission ,ode, using ZnSe or silicon substrates, or as free-standing films which were made as described for TGA.

2.3 Results and Discussion

2.3.1 Film Assembly

Figure 2-3 shows the per layer pair thickness for each of the four polyelectrolyte pairs over the assembly range of pH 3 – 6. PAH/PAA is the thinnest system, with an average layer pair thickness of less than 10 nm, due to the fact that PAH is strongly charged over this pH range. The LPEI/PAA and BPEI/PAA systems behave similarly with a peak layer pair thickness at pH 4 of about 115 nm when both polyelectrolytes are partially charged. Film assembly of these two systems below pH 2.5 and above pH 6 is essentially negligible. The PAMAM/PAA films are much thicker than the other systems, with a peak per layer pair thickness at pH 4 of ~170 nm. Considering that the extended diamter of a G4 PAMAM dendrimer in solution is somewhere between 5 and 7 nm,[15] this is a somewhat surprising result, suggesting perhaps the PAA chains make up the bulk of each layer pair. The per layer pair thickness for PAH/PAA and LPEI/PAA are consistent with those reported elsewhere.[11,23]

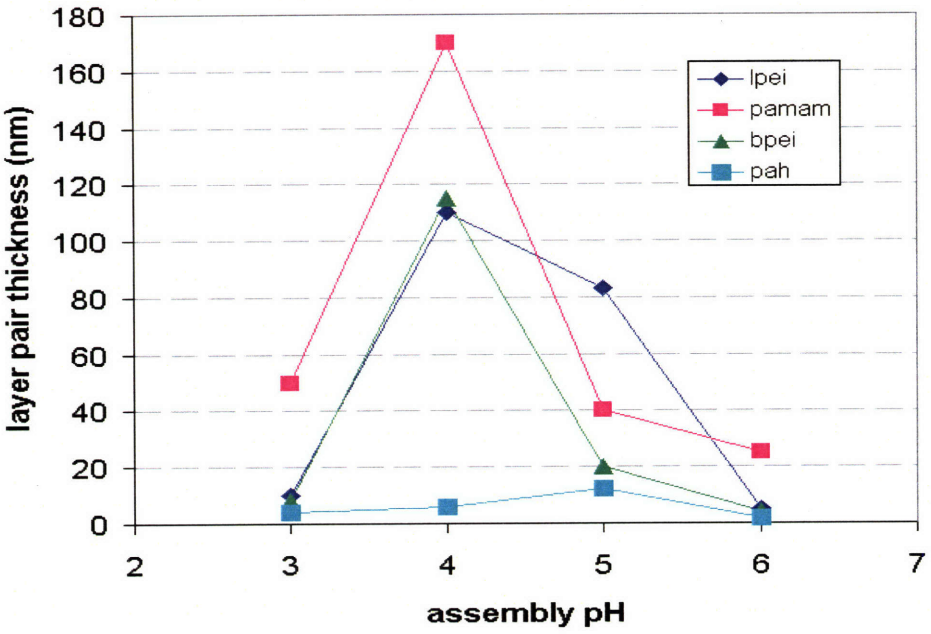

Figure 2-3: Growth curves of the polyelectrolyte systems examined in this work.

2.3.2 Morphology of PAMAM Containing Multilayers

The literature is full of examples of AFM images of LbL films composed of linear polyelectrolytes. Dendrimers, with their different molecular architecture are known to adsorb differently; and it is unclear if linear chains can interpenetrate them. Dendrimers are known to take on a flat conformation when adsorbed at a surface due to the high density of charged groups. Dendrimers, especially at lower generations are flexible, and will find a conformation in which the maximum number charged groups will attach to the surface. This can be seen in figure 2-2, in the AFM images of the PAMAM surfaces of PAMAM/PAA multilayers. The pH 5 and pH 6 surfaces are very smooth with dense layers of flattened dendrimers. The pH 3 case is, however, somewhat different. At pH 3, the PAMAM dendrimer is fully charged and extended in solution. The 1 micron phase image shows that the PAMAM surface is covered with clusters, or aggregates of PAMAM dendrimers. In this case, the self-repulsion of the positive charges makes it difficult for the dendrimer to flatten onto the PAA surface, which had also become less charged and therefore less attractive. Secondary van der Waals interactions between dendrimer interiors then cause them to aggregate and form these clusters.

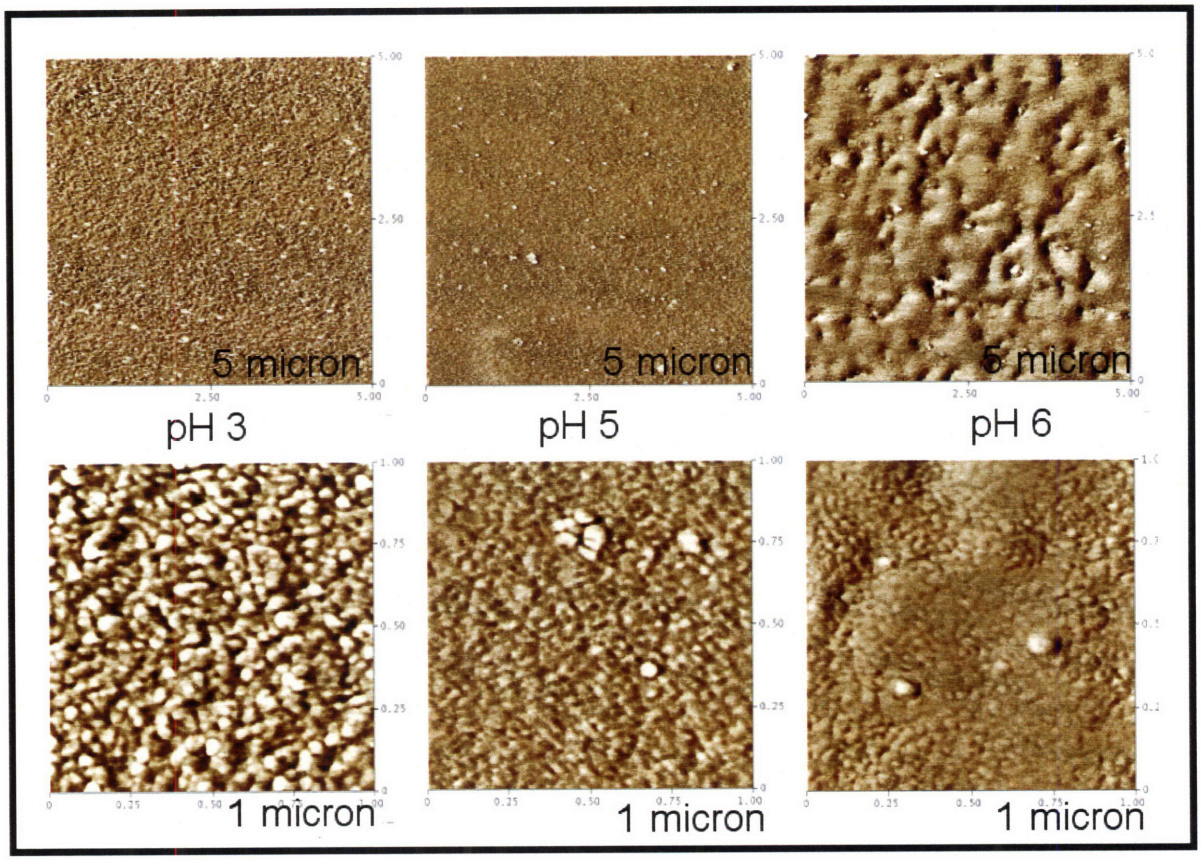

Figure 2-4: Phase images of PAMAM surfaces of PAMAM/PAA multilayers, 5.5 bilayers, PAMAM surfaces, assembled at different pH conditions. The pH 3 film shows aggregations of dendrimers on the surface will the films assembled at higher pH have a more compact surface morphology.

2.3.3 Degree of Ionization within LbL Films

Studies have repeatedly shown that the degree of ionization along the backbone of a polyelectrolyte chain is subject to change under the influence of its immediate environment as the polymer chain tries to find the minimum energy configuration. That is, in solution at a given pH a weak polyelectrolyte will have a specific degree of ionization, but the coulombic forces introduced by a second polyelectrolyte will affect that degree of ionization. Adsorption to a surface can also have an influence. Therefore, within a multilayer assembly, the degree of ionization of the various components is usually rather different than in solution. The pKa of PAA has been pbserved to shift 2-3 pH units within an LbL film as compared to in solution.[11] This shift in pKa can be determined by a number of factors; including the strength of interaction between the anionic and cationic groups.[24] In chapter 5 an example of the stronger interactions between LPEI and PAA when compared to PAA and a second polycations actually causes that second polycations to be displaced from solution.

FTIR studies of LPEI/PAA, BPEI/PAA, PAMAM/PAA, and PAH/PAA multilayers (which contain similar ionic crosslinks) were performed in order to determine what affect, if any, the molecular architecture and hydrophobicity of the polycations would have on the ionization of PAA. All four polycations have amine groups, which strongly complex to the carboxylic acid groups of PAA.

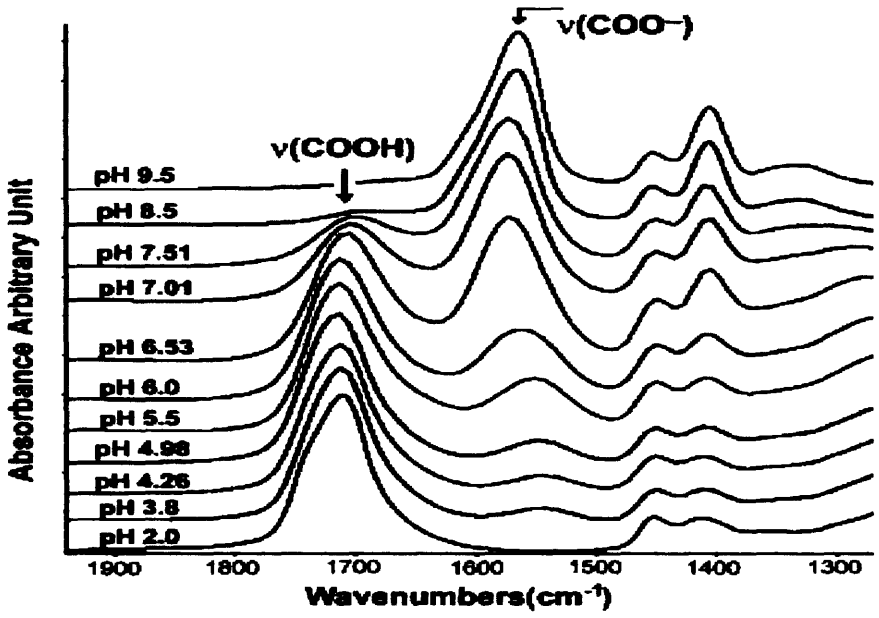

Figure 2-5: FTIR spectra of cast films of PAA taken at various pH values, taken from ref. 11.

Comparing figure 2-5 to the FTIR spectra of LPEI/PAA, PAH/PAA, PAMAM/PAA, and BPEI/PAA (shown in figures 2-6, 2-7, 2-8, and 2-9, respectively) it is clear that the amount of ionized carboxylic acid groups is much greater in all of the films that for the PAA cast from solution. This is, of course, due to the complexation between the polyelectrolyte pairs. Another clear (and to be expected) trend is the fact that (as for the cast films) the number of ionized carboxylic acid groups increases with pH.

Approximate percentage of ionized carboxylic acid groups was determined by taking a ratio of areas of the peak for neutral –COOH (at 1710) and ionized –COO^- (at 1540). Comparing the four polycations, films containing PAH are the most highly ionized, followed by BPEI, then LPEI, and finally PAMAM containing films, which contain the most free carboxylic acid (-COOH) groups. This result is summarized in figure 2-10, which plots the percentage of free carboxylic acid groups in each of the films. Figure 2-5 shows that PAA in cast films is between 10 – 30% ionized, whereas in the

multilayers the pH 3 percent of ionization ranges from 30 – 45% and the pH 6 percent ionization ranges from 70 – 90%.

PAH is the most strongly charged of the group, as well as most hydrophobic, explaining why it forms a large number of ionic crosslinks with PAA. The interior tertiary amines of the PAMAM dendrimers are largely uncharged at pH 5 and 6. At the lower pH values the dendrimers take on a more fully extended conformation, and it is difficult for PAA chains to penetrate to the interior. Although LPEI and BPEI are chemically similar, BPEI is more charged over the range of assembly conditions, partly explaining the difference in the degree of ionization of the films. Also, it is possible that the branched polymer is more easily able to penetrate the PAA surface at each adsorption step and thereby form more ionic crosslinks.

It is more difficult to determine the degree of ionization of the amine groups in the various LbL assemblies. Features (peaks or often shoulders) corresponding to charged and neutral amine groups are seen from 2500cm^{-1} to 3500cm^{-1}. Over this range features from hydrogen bonding, neutral carboxylic acid groups, water (in general –OH stretching), methylene groups of the polymer backbone, and amide linkages (present in PAMAM dendrimers) are all also present, making it impossible to precisely deconvolute the numerous peaks.

In figure 2-4, the LPEI/PAA FTIR spectra, a shoulder at about 2500 cm^{-1} can be seen; this feature is due to charged secondary amine groups, and is present at all pH values. A small features presents itself at abour 3300 cm-1 in the pH 5 and pH 6 spectra; this is due to free secondary amine groups. From these observations we can conclude that LPEI is highly charged within these assemblies, with free amine groups presenting themselves only at higher pH values. Considering that LPEI causes PAA to become more charged, it should be expected that the same happen for LPEI.

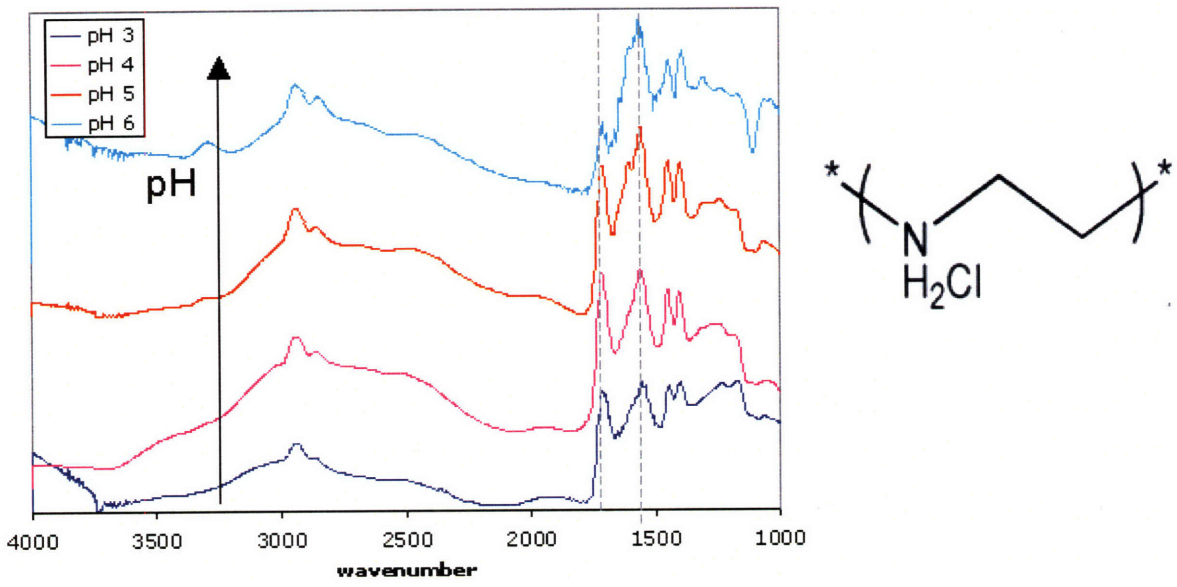

Figure 2-6:FTIR spectra pf LPEI/PAA multilayers assembled from pH 3-6. Spectra are shifted along the y axis arbitrarily for clarity's sake. Indicated are the peaks for free carboxylic acid at ~1710 and ionized carboxylic acid (-COO-) at ~1540.

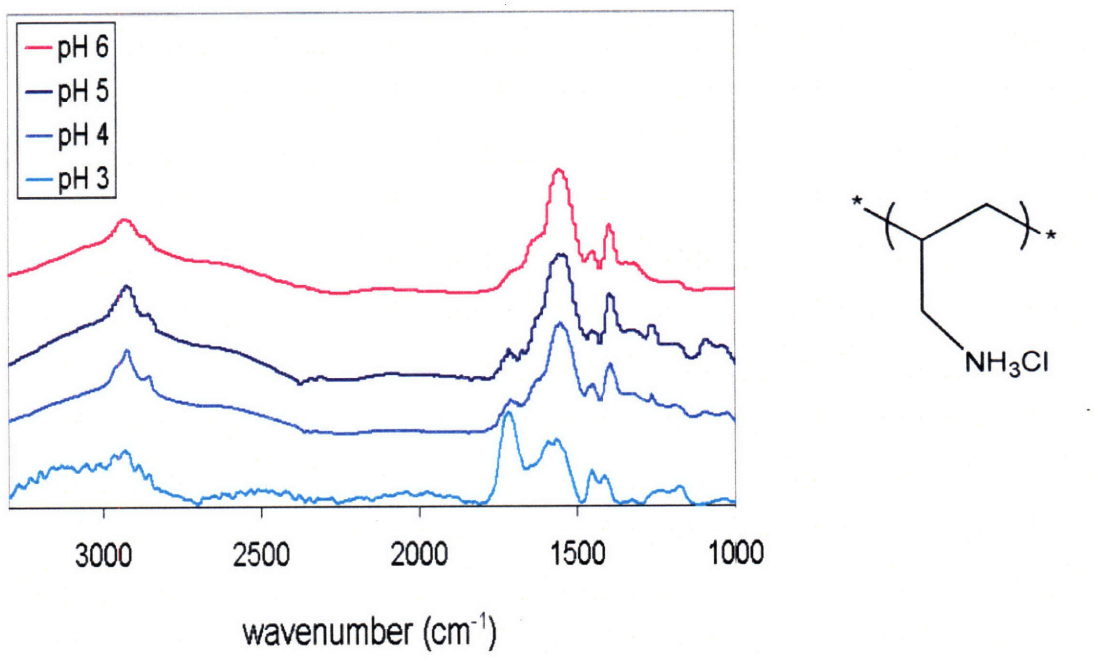

Figure 2-7: FTIR spectra of PAH/PAA multilayers

As seen in figure 2-5, the PAH/PAA case is more simple; the peak at about 3000 cm-1 is due to charged primary amines (although overlapping with features due to methylene groups), and it can be seen that the PAH chains are fully charged throughout the pH series.

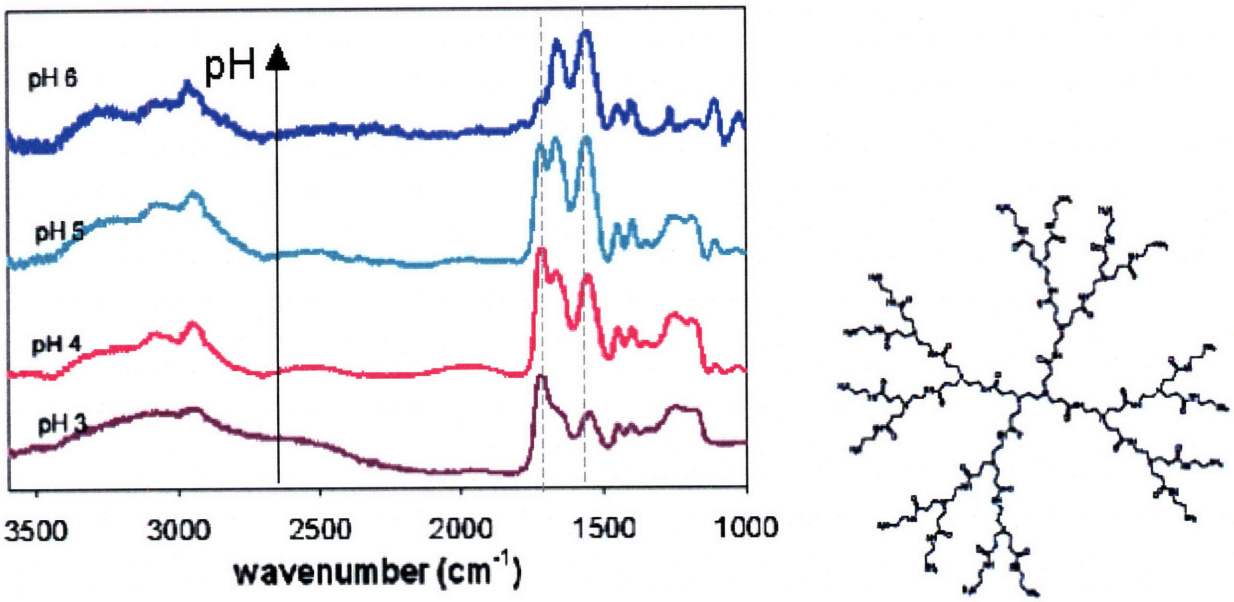

Figure 2-8: FTIR spectra of PAMAM/PAA multilayers.

The PAMAM/PAA films, seen in figure 2-6, are the least clear in terms of degree of ionization of amine groups because of the overlap with features from amide linkages. The shoulder at 2500 cm-1 attributed to charged tertiary amine groups can be seen in the pH 3 spectrum, as that is below the tertiary amine pKa for PAMAM. The broad shoulder from 3000 cm-1 to 3500 cm-1 indicate that free amine groups are present, even at the lowest pH. This can be explained by the previous observation that the compactness and stiffness due to self-repulsion of the dendrimer structure, especially at low pH, make it difficult to form many ionic crosslinks.

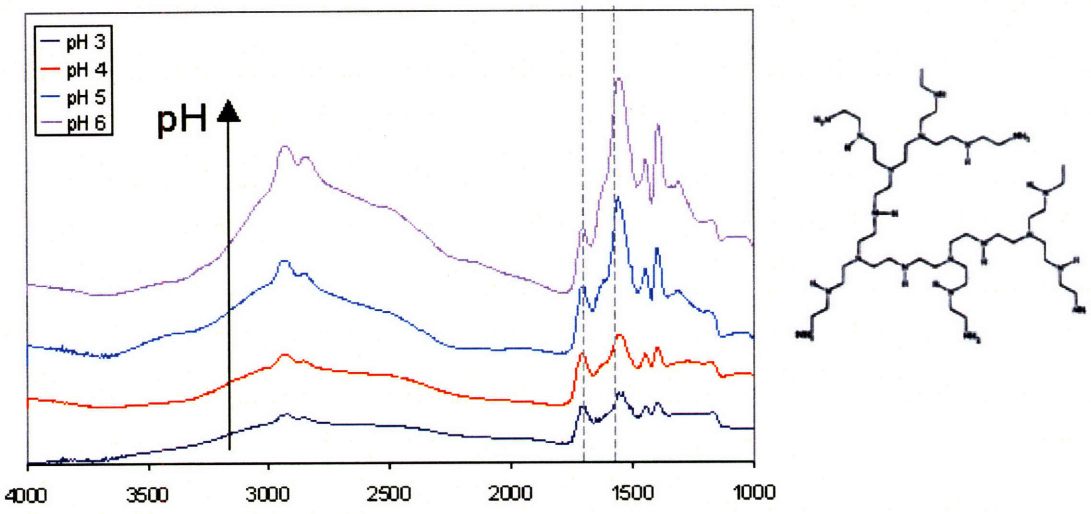

Figure 2-9: FTIR spectra of BPEI/PAA multilayers. Overall, these FTIR spectra show that for each polycations there is a different degree of ionization for the carboxylic acid groups, the most strongly ionized being PAH > BPEI > LPEI > PAMAM, which has the least degree of ionization of the carboxylic acid groups.

In the BPEI/PAA FTIR spectra (figure 2-7), the shoulder at 2500 cm-1 representing charged tertiary and secondary amine groups is seen to increase with pH, corresponding to the increased degree of ionization of carboxylic acid groups.

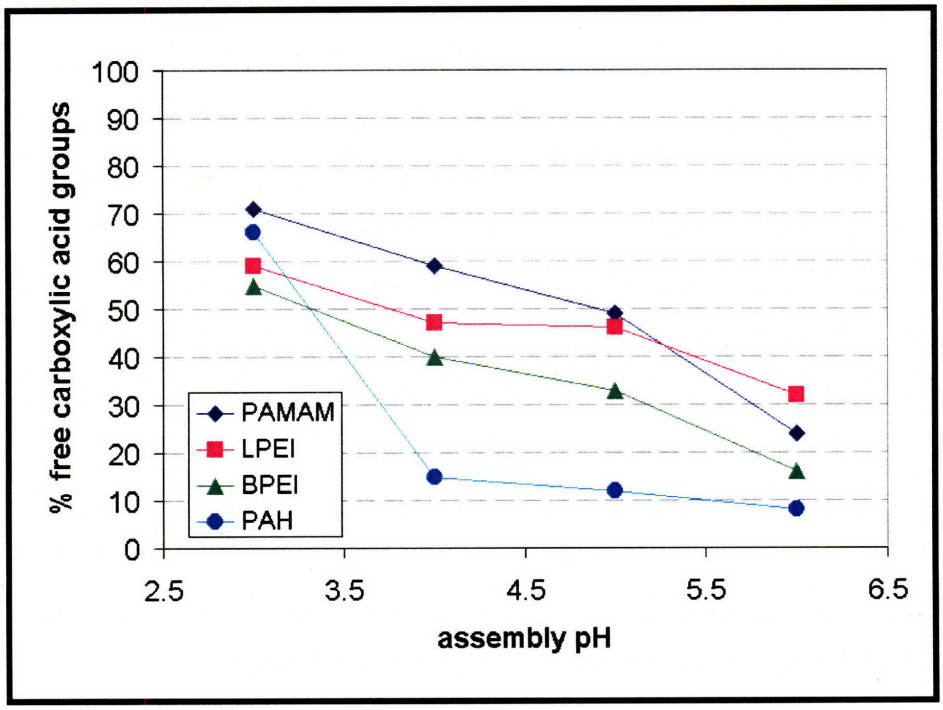

Figure 2-10: Percentage of available -COOH groups.

2.3.4 TGA of LbL films

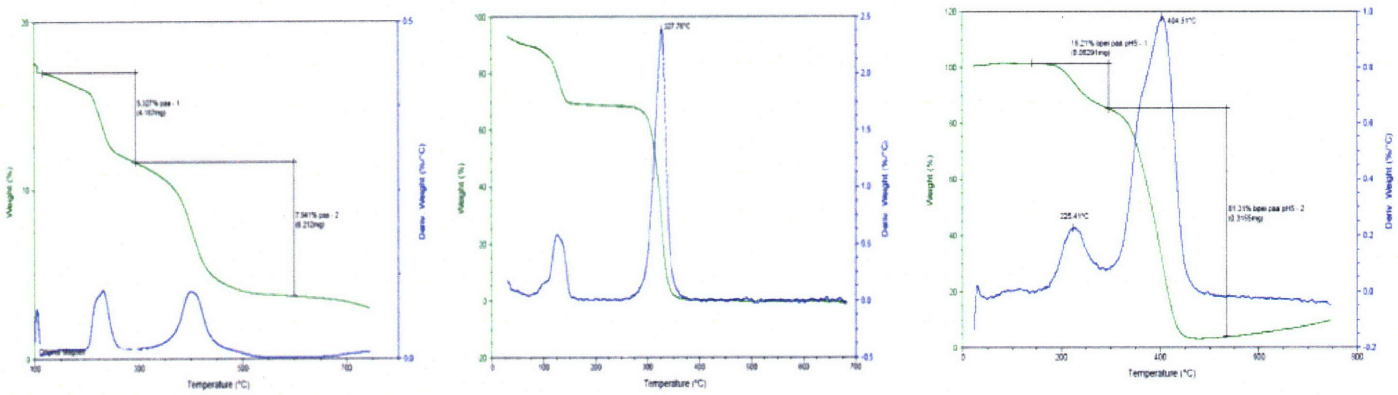

(a) (b) (c)

Figure 2-11: TGA of (a) pure PAA (b) pure LPEI and (c) LPEI/PAA multilayer assembled at pH 5.

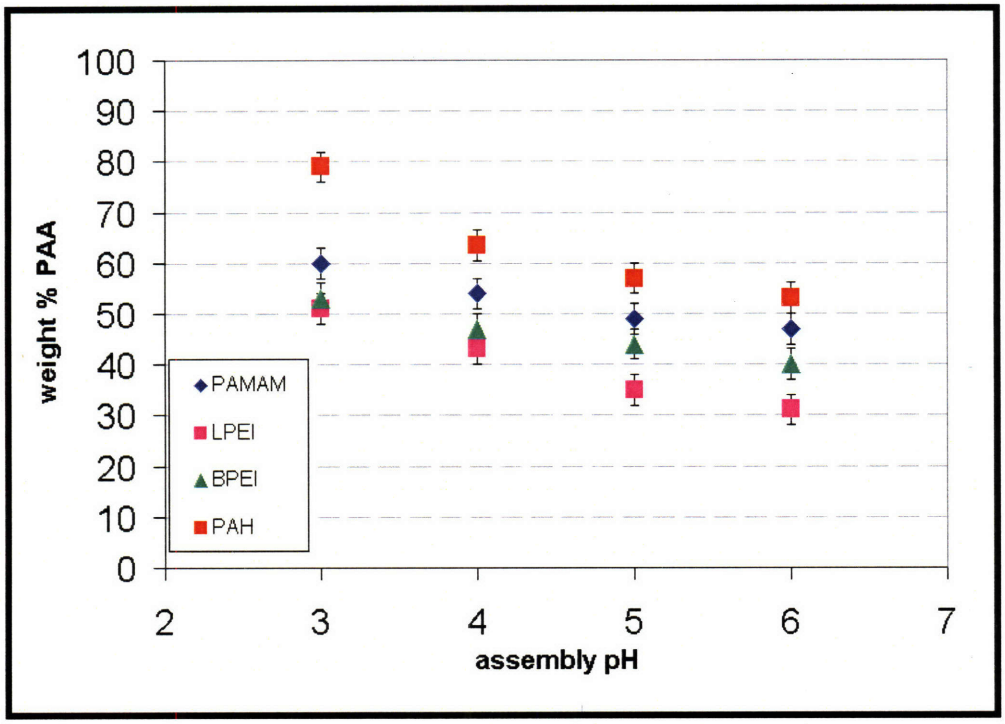

Figure 2-12: Composition of LbL films in terms of wt% PAA.

TGA data was collected of pure samples of the polyelectrolytes as well as the films assembled from pH 3 – 6. Figure 2-11 shows TGA data of (a) pure PAA, (b) pure LPEI, and (c) LPEI/PAA multilayer assembled at pH 5. By comparing the film's TGA curve to that of the pure components, it is possible to determine the relative composition within the film. Figure 2-12 shows the composition of the films assembled under different conditions in terms of weight percent PAA.

Figure 2-12 shows the relative compositions for the four sets of LbL assemblies across the assembly pH range of interest. Consistent to all four systems is that PAA content decreases with increasing pH. PAA is becoming more charged with increasing pH and the polycations less so, which is consistent with lower PAA content at higher pH value. From the four systems, the PAH films have the highest amount of PAA in them, ranging from ~85% at pH 3 to 55% at pH 6. The other systems have similar compositions, ranging from 50-60% PAA at pH 3 to 30-50% PAA at pH 6.

2.4 Conclusions

Here we have investigated some fundamental properties of LbL assemblies comprised of PAA in combination with polycations of amine functionality (LPEI, PAH, PAMAM dendrimer, and BPEI). While these polycations were chemically similar, they differed in solution state degree of ionization, molecular architecture, and hydrophobicity. These four assemblies were investigated in order to determine what if any affect these differences have on multilayer structures.

FTIR spectra show that complexation of PAA with all of these polycations causes PAA to become more charged than in solution state at the same pH conditions. However, this affect is different for each polymer, the films with PAH being the most strongly ionized, followed by BPEI, LPEI, and finally PAMAM. PAH is the most hydrophobic if the group and therefore the most likely to form ionic crosslinks. PAMAM's compact geometry limits access to its amine groups, and therefore forms few crosslinks.

AFM images of PAMAM surfaces confirm that PAMAM adsorbs in a manner somewhat different than linear polyelectrolyte chains. At low pH they form aggregates on the PAA surface, while at higher pH they flatten out onto the PAA surface, both of which are difficult configurations for the PAA chains to then penetrate and form many ionic crosslinks.

TGA data shows that the PAA content of the films decreases with increasing pH value – consistent with PAA becoming more charged and the polycations becoming less charged. The PAH/PAA films contain the highest wt % of PAA.

Chapter 2 References

1. Dubas, S. T.; Schlenoff, J. B. *Macromolecules* **1999**, *32*, 8153-8160.
2. Israels, R.; Leermakeers, F. A. M.; Fleer, G. J. *Macromolecules* **1994**, *27*, 3087-3093.
3. Hoogeveen, N. G.; Cohen Stuart, M. A.; Fleer, G. J.; Böhmer, M. R. *Langmuir* **1996**, *12*, 3675-3681.
4. Fery, A.; Schöler, B.; Cassagneau, T.; Caruso, F. *Langmuir* **2001**, *17*, 3779-3783.
5. Yoo, D.; Shiratorei, S. S.; Rubner, M. F. *Macromolecules* **1998**, *31*, 4309-4318.
6. Shiratorei, S. S.; Rubner, M. F. *Macromolecules* **2000** *33*, 4213-4219.
7. Steitz, R.; Jaeger, W.; v. Klitzing, R. *Langmuir* **2001**, *17*, 4471-4474.
8. Schoeler, B.; Kumaraswamy, G.; Caruso, F. *Macromolecules* **2002**, *32*, 889-897.
9. Glinel, K.; Moussa, A.; Jonas, A. M.; Laschewsky, A. *Langmuir* **2002**, *18*, 1408-1412.
10. Schoeler, B.; Poptoshev, E.; Caruso, F. *Macromolecules* **2003**, *36*, 5258-5264.
11. Choi, J.; Rubner, M. F. *Macromolecules* **2005**, *38*, 116-124.
12. Debreczeny, M.; Ball, V.; Boulmedais, F.; Szalontai, B.; Voegel, J.C.; Schaaf, P. *J. Phys. Chem. B* **2003**, *107*, 12734.
13. Weyts, K. F.; Goethals, E. J. *Makromol. Chem., Rap. Comm.* **1989**, *10*, 299.
14. Smits, R. G.; Koper, G. J. M.; Mandel, M. *J. Phys. Chem.* **1993**, *97*, 5745.
15. Bloys van Treslong, C. J.; Staverman, A. J. *Recueil, J. Royal Neth. Chem. Soc.* **1974**, *93*, 171.
16. Shepherd, E. J.; Kitchener, J. A. *J. Chem. Soc.* **1956**, *4*, 2448.
17. Tomalia, D. A.; Naylor, A. M.; Goddard, W. A. *Angewandte Chemie International Edition* **1990**, *29*, 138-175.
18. Malyarenko, D. I.; Vold, R. L. Hoatson, G. L. *Macromolecules* **2000**, *33*, 1268-1279.
19. Uppuluri, S.; Tomalia, D. A.; Dvornic, P. R. In *Polymeric Materials Encyclopedia*; Salamone, J. C., Ed.; CRC Press: New York, 1996; Vol. 3, pp 1824-1830.
20. Niu, Y.; Sun, L.; Crooks, R. M. *Macromolecules* **2003**, *36*, 5725-5731.
21. Cakara, D.; Kleimann, J.; Borkovec, M. *Macromolecules* **2003**, *36*, 4201-4207.
22. Diallo, M. S.; Christie, S.; Swaminathan, P.; Balogh, L.; Shi, X.; Um, W.; Papelis, C.; Goddard, W. A.; Johnson, J. H. *Langmuir* **2004**, *20*, 2640-2651.
23. Delongchamp, D., Hammond, P. T. *Chem Mater.* **2003**, *15*, 1165-1173.
24. Zacharia, N. S.; DeLongchamp, D. M.; Modestino, M.; Hammond, P. T. *Macromolecules* **2007**, *40*, 1598-1603.
25. Lutkenhaus, J. L; Hrabak, K. D.; McEnnis, K.; Hammond, P. T. *J. Am. Chem. Soc.* **2005**, *127*, 17228-17234.

Chapter 3

Application of Polyamine Containing LbL Films; Spray Deposition and Organic Vapor Permeation

3.1 Introduction

In the previous chapter four multilayer systems were introduced, and their basic properties examined. The next several chapters explore applications based on these different properties. Here we discuss an automated method for misting films that allows us to deposit films on a wider range of substrates, including porous membranes. We then test these films for permeation to chloroethl ethyl sulfide.

The LbL process is an attractive method that in principal could be used to conformally coat substrates of nearly any geometry and size with nanoscale control of film thickness and structure. Conventional "dipping" techniques for film deposition which work well in the laboratory setting are not so well suited for industrial applications due to the long deposition time and the limitation to substrate size inherent to dipping. Using an automated spraying process speeds up film formation allowing for large areas to be simultaneously coated, thus facilitating the coating of materials such as textiles.

In order to more quickly assemble multilayers, methods such as spincoating[1] and misting[2-4] have been considered. One of the first commercial products using LbL films was a contact lens developed by Cibavision, using a PAH/PAA multilayer to increase surface wettability. In order to make surface modification via LbL commercially viable, a one step process was developed, by which a soluble complex of the two polyelectrolytes was sprayed onto the contact lens. Several other groups have examined the properties of multilayers assembled by a spraying process, including simultaneously spraying the substrate with both polyions, and varying parameters such as rinsing time and distance away from the substrate. Misted multilayers can vary a great deal depending on small differences in the assembly conditions; droplet size, pressure, length of rinse cycle, etc. In order to eliminate this variability, we have automated the misting process for multilayer assembly.

The ability to coat a range of different substrates using this misting technique allows for the creation of ultrathin LbL membranes which span the pores of well-defined commericial membranes

such as track-etched polycarbonate (Nuclepore). Such membranes can then be assembled onto fibers and fabrics or on traditional membranes. We will utilize the automated misting method as a route to formation of LbL membranes; the automated nature of this process enables construction and testing of the different polyamine systems in the study assembled under differing conditions.

Thin films as membranes or diffusion barriers are used in a variety of applications, ranging from filtering and separation of components in solutions to food packaging, drug delivery and protection from corrosive gases.[8, 9, 10] LbL films have been used for pervaporation separation of alcohol/water mixtures[10, 11] and as nanofilters to separate sucrose from an aqueous solution.[5] It has been reported that permeability and transport in LbL film are correlated to factors such as ionic crosslink density and nature of the film's capping layer.[5]

Using misting to spray LbL films onto textiles, protective coating against corrosive gases, such as chemical warfare agents, could de designed. Here we demonstrate films properties as simple diffusion barriers to CEES vapor, but multiple functionalities could eventually be built into these films, such as chemical moieties that bind to or decompose gas molecules.

3.2 Experimental Details

***Materials*:** Poly(ethylene imine) (LPEI, MW = 25,000), poly(acrylic acid) (PAA, MW = 90,000) were purchased from Polysciences. Poly(amido amine) dendrimer (PAMAM G4, NH_2 surface, 22 wt% in methanol) was purchased from Dendritech. Polymer solutions were made using DI water at a concentration of 20 mmol with respect to the repeat unit, and adjusted to the required pH using HCl or NaOH. The ionic strength of the PDAC and SPS solutions was 0.1 mol NaCl. Spray-LbL tests were conducted on three and four inch diameter silicon wafers (Silicon Quest International), while dipped LbL tests were conducted on similar wafers which had been broken into 1cm by 5cm pieces. All silicon was cleaned with methanol and Milli-Q water, followed by a five minute oxygen plasma etch (Harrick PCD 32G) to clean and hydroxylate the surface.

***Film Deposition*:** For permeation measurements polyelectrolyte assemblies were sprayed onto Nuclepore membranes. For swelling and thickness measurements silicon substrates were used, and for TGA measurements polypropylene substrates. Silicon wafers were rinsed with methanol and then deionized (DI) water, and then exposed to oxygen plasma for 5 minutes. Nuclepore membranes were used as received for film assembly. Dipped film assembly was automated with a Carl Zeiss HMS DS-

50 slide stainer. The substrates were first exposed to the polycation solution for 10 min. followed by three rinse steps in Milli-Q water for a total of 2 minutes. The substrate was then exposed to the corresponding polyanion solution and rinsed similarly. The cycle was repeated for the required number of layer pairs requiring approximately 12.5 hours to complete a 25 layer pair film. To adjust the pH value of the polyelectrolyte solutions and rinse baths, dilute solutions of NaOH and HCl were used. Sprayed films were deposited using identical solutions and rinse pH values. All solutions were delivered by ultra high purity Argon (AirGas) regulated to 50 psi. The polycation was sprayed for 3 seconds and allowed to drain for 17 sec. before spraying with water for 10 sec. After a 10 second draining period the polyanion was sprayed and rinsed similarly. The cycle was then repeated for the desired number of layer pairs resulting in a 33 minute process to deposit a 25 layer pair film.

Film characterization: Permeation testing is conducted by sandwiching a Nuclepore Track-Etch Polycarbonate Membrane coated with the desired film in between two 1/16" thick butyl rubber gaskets. These membranes provided negligible resistance to mass transfer, allowing us to quantify the physical properties of the coatings independent of the underlying substrate. The butyl rubber has been shown to absorb negligible amounts of permeant compounds on time scales of interest to this test. The stack is then topped with a steel mesh to act as a high surface area support for permeant chemicals in the condensed phase. The membrane then acts as the only means of mass transfer between two portions of a sealed stainless steel test cell. Above the membrane, the stagnant vapor space contains a permeant compound at vapor liquid equilibrium (thus its vapor pressure), while an inert sweep gas is passed under the membrane at a known flow rate. All piping is constructed from stainless steel as well.

This sweep gas is then analyzed by a GOW-MAC Series 23-550 Total Hydrocarbon Gas Analyzer, equipped with an FID (hydrogen/oxygen flame) capable of 0.01 ppm contaminant detection. Since mass transfer is restricted to one dimension through the membrane, and no pressure gradient is induced across it, any contaminant reaching the detector is attributed to one dimensional diffusion through the membrane simplifying further calculations of permeation.

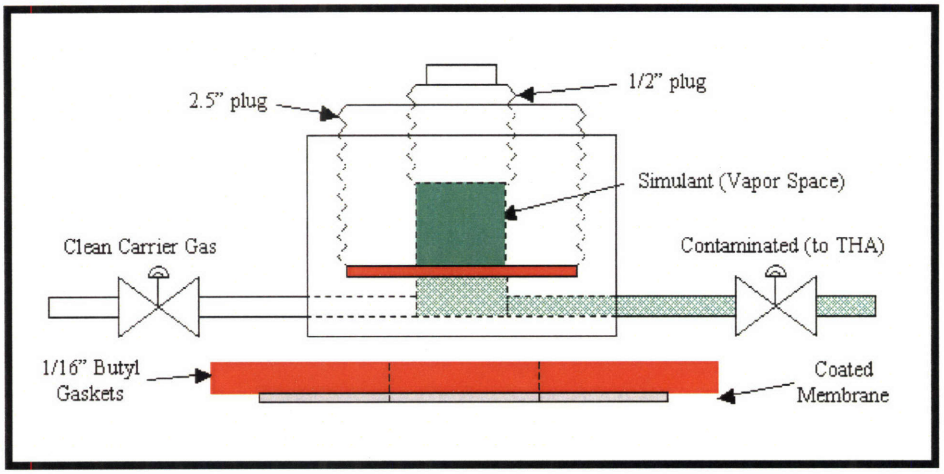

Figure 3-1: Schematic of permeation cell.

To measure film thickness, both profilometry and ellipsometry were used. A Tencor P10 profilometer was used, with a tip force of 3 mg to avoid penetrating the film.

3.3 Spray Deposition of Multilayers

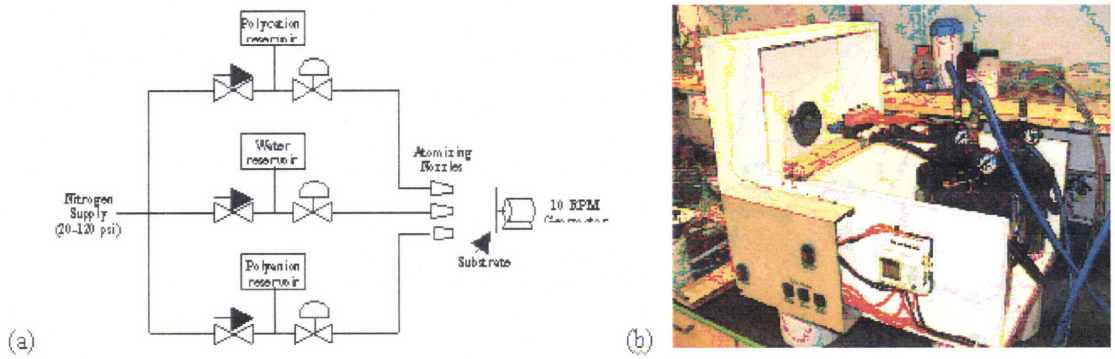

Figure 3-2: (a) Schematic of automated spraying system, and (b) photograph of automated spraying system.

The automated spray system, shown in figure 3.2, consists of three identical solenoid valves, each supplied with a constant head of fluid from either of two polyelectrolyte vessels or a rinse water vessel. Spray is then controlled by sequentially closing and opening the solenoid valves through the use of a logic relay capable of 10 ms accuracy in response time. Fluids then pass through atomizing nozzles that are each equipped with a prefilter. The substrate is mounted vertically on a sliding post allowing larger substrates to be placed further from the nozzle bank. To avoid drip patterns in the cascading film, the substrate is also rotated at 10 RPM. However, the reader should note that this speed is far too low to impart any centrifugal force to the liquid on the substrate. The rotation is

simply to minimize the effects of gravity as well as any irregularities in the pattern developed by the nozzles. Finally, to avoid contamination, all plumbing, including valve bodies, was constructed of poly(propylene).

With our spraying system we are able to uniformly coat porous substrates such as Nucleopore membranes, and hydrophobic substrates such as Dupont Tyvek. We are able to uniformly change the surface properties of Tyvek, indicating that there is a uniform film on the surface. This can be seen in Figure 3-3; (a) contact angle of water on uncoated Tyvek, and (b) contact angle of water on Tyvek coated with $(LPEI/PAA)_{100}$. The coated material exhibits a wetting contact angle more than 40° less than that observed on uncoated material, as seen in Figure 3-3. This macroscopic modification can be seen uniformly across the entire coated area, indicating successful coating of the entire substrate. Additionally, we have also shown the ability to spray hydrogen bonded films and films with TiO_2 nanoparticles.[7]

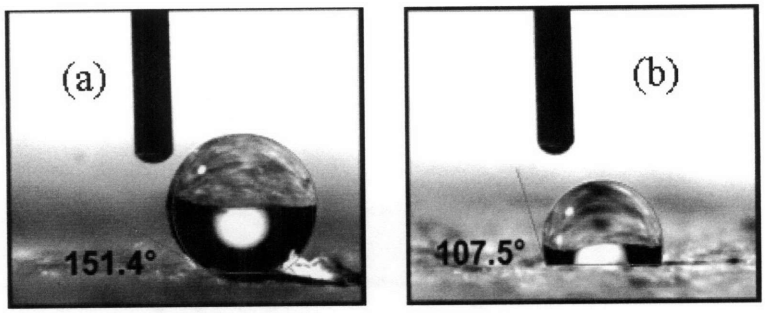

Figure 3-3: Contact angle of water on (a) uncoated Tyvek material and (b) Tyvek cloth misting with 100 layer pairs of LPEI/PAA.

The films created by spraying are thinner than those dipped, but they follow the same trends in terms of relative film thickness at different assembly conditions. Figure 3-4 shows the thickness for 50 layer pair sprayed LbL films for the different polyamine systems used in this work. As an example, a 50 layer pair PAMAM/PAA film at pH 4 is ~1250 nm thick, or 25 nm per layer pair whereas the dipped analogue is ~170 nm thick per layer pair. For another example, dipped LbL films of LPEI/PAA have been reported to have a thickness of approximately 100 nm per layer pair[6] at pH 4, whereas the misted layers have a thickness of only 6 nm per bilayer at pH 4. AFM images of the first layer pair of PAMAM/PAA both dipped and sprayed (seen in Figure 3-7) shows that in both cases "island" growth is initially seen, but that in the case of the sprayed film, these islands are smaller, likely due to the short exposure time. This then leads to lower surface roughness and eventually lower film thickness.

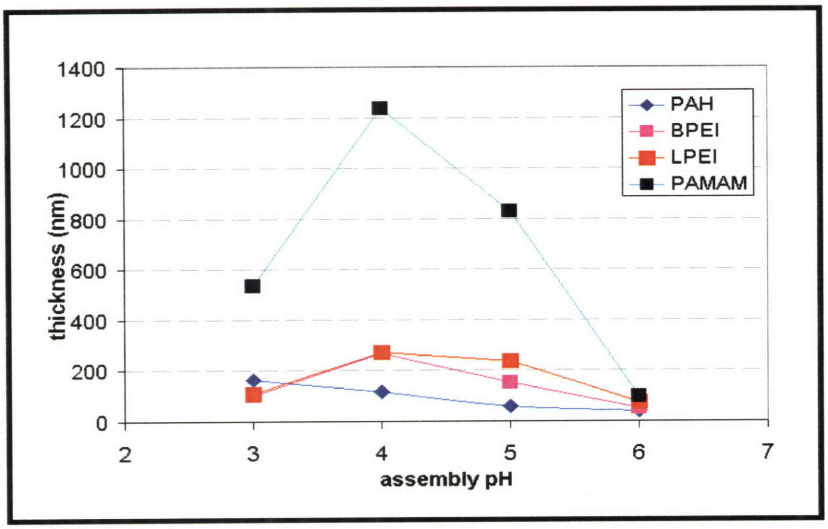

Figure 3-4: Thickness of sprayed 50 layer pair multilayer films.

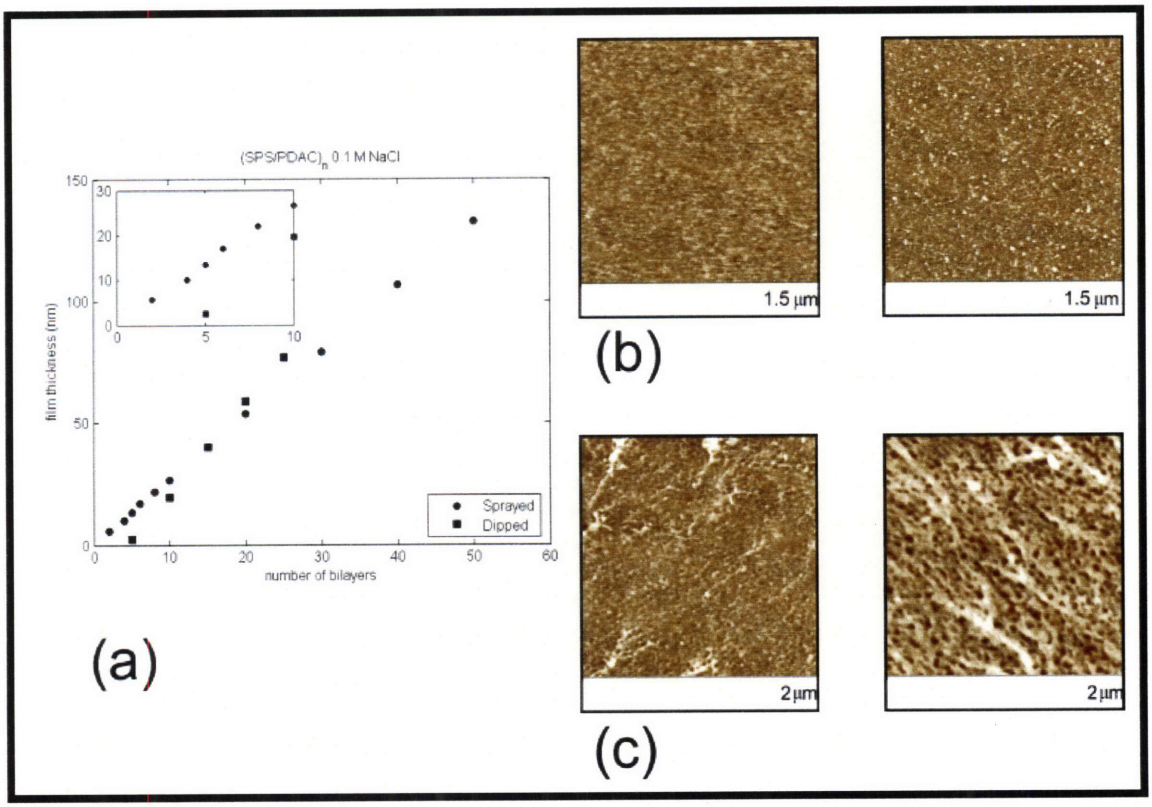

Figure 3-5 : (a) Growth curve of SPS/PDAC dipped vs. sprayed. (b) AFM images of the deposition of the first layer pair of SPS/PDAC, misted, and (c) AFM images of the first layer pair of SPS/PDAC dipped. All AFM images are 5 micron squares.

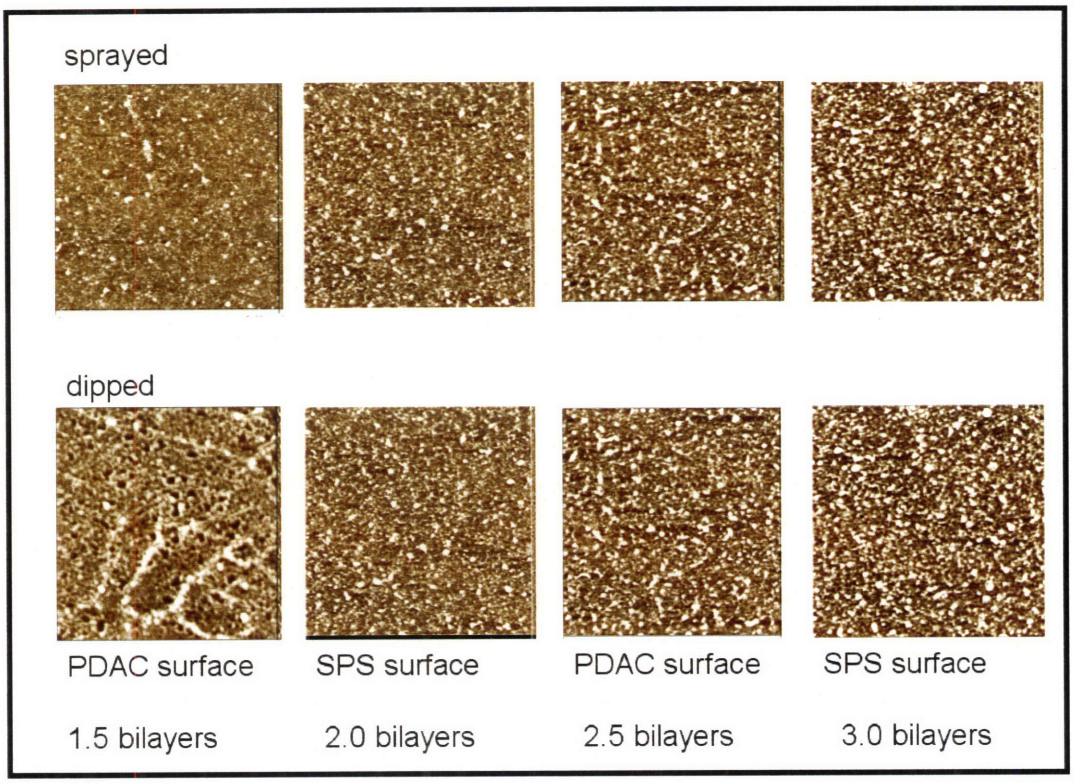

Figure 3-6: AFM images of sprayed vs. dipped SPS/PDAC multilayers, all images 5 micron squares. The dipped surfaces are more rough then the sprayed surfaces through the first 2 layer pairs, and are similar for both methods.

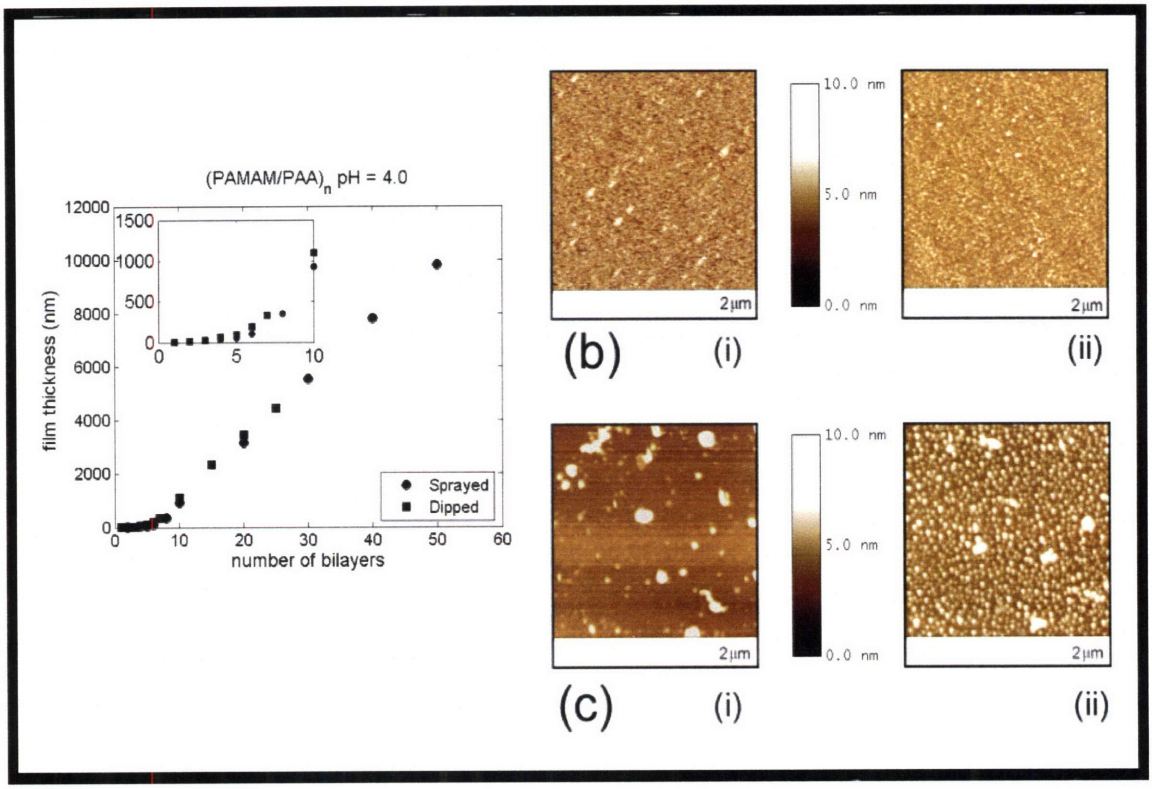

Figure 3-7: Growth curve for sprayed vs. dipped multilayers of PAMAM/PAA at pH = 4. The right hand images are AFM topology images of (b) sprayed PAMAM/PAA multilayers, (i) 0.5 layer pair and (ii) 1.0 layer pair. Images in (c) are of dipped PAMAM/PAA layers, (i) 0.5 layers pairs and (ii) 1.0 layer pairs. Dipped images slow larger initial island growth.

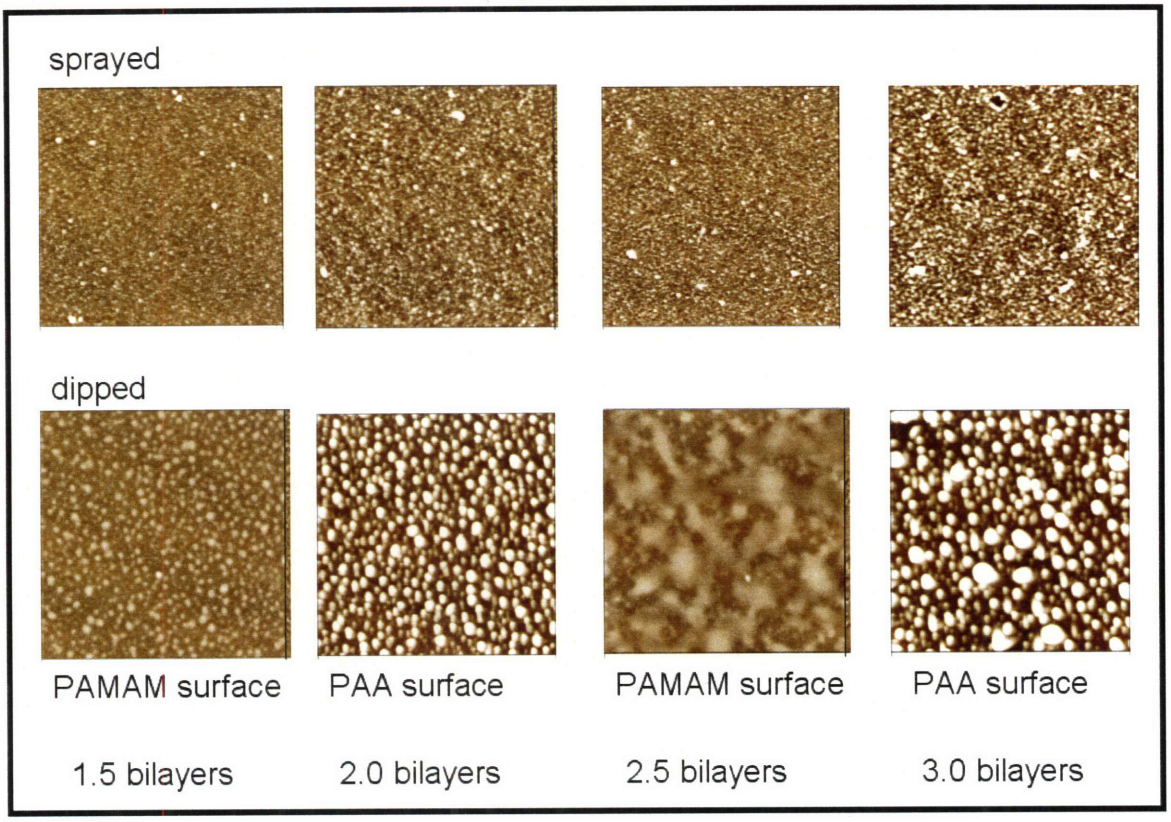

Figure 3-8: 5 micron height images of both sprayed and dipped PAMAM/PAA multilayers at pH = 4. Dipped surfaces show larger features, perhaps indicative of the reason that thicker films are formed.

3.4 CEES Vapor Permeability

In order to compare the properties of the different LbL systems as diffusion barriers, films of 50 layer pairs were misted onto Nuclepore membranes and exposed to the vapor of a mustard gas simulant (chloroethyl ethyl sulfide, or CEES, structure shown in Figure 3-9(a)) using the set up described in the experimental details. This set up measures instantaneous concentration of gas passing through the membrane in ppm at ten second intervals. An example of the instantaneous flux through an LPEI/PAA pH 4 film is shown in Figure 3-9(b).

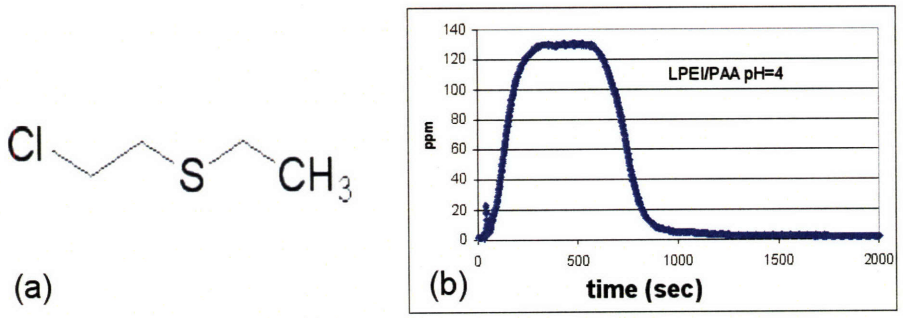

Figure 3-3-9: (a) Structure of chloroethyl ethyl sulfide, CEES. (b) Example of the raw instantaneous flux data collected for a LPEI/PAA pH 4 film. The measurement is ppm of CEES vapor in the carrier gas which sweeps through the cell below the membrane. The flux ramps up to a steady state plateau and then falls to zero as the CEES vapor in the cell crosses the membrane and is carried away by the flow of compressed air.

Net permeation, or net amount of vapor that has flowed through the membrane, can be determined by integrating the instantaneous flux curve, and should be equal to the amount of CEES placed in the cell at the beginning of the experiment. Our experimental results agree within 10% of this value, telling us that our cell is indeed airtight over the timescale of the experiment and that the rubber gaskets are not being swollen by the organic vapor.

Transport of the CEES vapor through our LbL films can be addressed using the solution-diffusion model; in which the permeant is thought to dissolve into the membrane and then diffuse down a concentration gradient.[8, 9] Diffusion across the membrane can then be described using Fick's law, which in this case is a function of the "permeability" of the membrane, considered a constant property for a given material exposed to a given permeant partial pressure gradient. The permeability is defined as the product of the solubility of the permeant in the membrane and the diffusivity of the permeant in the membrane (i.e. the rate at which the CEES vapor permeates the LbL film is dependent on how much can be dissolved into the film and then how quickly it diffuses through the film).

In order to determine the solubility and permeability of the permeant in the membrane, steady state flux must be reached in the diffusion cell. This steady state regime can be seen in the flat plateau that is reached in the data shown in Figure 3-9 (b). In our tests we used a fixed amount of CEES vapor in each case, which was not always enough to reach this steady state. Therefore, we have calculated a "peak" permeability based on the highest flux value reached during the test. The definition of this peak permeability is shown in Equation 1. Permeability is the product of the mass flux and the

membrane thickness divided by the product of the cross-sectional area and pressure gradient. This value a materials property, and is independent of membrane thickness. The flux through a thinner membrane will be higher than that through a thicker membrane at the same pressure gradient, so the thickness is canceled out in the product of these two terms.

$$P = \frac{q \cdot t}{A \cdot \Delta p} = \frac{cm^3(STP) \cdot cm}{s \cdot cm^2 \cdot cmHg}$$

Equation 3-1: definition of peak permeability. Variables used to are defined as follows: q is the instantaneous flux, t is the membrane thickness, A is the cross-sectional area of membrane, and Δp is the pressure difference across the membrane.

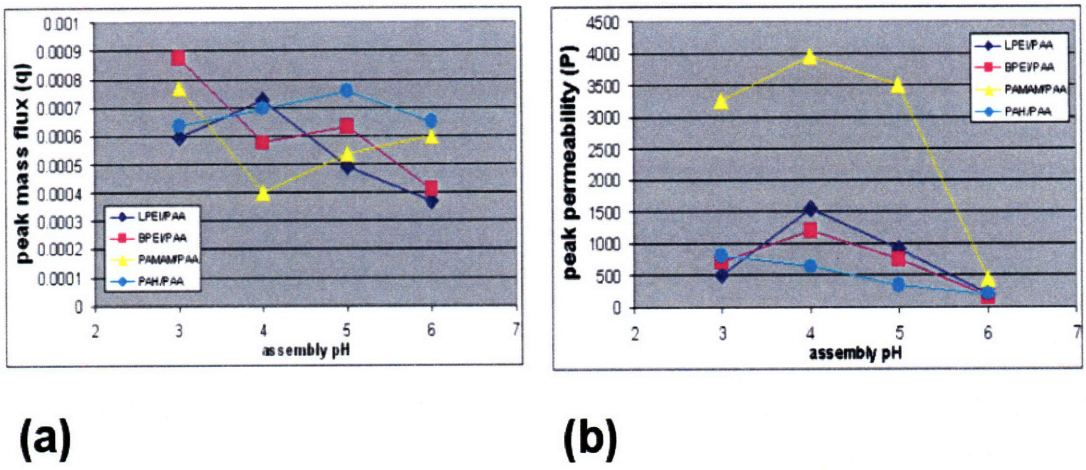

Figure 3-10: (a) peak mass flux values and (b) peak permeability values as defined by eqn. 1.

Figure 3-10 shows both the peak mass flux (Figure 3-10 (a)) and in part (b) the peak permeability values as defined by Equation 1. When comparing permeability values to film thickness (Figure 3-4) the two seem to correlate. PAMAM films have by far the highest permeabilities, while the other systems have values similar to each other. This correlation of thickness and permeability can be explained considering the relationship between film densities and their thickness. All of the membranes tested were 50 layer pairs. The films that deposited as thick layers also have less ionic crosslinks, a lower density, and a higher fraction of air. Therefore the organic vapor diffuses more quickly through these films. In chapter two we saw that PAMAM films have overall the greatest

amount of free carboxylic acid groups, and PAH the lowest amount, and here we see that PAMAM films have the highest permeability and PAH the lowest permeability.

To determine values of diffusivity for our various membranes, we used the time lag method. The total flux through the membrane is calculated, given in Equation 3-2. The quantity $l^2/6D$ is the "time lag" and can be determined directly from the plot of Q vs. time, from which values of D can be found. Figure 3-11 shows the diffusivity values for the LbL films, based on time lag calculations. PAMAM films have diffusivities an order of magnitude higher than the other films (~10-9), which all have similar diffusivity values on the order of 10^{-10}.

$$Q = \frac{DC_0}{\ell}\left(t - \frac{\ell^2}{6D}\right)$$

Equation 3-2: Total flux Q through membrane as a function of time. D is the diffusivity, λ is the membrane thickness, and C_0 is the initial concentration of the permeant on the feed side of the membrane.

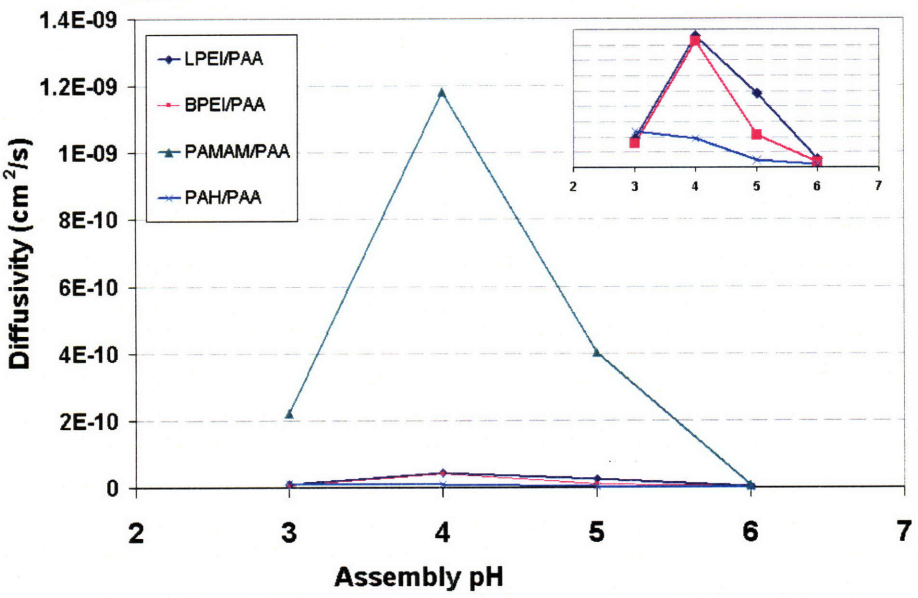

Figure 3-11: Diffusivity values of CEES vapor in the 16 LbL films. Diffusivity is proportional to the square of the membrane thickness, meaning that PAMAM films exhibit diffusivities an order of magnitude higher than the other films, on the order of 10^{-9} cm^2/s. The inset shows a close up of the

values for the BPEI/PAA, LPEI/PAA, and PAH/PAA multilayers, which are on the order of 10^{-10} cm^2/s.

Based on the quotient of the peak permeability and the diffusivity values we calculated an "implied" solubility for the different membranes, shown in Figure 3-12. While these solubility values cannot be considered to be material properties, since our data was not collected at steady state, they are indicative of the relative trends within the different LbL systems. The strong thickness dependence of the diffusivities and therefore permeabilities is not seen in the solubility values. The amount of CEES that can dissolve into a particular LbL film is based solely on interactions between the CEES molecules and the film, regardless of film thickness. We see that PAH/PAA films have the highest solubility values, followed by BPEI/PAA and LPEI/PAA with similar values, and then the PAMAM/PAA films. This trend roughly corresponds to the degree of ionization of carboxylic acid groups in the LbL films, or the basicity of the polycations. CEES is a polar molecule, and the amine groups interact with the dipole of the chlorine atom. The more basic amine groups interact more strongly. Within each polyelectrolyte pair, there is an increase in the solubility with increasing ionization. Polarity plays a role here, and as the ionic crosslink density becomes higher interactions with the CEES are stronger.

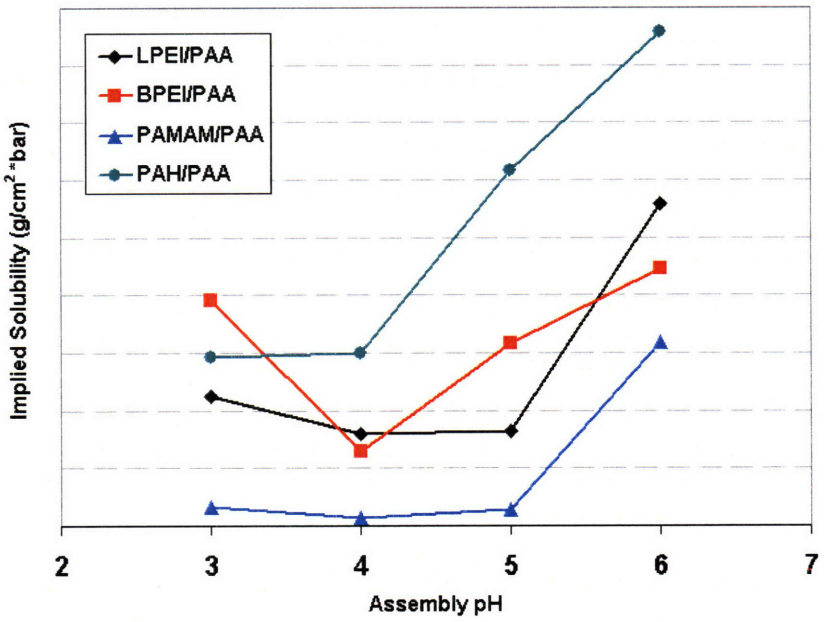

Figure 3-12: Implied solubilities defined as the quotient of peak permeability and diffusivity.

3.5 Conclusions

A method of "misting" LbL films onto substrates was automated. This process produces LbL films that are much thinner than those made by conventional "dipping" and more quickly (approximately a ten fold decrease in time needed). During the first several layer pairs, LbL films growth begins as islands adsorbed to the substrate that eventually are covered over to make a continuous film. This is also seen for misted films, but the "islands" are much smaller, probably due to the decreased amount of time the polyion is exposed to the substrate at each deposition step. Using the automated misting technique, we are able to expand the possible substrates for LbL deposition, including commercially available membranes. This allows us to test the properties of the various polyamine containing LbL films as diffusion barriers.

The misting technique was used to deposit LbL films of 50 layer pairs onto Nucleopore membranes, which were then exposed to CEES vapor in the permeation cell developed for this set of measurements. Although steady state observations were not always made, values for diffusivity were calculated using the time lag method, and "instantaneous" permeability and solubility values were calculated. It was observed that permeability to CEES correlates to density and ionic crosslinking of the membrane. Highly ionized systems that deposit in flat, tightly crosslinked layers are much less permeable to CEES vapor than those systems that deposit in thick, "loopy" layers.

Permeability as defined by the solution-diffusion model is the product of diffusivity and solubility. Using the time lag method we calculated diffusivity values and could therefore fins solubilities of CEES vapor in our systems. Diffusivity trends were similar to overall permeability; PAMAM containing films had diffusion constants higher by an order of magnitude compared to the others. Solubility, however, showed the opposite trend. CEES vapor was the least soluble in PAMAM films and most soluble in PAH/PAA films. Also, within each system CEES became more soluble with increasing pH and carboxylic acid ionization. As CEES is a polar molecule its vapor is most soluble in the membranes with the highest ionic crosslink densities.

Chapter 3 References

1. Cho, J.; Kim, S.; Char, K. *Kor J. Chem. Eng.* **2003**, *20(1)*, 174-179.
2. Schlenoff, J. B.; Dubas, S. T.; Farhat, T. *Langmuir* **2000**, *16*, 9968.
3. Izquierdo, A.; Ono, S. S.; Voegel, J. C.; Schaaf, P.; Decher, G. *Langmuir* **2005**, *21*, 7558.
4. Porcel, C. H.; Izquierdo, A.; Ball, V.; Decher, G.; Voegel, J. C.; Schaaf, P. *Langmuir* **2005**, *21*, 800.
5. Miller, M. D.; Bruening, M. L. *Chem. Mater.* **2005**, *17*, 5375-5381.
6. DeLongchamp, Dean M.; Hammond, Paula T. *Chem. Mater.* **2003**, *15(5)*, 1165-1173.
7. Krogman, K. C.; Zacharia, N. S.; Schroeder, S.; Hammond, P. T. *Langmuir*, **2007**, 23, 3137-3141.
8. Murty, L. V. R.; Chauhan, R. S. J. Appl. Polymer Sci. 1998, 68(12), 2057-2062.
9. Semwal, R. P.; Banerjee, S.; Chauhan, L. R.; Bhattacharya, A. J.; Rao, N. B. S. N. *Appl. Polymer Sci.* **1998**, *60*, 29-35.
10. Dubey, V.; Gupta, A. K.; Maiti, S. N. *J. Polymer Sci. B* **2002**, *40(17)*, 1821-1827.
11. Krasemann, L.; Toutianoush, A.; Tieke, B. *J. Membrane Sci.* **2001**, *181(2)*, 221-228.
12. Meier-Haack, J.; Lenk, W.; Lehmann, D.; Lunkwitz, K. *J. Membrane Sci.***2001**, *184(2)*, 233-243.
13. Rivin, D.; Lindsay, R. S.; Shucly, W. T.; Rodriguez, A.; *J. Membrane Sci.* **2005**, *246*, 39-47.
14. Wijmans, J. G.; Baker, W. R. *J. Membrane Sci* **1995**, *107*, 1-21.

Chapter 4

Metal Nanoparticle Formation in PAMAM Containing Multilayers

4.1 Intro: Nanoparticles in LbL Assemblies

Metal and other inorganic nanoparticles (NPs) exhibit a broad range of unique properties not found in bulk materials due to their size and electronic structure. These include optical, magnetic, and electronic properties that make NPs interesting for applications ranging from sensing to data storage.[1, 2] Not only do size and composition determine nanoparticle properties, but spatial ordering and interaction with surrounding media play a role as well.[3] Incorporation into thin films can provide the basis for tuning these interactions and therefore achieving desired properties. Immobilization in a polymer matrix can also prevent the aggregation of particles that often happens in solution, thereby preserving their properties.

LbL assembly presents itself as an ideal platform for the incorporation of inorganic NPs. LbL allows for both control of the spatial placement of the film components and for tuning of the interaction among those components and with the surrounding environment. Particles that have been synthesized in such a manner that they have ionic surfaces can be directly incorporated.[4, 5] Metal oxides such as titania or silica lend themselves especially well to this process as they already have a native negative charge.[6] Even quantum dots[7] and gold NPs[9] have been incorporated into LbL films via this route. Caruso, *et al* used a silica NP containing multilayer was exposed to HF post assembly in order to dissolve the particles and create a nanoporous structure.[8] In another case, Fery and workers introduced covalent crosslinks into a gold NP containing film in order to improve mechanical stability.[10]

One of the difficulties with directly incorporating NPs into a multilayer is achieving adequate packing density. Strategies to increase packing of gold NPs in a film include infiltrating a multilayer with NPs post assembly, or individually coating gold NPs with polyelectrolytes and then depositing these coating particles on a surface.[11]

Another method for creating a polyelectrolyte-NP composite film is to synthesize the NPs within the LbL films. Two strategies are often used to grow metal NPs inside of LbL films. The first, as shown in figure 4-1 (1) is to assemble the film, then soak it briefly in a metal salt. The metal ions will then complex with free functional groups within the film. The film is then exposed to a reducing agent, such as sodium borohydride or a hydrogen atmosphere, and the metal ions are reduced to

discrete NPs.[12-14] The second method, as shown in figure 4-1 (2) is to first complex a metal salt with a polyelectrolyte, then assemble the film, and similarly expose it to a reducing agent.[15] The complexation between the metal ion and the polyelectrolyte could either be electrostatic (as in the case of carboxylic acid groups and metal ions) or could be a ligand to metal charge transfer interaction (as in the case of amine groups and metal ions). Caruso, *et al* in one case used polyelectrolyte complexed with titania precursor to create gold-titania core shell particles.

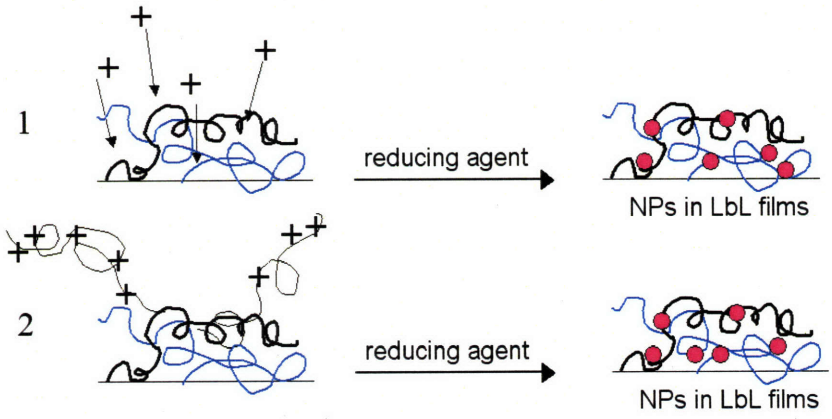

Figure 4-1: Schematics 1 and 2 show commonly used methods to form metal NPs in LbL films. In (1) a pre-formed film is exposed to a metal salt, and metal ions complex with functional groups in the film. The film is then exposed to a reducing agent. In (2) metal ions are complexed with a polyion in solution, the film is formed with this polyelectrolyte-metal ion complex, and then exposed to a reducing agent.

Examples of both of these strategies for metal NP formation can be seen in Figure 4-2. Figure 4-2 (a) shows a cross-sectional TEM image of an LbL film, in which sections have been impregnated with Ag NPs, taken from reference 14. The dark areas of the image are the Ag NPs. The film alternates sections of PAH/PAA multilayer with PAH/sulfonated poly(styrene) (SPS) multilayer. Ag^{+} ions only complex with the carboxylic groups of the PAA chains, and therefore the Ag NPs are selectively placed. Ag NPs have been used in LbL films both for their optical properties and for their antimicrobial properties.[29] In Figure 4-2 (b) Pd^{2+} ions are complexed to LPEI, then the LbL film is assembled (onto alumina microparticles). Pd NPs were selected in this case because of their ability to catalyze a number of organic reactions, including hydrogenation. Bruening, *et al* [15] showed that encapsulating Pd NPs in their LbL film improves the selectivity of hydrogenation of a series of

unsaturated alcohols, even more so than using dendrimer encapsulated NPs in solution. This is likely due to the restriction of active sites on the NPs by the polymer matrix.

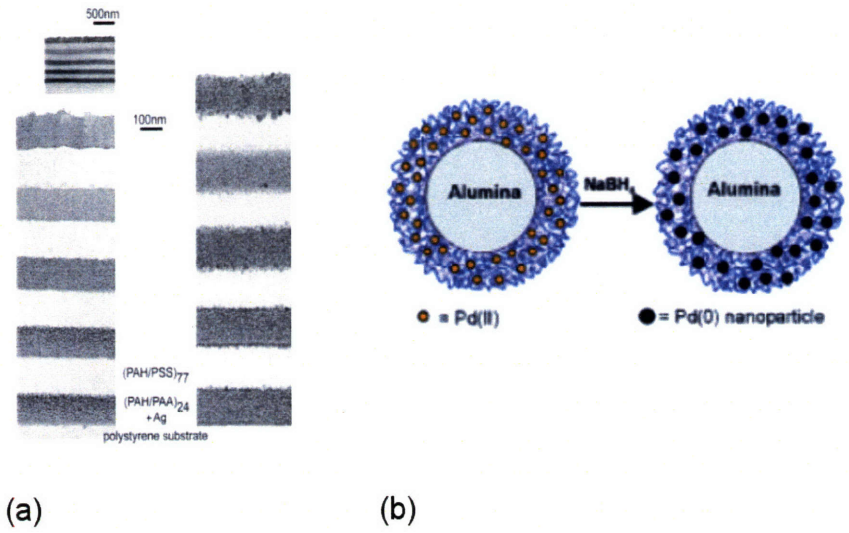

Figure 4-2: Examples of fabrication of metal NPs in LbL films. Figure (a) shows an optical Bragg stack formed by alternating sections of LbL film with Ag NPs and PAH/SPS multilayer.[11] Ag^+ ions are complexed to carboxylic acid groups in a pre-formed multilayer and then reduced into particles. Figure (b) shows microparticles coated with Pd NP containing multilayers. [15] The Pd NPs are formed by first complexing Pd^{2+} ions to LPEI chains, forming the multilayers, and then reducing the ions.

The synthesis of metal NPs within PAMAM dendritic core is a well known procedure, first demonstrated by Crooks.[17-19] Synthesis of nearly any transition metal NP as well as certain semiconducting NPs has been shown. In a solution of dendrimers, positive metal ions will partition to the dendrimer's interior due to interactions with the lone pair of the nitrogen of the tertiary amine groups. There is a ligand to metal charge transfer between the amine group and the metal ion. Spectroscopy has further demonstrated that in the case of Cu^{2+} ions coordinate not only with the tertiary amine groups, but also the nitrogen atoms of the amide linkages as well as water molecules from the surrounding environment.[17] A schematic of the proposed coordination of silver ions in the interior of a PAMAM dendrimer can be seen in Figure 4-3. Depending on the ratio of metal salt to dendrimer, the size of the NPs can be precisely controlled to as small as clusters of less than 150 metallic atoms.[20] Since dendrimers are extremely monodisperse, using them as a template for metal NP synthesize results in highly monodisperse particles.

One of the most promising applications for these dendrimer encapsulated NPs is catalysis. Pd NPs, for example, are highly active as non-selective catalysts for a number of reactions. The smaller the particles, the more active they become, but they also have a greater tendency to aggregate. Separating the particles inside a dendrimer core solves this problem. Also, selectivity can increase with NP monodispersity, another advantage to using a dendritic template. PAMAM encapsulated Pd nanoparticles have been shown to improve to be good catalysts for simple alcohol hydrogenations,[24] Heck reactions,[27] Suzuki coupling reaction,[23] and the Stille reaction.[26] It has also been shown that dendritic encapsulation of NPs will increase selectivity, as larger substrates are sterically hindered from entering the dendrimer's interior.

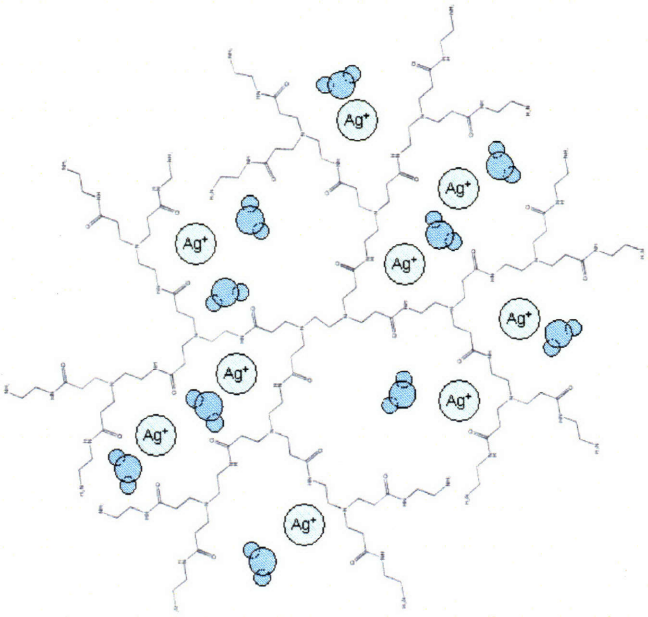

Figure 4-2: Silver ions are coordinated with the interior of the PAMAM dendrimer via interactions with the amide linkages, tertiary amine groups, as well as water molecules.

We propose here yet another route to the formation of metal NP-polyelectrolyte composite thin films. PAMAM dendrimers can be used as a template for the synthesis of NPs within an LbL film. Our strategy is schematically depicted in Figure 4-4. PAMAM dendrimers either with metal ions in their interior or with reduced NPs will be used as the polycationic component of the LbL film. The exterior amine groups of the dendrimer will remain free to form ionic crosslinks. In this way the exact placement of NPs within the LbL structure can be controlled. The choice of PAMAM as a template for NP synthesize makes sense because of the benefits of monodispersity of the resulting NPs, but as seen in previous chapters, PAMAM/PAA films have the greatest number of free carboxylic acid

groups. Therefore, a second type of NP could be synthesized inside the multilayer using these free carboxylic acid groups.

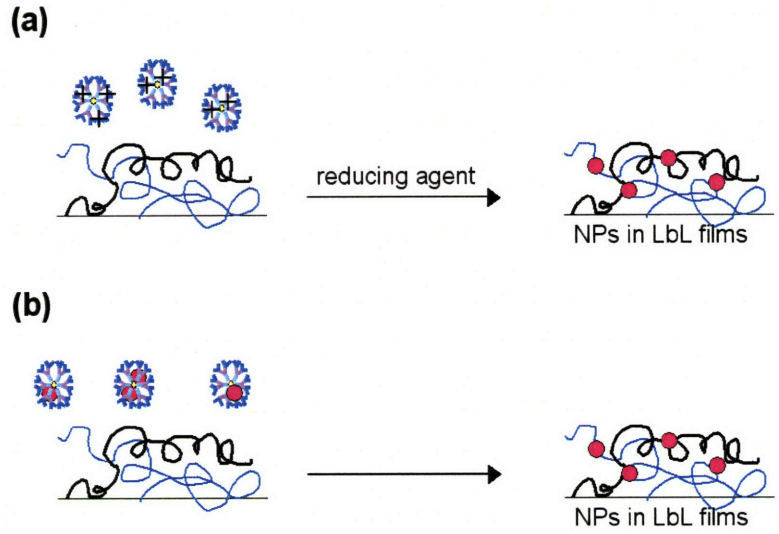

Figure 4-4: Strategies for forming dendrimer-NP multilayer. (a) Forming a PAMAM-metal ion complex, assembling the multilayer, and then exposing to a reducing agent. (b) Forming metal NPs inside PAMAM dendrimers and then assembling the multilayer.

4.2 Experimental Details

Materials**:** Poly(acrylic acid) (PAA, MW = 90,000) was purchased from Polysciences. Poly(amido amine) dendrimer (PAMAM G4, NH_2 surface, 22 wt% in methanol) was purchased from Dendritech. Poly(allylamine hydrochloride) (PAH, MW = 70,000), silver nitrate, sodium borohydride, and palladium(II)acetate were purchased from Sigma Aldrich. Polymer solutions were made using DI water at a concentration of 20 mmol with respect to the repeat unit, and adjusted to the required pH using HCl or NaOH. Si wafers were purchased from Silicon Quest All silicon was cleaned with methanol and Milli-Q water, followed by a five minute oxygen plasma etch (Harrick PCD 32G) to clean and hydroxylate the surface. Glass and quartz slides from VWR were cleaned by sonication for 10 minutes in each of a series of solvents; dichloromethane, acetone, methanol, and then DI water, and then exposed to 5 minutes of oxygen plasma etch.

Synthesis of PAMAM encapsulated metal NPs: in our studies we synthesized dendrimer encapsulated metal nanoparticles of both silver and palladium. For the synthesis of silver nanoparticles we prepared a 10 mM solution of PAMAM G4 and 5 mM of silver nitrate ($AgNO_3$) in DI water. After adding the silver salt we added continuously and with stirring $NaBH_4$ up to a

concentration of 50 mM, this assured the reduction of all the silver ions in solution. After doing this a deep orange solution of nanoparticles was obtained, and the pH adjusted to the desired level using HNO_3 and NaOH. For the case of Palladium nanoparticles the procedure was similar, and the salt used was Palladium (II) acetate ($Pd(AcCOO)_2$). The only difference for this synthesis was that, due to the low solubility of $Pd(AcCOO)_2$ in water, the palladium salt was dissolved in acetone prior to the preparation of the solution. The concentration of acetone after the solution was obtained was less than 5 % v/v.

Synthesis of Copper particles using PAA as a template: A solution 20 mM in PAA and 2 mM in CuCl2 was prepared. Excess NaBH4 was added with stirring to the solution until the concentration of $NaBH_4$ reached 20 mM. At that point all the Copper ions were reduced into nanoparticles, and the resulting solution had a deep green-brownish color. After doing this the pH was adjusted to the desired level using HCl and NaOH.

LbL films were constructed as follows according to the alternate dipping method using an automated Carl Zeiss HMS Series Programmable Slide Stainer.[8] Briefly, pretreated substrates were submerged in a polycationic dipping solution for 10 minutes followed by a cascade rinse cycle consisting of three deionized water rinsing baths (30, 45, and 60 seconds, respectively). Substrates were then submerged in a polyanionic solution for 10 minutes followed by the same cascade rinsing cycle, and the entire process was repeated as desired. Following deposition, films were immediately removed from the final rinsing bath and dried thoroughly under a stream of dry nitrogen gas.

4.3 Results and Discussion

As described above, we created metal NP-polymer composite films using metal ion-PAMAM dendrimer complexes. Although a film with PAMAM-ion complexes can be used to create a metal NP containing film, but we found no advantage to this strategy; in fact it may be preferable not to expose the entire film to a harsh reducing atmosphere. It may be desirable, however, for other applications to incorporate metal ions in an LbL assembly, in which case PAMAM-ion complexes would be ideal. We instead present here results from assembling PAMAM encapsulated metal NPs with PAA. Figure 4-5 shows the UV-vis absorbance of Pd NP containing multilayers of PAMAM/PAA assembled at pH 5. These films grow linearly with number of bilayers, and the plasmon resonance peak for Pd also grows linearly. This indicates that the Pd NPs are incorporated at a similar rate as the PAMAM; that is, they are not lost during film assembly. We have then created a

composite in which we precisely know the location of the metal nanoparticles. A film could be assembled in which only one of the PAMAM deposition steps included the encapsulated NPs, giving a film with precisely one line of NPs deposited at any part of the film.

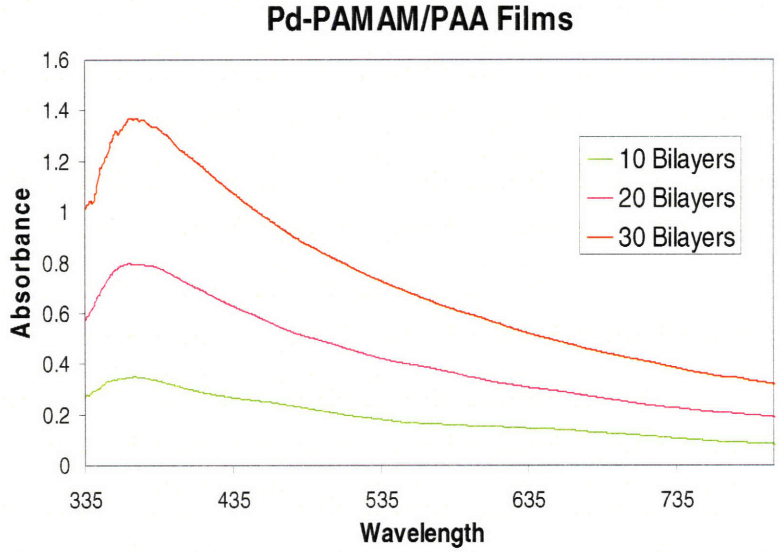

Figure 4-5: UV-vis plot showing the absorbance of Pd NP containing films as a function of number of bilayers. There is a linear increase with the number of bilayers of the plasmon resonance peak, indicating that the metal NPs do remain within the dendrimers throughout film formation.

In a second case we incorporate two different types of nanoparticles into one film. Figure 4-6 shows the UV-vis of a film with PAMAM encapsulated Pd nanoparticles and Cu nanoparticles synthesized by complexation with the carboxylic acid groups of PAA chains. The two separate surface plasmon peaks indicate the presence of two types of nanoparticles. By reducing the nanoparticles prior to assembly, we are able to add multiple NPs in a fixed ratio and in a fixed location (i.e. either coordinated to PAA chains or to PAMAM molecules).

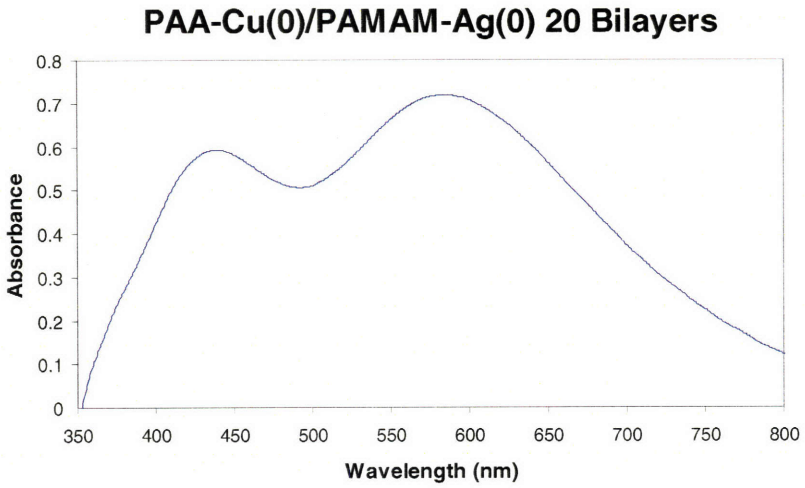

Figure 4-6: UV-vis spectrum showing plasma resonance for two different metal NPs within the same film.

Palladium NPs have many catalytic applications, and we have demonstrated the hydrogenation of allyl alcohol using our Pd NP-polyelectrolyte composite films. For the following reactions we prepared a Pd based catalyst by depositing 10 bilayers of PAMAM with Pd nanoparticles and PAA over a porous metallic substrate. All the solutions were prepared at pH 3. The hydrogenation reactions were carried out using a Hydrogen saturated atmosphere, at atmospheric pressure and ambient temperature. The conversions were estimated using NMR spectrometry. We also observe in certain occasions the formation of the isomerization byproduct, propanal. We did not account for the formation of this byproduct in our estimation of conversion, since it varied for run to run.

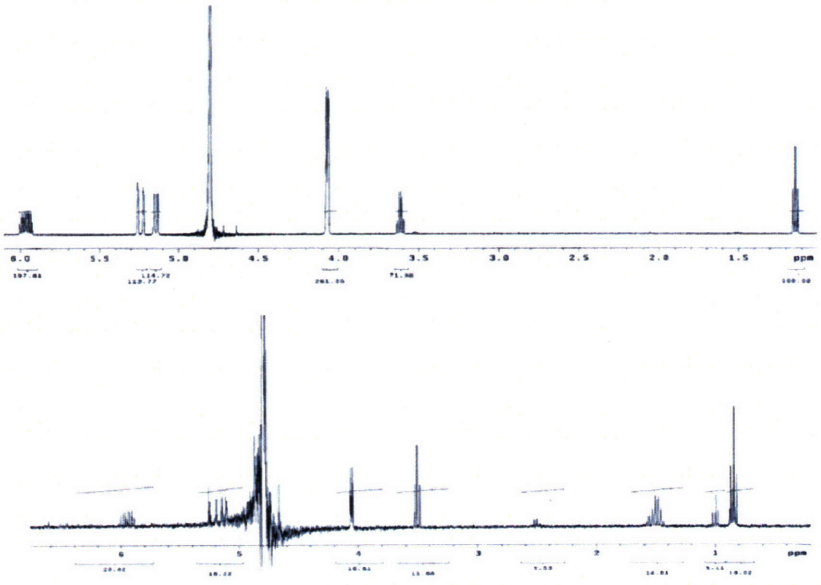

Figure 4-7: NMR of allyl alcohol before (above) and after (below) reaction confirms that the hydrogentation did take place.

The reaction was carried out using 4 cm^2 of catalyst. The reaction solution consisted of 30 mL of 10 mM allyl alcohol in D_2O. The film was created from solutions at pH 3. Figure 4-8 shows the conversion of the reaction as a function of time, over a 4 hour period. The conversion increased linearly with time as observed in Figure 4-8.

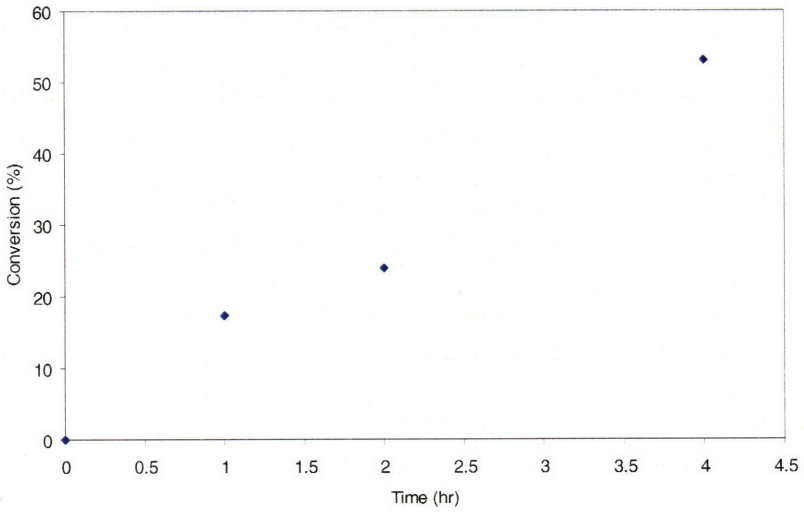

Figure 4-8: Percent conversion of the hydrogenation of allyl alcohol using Pd NP-polyelectrolyte composite film as catalyst.

Catalyst Recycle

The catalyst was also recycled to test its catalytic activity. Initially a hydrogenation reaction of 20 mL of 10 mM Allyl Alcohol was carried out for 3.5 hours. Immediately after this reaction was completed another 3.5 hour reaction was performed. Then the catalyst was allowed to react with allyl alcohol in the presence of hydrogen gas for 4 days, and at the end of this period a fresh 10 mM solution of allyl alcohol was allowed to react for 3.5 hours with this catalyst. After analyzing using NMR techniques, we found that the activity of the catalyst increased with use. Table 4-1 summarizes the results. The more times the film is used, the greated the efficiency achieved. We attritube this to swelling of the film and increased access to reaction sites on the NPs.

Time of use	Conversion (%)
0	15
3.5 hour	23
4 days	30

Table 4-1: Catalyst efficiency increases with number of times used, due to film swelling and increased access to NP reaction sites.

Two reactions were carried out simultaneously using 15 mL of a 10 mM solution of allyl alcohol and 6.6 and 2.2 cm^2 of catalyst respectively, for a period of 5 hours. The conversions for both cases were 100% and 56.30 respectively, telling us that a relatively small amount of film is necessary to complete the reaction.

4.4 Conclusions

A number of groups have successfully demonstrated incorporation of metal NPs into LbL assemblies, for applications ranging from a Bragg stack[1] to sensors[9] to antimicrobial coatings.[10] Methods of incorporating metal NPs include adsorbing hydrophobic nanoparticles or surface modified, charged nanoparticles, but more commonly NPs are synthesized *in situ*. Examples include the two following strategies; 1) soaking a film containing PAA in a metal salt, the salt ions will displace H+ ions and complex with –COOH groups. The film is then exposed to a reducing agent, and 2) coordinating metal ions with an amine functionalized polymer such as LPEI, then assembling the multilayer, and then exposing it to a reducing agent.

PAMAM dendrimers are well known for their use as templates for nanoparticles synthesis. Metal ions coordinate with the inner amine groups and amide linkages and then can be reduced; good control over solution stoichiometry can lead to extremely monodisperse NPs over a range of sizes (depending on how many metal ions are sequestered into each dendrimer). Given our previous results in Chapter 2, we believe that many of the interior amine groups of the PAMAM do not participate in forming ionic crosslinks within PAMAM/PAA assemblies, simply due to their close proximity to one another. Therefore, we can use those inner amine groups either before film assembly or after film assembly with no change in LbL structural properties (ie film thickness, degree of crosslinking).

By first synthesizing metal NPs within PAMAM dendrimers and then assembling LbL films, we have a greater control of the placement of those metal NPs within the film. It is also then possible to synthesize a second NP using the other polyelectrolyte. One example that we demonstrated was the synthesis of Ag NPs within PAMAM core, assembling a film with PAA, exposing this film to copper salt, then a reducing agent to form Cu NPs outside of the dendrimers. We also show that the intensity of the surface plasmon grows linearly with number of bilayers when assembling LbL films using dendrimer encapsulated NPs, giving a good indication that the NPs stay within the dendrimer interiors.

Pd nanoparticles are non-selective catalysts for hydrogenation reactions. Encapsulation both within dendrimers and also within LbL assemblies has been shown to improve catalyst selectivity. We synthesized Pd NPs in G4 PAMAM dendrimers, then assembled LbL films of PAMAM-Pd(0)/PAA. These films were placed in aqueous solution of allyl alcohol. NMR shows that the Pd NPs did catalyze the hydrogenation of allyl alcohol.

Chapter 4 References

1. Fendler, J. H. *Adv. Mater.* **2002**, *114*, 1006.
2. Jin, R.; Cao, Y. C.; Hao, E.; Metraux, G. S.; Schatz, G. C.; Mirkin, C. A. *Nature* **2003**, *425*, 487.
3. Peng, S.; Manna, U.; Yang, W.; Wickham, J.; Scher, E.; Kadavanich, A.; Alivisatos, A. P. *Nature* **2000**, *404*, 59.
4. Serizawa, T.; Takeshita, H.; Ahashi, M. *Langmuir* **1998**, *14*, 4088-4094.
5. DeLongchamp, D.; Hammond, P. T. *Adv. Func. Mater.* **2004**, *14*, 224-232.
6. Lvov, Y.; Ariga, K.; Onda, M.; Ichinose, I.; Kunitake, T. *Langmuir* **1997**, *13(23)*, 6195-6203.
7. Hao, E.; Zhang, H.; Yang, B.; Ren, H.; Shen, J. *J. Colloid Surface Sci.* **2001**, 238(2), 285-290.
8. Li, Q.; Quinn, J. F.; Wang, Y.; Caruso, F. *Chem. Mater.* **2006**, *18*, 5480-5485.
9. Schmitt, J.; Decher, G.; Dressick, W. J.; Brandow, S. L.; Geer, R. E.; Shashidhar, S.; Calvert, J. M. *Adv. Mater.* **1997**, *9(1)*, 61-65.
10. Lu, C.; Dönch, I.; Nolte, M.; Fery, A. *Chem. Mater.* **2006**, *18(26)*, 6204-6210.
11. Caruso, F.; Spasova, M.; Salgueiriño-Maceira, V.; Liz-Marzán, L. M. Adv. Mater. 2001, 13(14), 1090-1094.
12. Wang T.C., Rubner M.F., Cohen R.E. *Chem. Mater.* **2003** *15(1)*, 299-304
13. Joly, S.; Kane, R.; Radzilowski, L.; Wang, T.; Cohen, R. E.; Thomas, E. L.; Rubner, M. F.*Langmuir*, **2000**, *16*, 1354-1359.
14. Wang T.C.; Cohen R.E.; Rubner M.F. *Adv. Mater.* **2002** *14(21)*, 1534+
15. Kidambi, S.; Dai, J.; Li, J.; Bruening, M. L. *J. Am. Chem. Soc.* **2004**, *126*, 2658-2659.
16. Mayya, K. S.; Gittins, D. I.; Caruso, F. *Chem. Mater.* **2001**, *13*, 3833-3836.
17. Zhao, M.; Sun, L.; Crooks, R. M. *J. Am. Chem. Soc.* **1998**, *120*, 4877-4878.
18. Lemon, B. I.; Crooks, R. M. *J. Am. Chem. Soc.* **2000**, *122*, 12886-12887.
19. Zhao, M.; Crooks, R. M. *Chem. Mater.* **1999**, *11(11)*, 3379-3385.
20. Knecht, M. R.; Garcia-Martinez, J. C.; Crooks, R. M. *Chem. Mater.* **2006**, *18(21)*, 5039-5044.
21. Scott R.W.J.; Wilson OM, Crooks RM. *J. Phys. Chem. B.* **2005**, *109*, 692-704
22. Crooks, R. M.; Zhao, M.; Sun, L.; Chechik, V.; Yeung, L. K. *Acc. Chem. Res.***2001**, *34*, 181-190.
23. Li, Y.; Boone, E.; El-Sayed, M. A. *J Phys Chem B* **2001**, *105*, 8938-8943.
24. Niu, Y.; Yeung, L. K.; Crooks, R. M. *J. Am. Chem. Soc.* **2001**, *123*, 6840-6846.
25. Rahim, E. H.; Kamounah, F. S.; Frederiksen, J.; Christensen, J. B. *Nano Lett.* **2001**, *1(9)*, 499-501.
26. Garcia-Marquez, J. C.; Letzutekong, R.; Crooks, R. M. *J. Am. Chem. Soc.* **2005**, *127*, 5097-5103.
27. Yeung, L. K.; Crooks, R. M. *Nano Lett.* **2001**, *1(1)*, 14-17.
28. Yu, A. M.; Liang, Z. J.; Cho, J. H; Caruso, F. *Nano Letters* **2003**, *3(9)*, 1203-1207.
29. Li, Z.; Lee, D.; Sheng, X. X.; Cohen, R. E.; Rubner, M. F. *Langmuir* **2006**, *22(24)*, 9820-9823.

Chapter 5
Controlling LPEI/PAA Interdiffusion

5.1 Introduction

Advanced applications require the bottom-up assembly of complex heterostructured LbL assemblies, where a film is composed of layers of different polyelectrolyte pairs that can form various functional components of a device. Recently, we have found that the bottom-up assembly of complex heterostructures often yields unexpected results, because individually assembled polyelectrolyte pairs can behave differently during heterostructure assembly than when constructed as isolated structures. Such disrupted heterostructure assemblies are caused by complex interactions between polyelectrolyte pairs, which are governed by the ionization density and distribution along the polyelectrolyte backbone.[3, 4, 5, 15, 26, 29] Studies of the layer-by-layer process have recently revealed that in such cases, the system can no longer be treated as a kinetically frozen matrix with a fixed charged surface; instead, the polyelectrolyte complex can be considered to be a dynamic network of chains in which ionic bonds can be formed or displaced throughout the thickness of the film. Gaining a greater understanding of and control over the inner structure of these assemblies is very important if one is to ultimately control and construct novel heterostructures from these systems. [8]

Typical LbL films exhibit linear growth; after the first few layer pairs, each subsequent layer pair thickness reaches a steady state value. Recently, systems growing in a superlinear fashion have been observed.[10-13] In electrostatically bound films, exponential growth has been observed in films that are assembled from partially solvated polymers,[10] systems with strong hydrogen bonding,[11] or in systems of biological polymers.[12] It has been suggested that in certain cases nonlinear growth results from the increasing fractal roughness of the film surface, creating more film surface area with each adsorption step.[30, 32] In other cases, direct evidence shows that interdiffusion of polyions within the LbL film cause superlinear growth.[15] In these cases, the depositing polymer not only adsorbs onto the film's surface, but also enters the bulk of the film, creating a "reservoir" of excess unpaired polyelectrolyte. At the next step of film assembly, the contents of this reservoir are attracted to the now oppositely charged surface, polyelectrolyte is drawn out from the bulk film, and complexes with oppositely charged polyelectrolyte at the surface. As film thickness increases, the size of this reservoir increases, leading to superlinear growth. It is also possible for free polyions to exchange with

polymer chains that are already a part of the bulk film.[15, 16] This exchange can be either a polyion reversibly exchanging with itself, or irreversibly replacing another polymer, which forms a complex that is less energetically favored.[15, 33] Diffusion within an LbL assembly, while typically promoting disorder within the bulk film, can in certain instances be used to segregate and order species at the surface, as shown recently in the assembly and entropic ordering of viruses within an LbL assembled thin film.[16]

When interdiffusion occurs during assembly, one might expect heterostructure assembly to be disrupted when including a superlinearly growing LbL layer. Our system is composed of one polyelectrolyte pair – $(PXV/PAA)_n$ – incorporating a strong polycation with a fixed ionization density and charge distribution,[10] and one pair – $(LPEI/PAA)_n$ – incorporating a weak polycation with a labile ionization density and charge distribution that is dependent upon the local environment.[26, 34] Although these two pairs differ only by the type of polycation, they exhibit very different assembly behavior in isolation, and when a multilayer of $(LPEI/PAA)_n$ is assembled atop $(PXV/PAA)_n$, the assembly of the heterostructure is disrupted. Here we investigate the the nature of polyelectrolyte exchange that happens in these systems, demonstrating the true dynamic nature of the interdiffusion process, and its dependence on factors such as molecular weight. The driving force for polyion exchange in these systems is shown to be due to differences in the acid-base interactions between LPEI and PXV with PAA, and a resulting difference in the degree of ionization of the polyacid. Inserting a blocking layer between the two multilayers prevented any disruption of the heterostructure, and allowed straightforward heterostructure assembly, proving that disruption of this system results from LPEI interdiffusion. The applicability of this approach was further demonstrated in the construction of an LbL electrochromic device consisting of a coloring electrode and electrolyte. The use of blocking layers to manipulate growth modes in LbL assembled heterostructures[18, 19] provides the precise control necessary to purposefully vary composition for true bottom-up assembly of complex devices. The added ability to isolate, or compartmentalize, portions of the LbL film may also lead to new applications.

5.2 Experimental details

Materials. Poly(hexylviologen) was synthesized by refluxing 4,4′-bipyridine and 1,6-dibromohexane (Sigma Aldrich)[†] overnight in acetonitrile that had been dried over molecular sieves. The precipitate was then washed with acetonitrile and dried. Static Light Scattering (SLS) gave a weight average molecular weight of 150,000 g/mol, and end group analysis via NMR gave a weight of ~292,000 g/mol (see Appendix A for details about MW determination). Linear(polyethylene imine), ≈25 kDa and ≈250 kDa, as well as poly(acrylic acid)of ≈90 kDa in 25 % (by mass) aqueous solution, were purchased from Polysciences. Poly(allylamine hydrochloride) (PAH) was purchased from Sigma Aldrich. All chemicals were used as received. The chemical structures of these polyelectrolytes are shown in Figure 5-1. Polyelectrolyte primary chemical structures: the primary and secondary amines as well as carboxylic acid are shown in their protonated (low pH) form

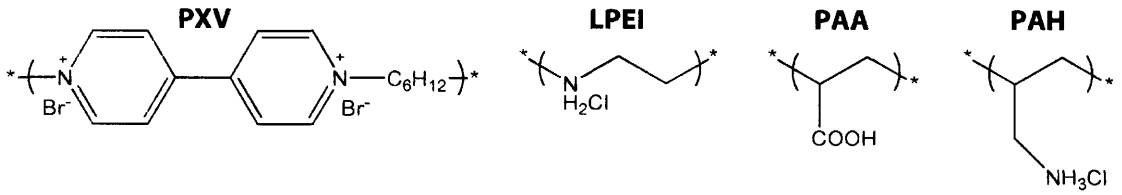

Figure 5-1. Polyelectrolyte primary chemical structures; the primary and secondary amines as well as carboxylic acid are shown in their protonated (low pH) form

Sample preparation and characterization: Film assembly was automated with a Carl Zeiss HMS DS-50 slide stainer. The substrates were exposed first to polycation solution for 10 min followed by three rinses in Milli-Q water, then a 10 min exposure to the polyanion solution followed again by rinsing. All polyelectrolyte solutions were 20 mM with respect to the polymer repeat unit. The pH of the polyelectrolyte solutions was adjusted with dilute aqueous solutions of HCl or NaOH, salt was not added to any polyelectrolyte solution. The pH of the rinse baths was adjusted to match that of the polyelectrolyte solutions; potassium phthalate buffer was used to adjust to pH 4 and HCl was used to adjust to pH 5.

[†] Certain equipment, instruments or materials are identified in this paper in order to adequately specify the experimental details. Such identification does not imply recommendation by the National Institute of Standards and Technology nor does it imply the materials are necessarily the best available for the purpose.

Glass substrates were cleaned in a Bransonic ultrasonic cleaner for 15 min each in dichloromethane, acetone, methanol, and deionized water. The water cleaning was repeated twice. Immediately prior to film assembly the substrates were exposed to oxygen plasma for five minutes. Silicon substrates were ultrasonically cleaned first in a solution of 70 % H_2SO_4 and 30 % H_2O_2 and then a mixture of 50 % NH_3OH 50 % H_2O_2.

Thickness measurements were performed by ellipsometry and profilometry. A Gaertner single wavelength ellipsometer was used for films less than 100 nm thick. Ellipsometry was performed at a single incident angle of 70°, and the refractive index was fixed at 1.45. A Tencor P10 profilometer was used to measure thicker films, films which were not optically clear, and for all surface roughness measurements. A tip force of 3 mg was used to avoid penetrating the film. In all cases, films were dried in a nitrogen stream prior to measurement.

FTIR measurements were performed using a Nicolet Magna 860 Fourier Transform Infra-Red Spectrometer with a DTGS detector. Films were assembled on silicon substrates, or assembled as free standing films on poly(propylene) substrates as described elsewhere,[37] and examined in transmission mode. To probe the exchange process, 25 layer pair films of (PXV/PAA) were soaked in 20 mM LPEI solution of different molecular weights, dried with nitrogen and scanned by FTIR for different immersion times. (PXV/PAA) films were kept hydrated in DI water at pH 4 or 5 (matching assembly conditions) from the time assembled until the exchange experiment was performed.

The extent of ionization was calculated from the ratio of the peak area at 1560 cm^{-1} to the sum of the peak areas at 1560 cm^{-1} and 1710 cm^{-1}. We assume that the coefficients of extinction are the same for the protonated carboxyl at 1710 cm^{-1} and the deprotonated carboxyl at 1560 cm^{-1}. In LPEI/PAA films, peaks at 1610 cm^{-1} (corresponding to $-NH^{2+}$) and 1650 cm^{-1} (corresponding to N-H deformation vibrations) overlap with the peak at 1560 cm^{-1} for the ionized carboxyl groups. To separate these peaks, Origin was used to fit Gaussian distributions to each peak.

Electrochemical potential control and current sensing were performed using an EG&G 263A potentiostat/galvanostat. Electrolyte was 0.1 M KCl, counter electrode was 2 cm^2 of platinum foil, and reference electrode was K-SCE. The three electrode cell was constructed in a similar fashion to one previously described[10]

5.3 Results and Discussion

5.3.1 Film Assembly

The design of our model heterostructure first required a study of the assembly of the two pairs of polyelectrolytes in isolation. PXV/PAA and LPEI/PAA films were assembled over a range of pH conditions atop the clean native oxide surfaces of silicon wafers to determine the assembly conditions for maximum film thickness. The pH of assembly controls the ionization density of the PAA and LPEI in solution, and therefore it should strongly influence the thickness, crosslink density, and morphology of the films that result.

Previous studies of LPEI/PAA films indicate a maximum thickness when assembled at pH 4.0 to 4.5[24] This pH coincides with the pK_a of LPEI in solution, which is 4.0 to 5.0.[38, 39, 40] The pK_a of PAA in solution to ranges from about 5.5 to 6.5.[41, 42, 43] In our previous work, we proposed that the thickest films were observed in this pH regime because both polymers were only partially ionized, allowing for coiled, or loopy deposition of both polyelectrolytes. The layer-by-layer deposition of weak polyelectrolytes or hydrogen bonding systems in this weakly ionized pH regime often creates films with an individual layer pair thickness of 100 nm or greater, which is much thicker than LbL films formed from strong polyelectrolytes,[24, 28] and indeed thicker than the radius of gyration of the polyelectrolytes. This unusual behavior may result because weak polyelectrolytes can redistribute their ionization density to adopt lower energy configurations. Additional causes may include hydrogen bonding and acid base interactions, which do not occur in strong polyelectrolytes.[26, 44]

We observed maximum film thickness to occur between pH 4 and 5, which is consistent with our previous work.[24] LPEI/PAA films exhibit average thicknesses of (70 to 90) nm per layer pair, with an rms roughness of (1 to 2) nm. Between pH 4 and pH 5 (and especially towards the lower end of this pH range) both polyelectrolytes are partially ionized. At pH lower than 2.5, when both LPEI and PAA are fully protonated, the per-layer pair thickness decreases and film formation is negligible. Film formation is also limited at pH values higher than 6, where PAA is fully ionized and therefore adsorbs in thin, flat layers.

The increase of LPEI/PAA film thickness with layer pair number as shown in Figure 2 shows an initial regime of exponential like growth, which lasts until around 15 layer pairs, after which growth becomes linear. While the phenomenon of early superlinear growth is universally reported for LbL assembled films, the superlinear regime is usually confined to the first 3-5 layer pairs.[23]

Films of $(PXV/PAA)_n$ were also assembled atop native silicon oxide over a similar pH range. Although PXV is not expected to change its ionization density with pH, the PXV solutions were adjusted to match the pH of the PAA solutions so that the polyanion would not change its ioni zation density during film assembly. The rms roughness of the $(PXV/PAA)_n$ films in the pH 4 and 5 cases is similar, averaging 8.1 nm and 12.1 nm, respectively. Growth is linear, with average per layer pair thicknesses of 55 nm for pH 4 and 60 for pH 5.

After the growth of the individual multilayers in isolation was studied, the model heterostructure was designed and assembled. Our original design consisted of a base electrochromic multilayer of $(PXV/PAA)_{20}$, followed by an ion conductive $(LPEI/PAA)_n$ multilayer, which was assembled at both pH 4 and pH 5. For simplicity, the $(PXV/PAA)_{20}$ multilayer was always assembled under the same pH conditions as the $(LPEI/PAA)_n$ multilayer. Figure 3 shows growth curves of the $(LPEI/PAA)_n$ multilayer assembled atop the base $(PXV/PAA)_{20}$ multilayer. The growth mode of the $(LPEI/PAA)_n$ multilayer atop the $(PXV/PAA)_{20}$ multilayer is similar to that of $(LPEI/PAA)_n$ in isolation atop the silicon oxide surface, in that it grows linearly over a large number of layer pairs. However, the pH 4 system grows to ≈90 % of the thickness that it does on bare silicon oxide, while the pH 5 system grew to only ≈27 % of the thickness on silicon oxide. The fact that the $(PXV/PAA)_{20}$ multilayers assembled at both pH 4 and pH 5 have similar surface roughness indicates that a changing substrate surface area did not cause the change in $(LPEI/PAA)_n$ growth.

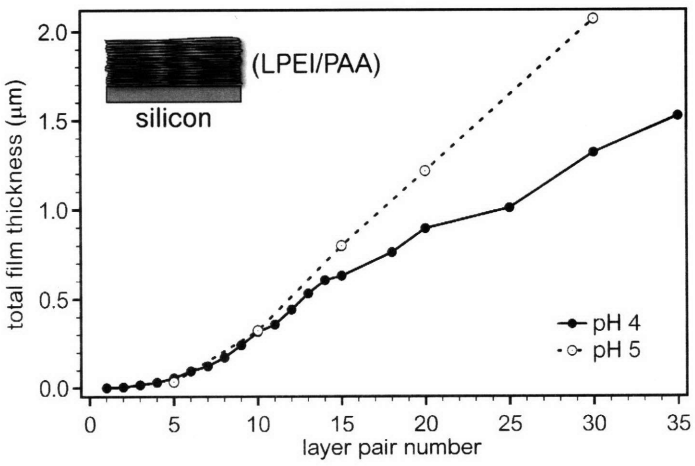

Figure 5-2. Growth curves for LPEI/PAA assembled at pH 4 and 5. A non-linear growth regime is observed for the first 15 layer pairs, and then a linear, steady state growth regime is reached. Standard uncertainty of film thickness measurement is ±10 %.

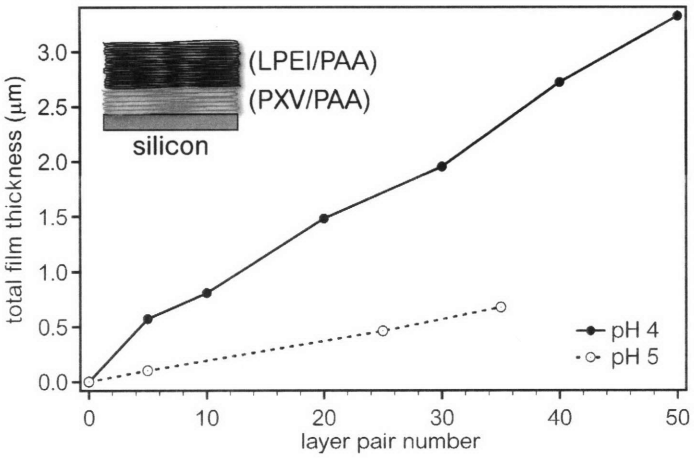

Figure 5-3. Growth curves for LPEI/PAA grown over PXV/PAA at pH 4 and pH 5, showing linear trends for both cases but with greater variance for the pH 4 case.. Standard uncertainty of film thickness measurement is ±10 %.

Despite the similarity in growth mode and thickness, the model heterostructure assembled at pH 4 (shown in Figure 4) undergoes an extreme change in film morphology. The films become optically opaque after only a few layers of LPEI/PAA are assembled, indicating a roughness increase to several hundred nm or greater. Figure 4(a) shows that this change in opacity is accompanied by pitting on the heterostructure film surface. In contrast, when the $(LPEI/PAA)_n$ multilayer is assembled atop $(PXV/PAA)_n$ at pH 5, there is slightly increased opacity in the film, but no significant change in structure, as shown in Figure 4(b).

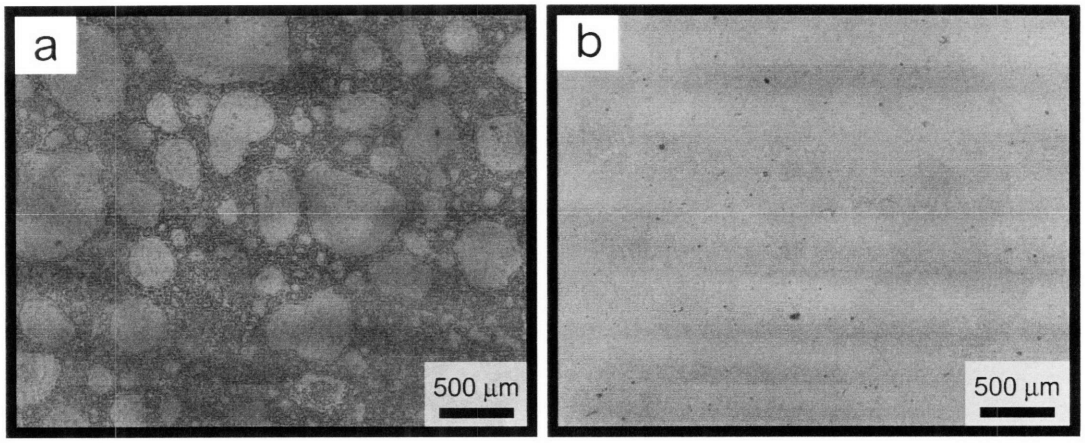

Figure 5-4. Surface of PXV/PAA + LPEI/PAA LbL film assembled at (a) pH 4, showing an uneven, roughened film surface and (b) pH 5, showing a smooth film.

5.3.2 FTIR Analysis

To probe the differences between $(LPEI/PAA)_n$ interactions and $(PXV/PAA)_n$ interactions, FTIR spectroscopy was used to measure the local chemical environment within the two systems assembled in isolation. Further FTIR spectroscopy experiments were used to observe the displacement of PXV by LPEI within the model heterostructure.

The degree of ionization along the backbone of a weak polyelectrolyte is known to vary from solution when within an LbL assembled film;[26] it depends strongly on the local environment of the polymer chain. Ionization distribution and ionization density along the polymer backbone are important factors in the stable formation of LbL films,[28] and weak polyelectrolytes may exhibit ionization redistribution to stabilize the resulting LbL film.[35, 37] Several reports indicate that the carboxylic acid groups of PAA are more readily ionized in the presence of weak polycations.[26, 27]

Figure 5 shows FTIR absorbance spectra for PAA cast from aqueous solution, PXV/PAA multilayers, and LPEI/PAA multilayers, assembled both at pH 4 and pH 5. Peaks at 1710 cm^{-1} correspond to –COOH asymmetric stretching, and those at about 1560 cm^{-1} and 1400 cm^{-1} correspond to the $-COO^-$ asymmetric and symmetric stretches, respectively. The multilayer films exhibit more ionized (or bound) carboxylic acid groups than the cast PAA films exhibit.

The PXV/PAA and LPEI/PAA multilayers assembled at pH 4 exhibit a clear difference in the extent of PAA ionization. For PXV/PAA, the extent of ionization is 19.5 %, whereas for LPEI/PAA

the extent is 53 %. For films assembled at pH 5, there is a smaller difference, with 38.5 % PAA ionization in PXV/PAA, and 54 % in LPEI/PAA. For details as to how the degree of ionization within the films was calculated, please see the Supporting Information. When assembled at pH 5, both systems have a relatively similar proportion of ionic crosslinks. At pH 4, LPEI/PAA is a more ionically crosslinked complex.

This result suggests a mechanism for the destabilization of the PXV/PAA multilayer within the model heterostructure. The formation of ionic crosslinks is energetically favored, and LPEI promotes more ionic crosslinks. LPEI appears to "titrate" PAA so that it becomes more ionized and capable of forming additional electrostatic crosslinks. Therefore, the spatial displacement of PXV by LPEI within the first multilayer is energetically favored. The wholesale rearrangement of film structure that accompanies this displacement may be responsible for the dramatic roughening of the film surface and the formation of pits. At pH 5, PAA ionization is more similar for the $(LPEI/PAA)_n$ and $(PXV/PAA)_n$ systems, and the driving force for PXV displacement is smaller, leading to slower film destabilization.

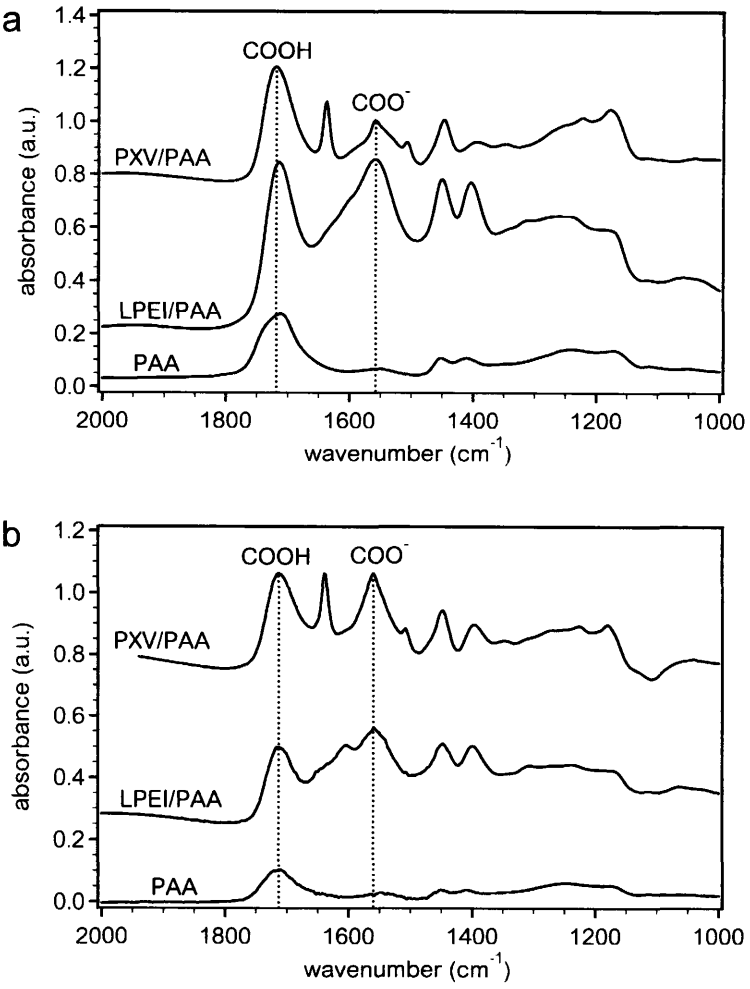

Figure 5-5. FTIR spectrum of cast PAA films, LPEI/PAA multilayers, and PXV/PAA multilayers assembled at (a) pH 4 and (b) pH 5. In all four films PAA becomes more ionized in respose to its environment, more so when complexed with LPEI than PXV. The difference in PAA ionization for the two systems is much greater at pH 4 than at pH 5. Spectra are vertically offset for clarity.

The displacement mechanism for model heterostructure destabilization can be confirmed by exposing the base $(PXV/PAA)_n$ multilayer to LPEI solution and monitoring the film composition over time. Similar experiments have been used to probe the relative strength of the interactions between polyelectrolytes within an LbL assembly.[32] Figure 6 shows the compositional progression of $(PXV/PAA)_{25}$ films immersed in various solutions of LPEI. Over time several changes can be observed in the FTIR spectra of the immersed films. A peak at 1640 cm^{-1}, which corresponds to C=C stretching, decreases, whereas a secondary amine peak ($-NH^{2+}$) at 1610 cm^{-1} becomes present and

grows as the extent of PAA ionization increases. Also, a peak at 1400 cm^{-1}, which corresponds to the C-H deformation vibrations of the backbone of LPEI (corresponds to stretching of the C-H bonds of carbon singly bonded to nitrogen), grows as the exchange takes place. This change in composition clearly illustrates the interdiffusion of LPEI into the PXV/PAA bulk, the displacement of PXV with LPEI, and the corresponding increase in electrostatic crosslinking involving PAA. For 25 kDa LPEI solution at pH 4, the C=C peak completely disappeared after 12 hr, and the percentage of ionized carboxyl groups increased from 18% to 60%. For immersion in 250 kDa LPEI solution, the same replacement occurs but at a slower rate. After 2 days in the 250 kDa LPEI solution, C=C remains, and the ratio of ionized to neutral carboxyl groups changed from 19% to 44%, indicating incomplete exchange. Immersion in pH 5 25 kDa LPEI solution creates a similar trend; disappearance of the C=C peak occurs, as well as an increased ionization of carboxyl groups, but at a slower rate than immersion in pH 4 solution. These results confirm that LPEI is the diffusing species within the multilayer (if it was PAA, the molecular weight of the LPEI should not change the time for the process to occur), and that the driving force for this exchange process is stronger at pH 4 than at pH 5.

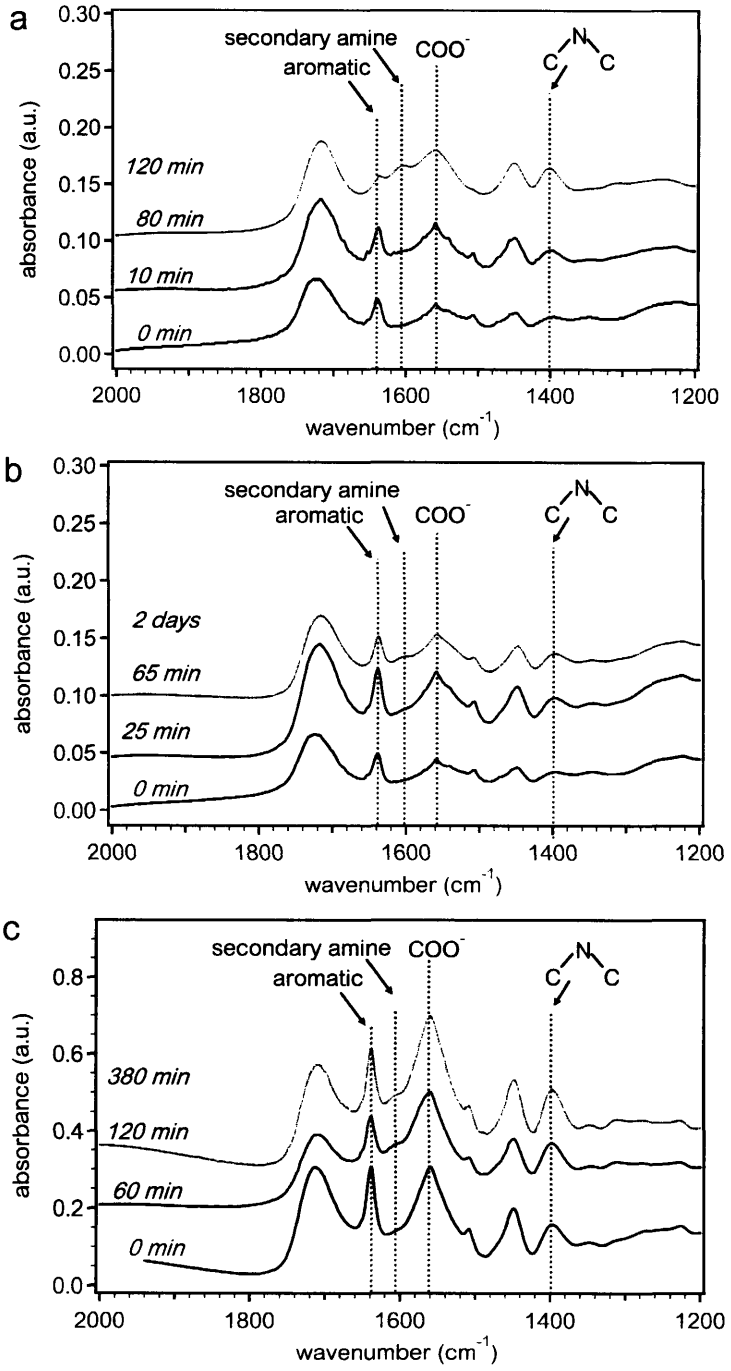

Figure 5-6. FTIR spectrum showing progression of LPEI exchanging with PXV at (a) 25 kDa LPEI at pH 4,, (b) 250 kDa LPEI at pH 4 and (c) 25 kDa LPEI at pH 5. Exchange occurs in all three cases, most quickly at pH 4 for the 25 kDa LPEI, showing both that the process is diffusion limited and that the driving force for exchange is less at pH 5. Spectra are vertically offset for clarity.

From this set of experiments we propose that the driving force of the displacement is the preferential complexation of PAA with LPEI over PXV. This must be more than simply the formation of new ionic crosslinks, because if this were the case, after the new ionic bonds between LPEI and PXV were formed there would be no reason for PXV to become displaced. We suggest that the enthalpy of the acid-base interactions is much stronger than the interaction of the viologen units with the carboxylic acid groups. Figure 5-7 sketches a proposed mechanism for this process. (1) The PXV/PAA multilayer is exposed to LPEI in solution, which diffuses into the multilayer. (2) The LPEI has the affect of ionizing some of the free carboxylic acid groups. (3) New ionic crosslinks are formed between free carboxylic acid groups and amine groups. Viologen units are also displaced and new bonds form between acid groups previously bonded to viologen units and amine groups. (4) PXV is ejected from the multilayer into the solution, and an LPEI/PAA multilayer structure is left.

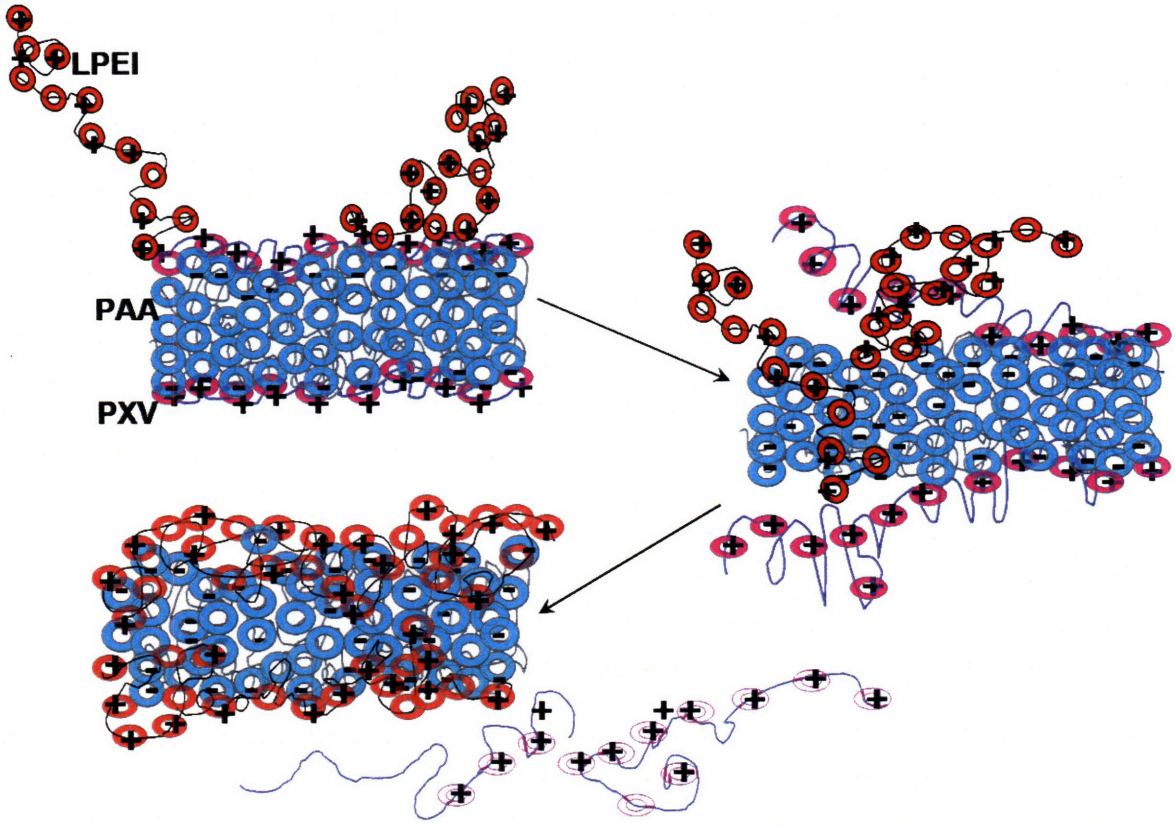

Figure 5-7: LPEI diffusing into and replacing PXV in a PXV/PAA mutliayer. PXV is eventually ejected from the structure.

5.3.3 Mobility of Other Weak Polycations within PXV/PAA Multilayer

We have previously demonstrated that LPEI, at pH 4 and 5, is able to exchange with the PXV in a PXV/PAA multilayer. In these studies, we also found that higher molecular weight LPEI (250,000 g/mol as opposed to 25,000 g/mol) takes longer to exchange with the PXV, consistent with the proposed mechanism that the LPEI chains diffuse through the pre-existing multilayer structure. It was also demonstrated that the exchange process occurs more slowly when both the PXV/PAA multilayer was assembled at pH 5 and the LPEI solution was adjusted to pH 5 during assembly as compared to pH 4. This exchange process appeared to be related to the difference in the various films' degree of ionization, which in turn determines the density of electrostatic crosslinks that stabilize the multilayer. When assembled at pH 4, the carboxylic acid groups of the PXV/PAA multilayers are ~20% ionized, while LPEI/PAA multilayers are ~50% ionized. In the pH 5 case, the PXV/PAA multilayer acid groups are ~40% ionized and the LPEI/PAA multilayer contains acid groups that are ~55% ionized. The lower degree of acid ionization in PXV/PAA films indicates that there must also be a lower number of ionic crosslinks, resulting in an LbL film with a looser network, thus making it easier for polymer chains to penetrate the film. Furthermore, the loss of charged anionic acid sites in the film at lower pH values leads to fewer "sticky" sites for the attachment of polyamine groups, thus increasing the mobility of polyamine chains within the film at lower pH. The enhancement of polyion chain mobility within the multilayer via the generation of multilayers with low ionic crosslink density and/or fewer charge sites, however, is not singularly sufficient for the interdiffusion and exchange process; many multilayers are generated at conditions yielding low degrees of ionization, but do not exhibit interdiffusion behavior. An additional consideration must also be the contribution to chain mobility resulting from the composition of the diffusing polymer component. The degree to which the polymer chain is hydrated during the adsorption and interpenetration process impacts localized polymer segment mobility; furthermore, chain size (i.e., molecular weight) and topology (branched structure) directly impacts the kinetics of diffusion. The interdiffusing polymer's charge density, rigidity or flexibility, and solubility within the multilayer matrix are all potential factors in chain mobility.

The above two issues relate to the kinetic barriers that affect penetration and diffusion of polyion chains within the multilayer during the adsorption process. A third factor that appears to play a particular role in the interdiffusion and exchange between polyions within the film is the thermodynamic driving force for this exchange, whether it be due to chemical partitioning or specific chemical interactions. In the particular model system of interest here, this driving force is the

difference in the relative affinity of the basic amine groups in the polyamine over the quaternized pyridinium groups in PXV due to strong acid-base interactions between acid and amine groups, as demonstrated by significant shifts in acid ionization in the presence of LPEI.

It is important to determine what conditions and aspects of the interdiffusing polyion species allow them to diffuse and exchange with polymer in underlying layers of an LbL film. By examining this behavior with the PXV/PAA model system and a range of polyamines, it is hoped that a greater understanding of this phenomenon be achieved, particularly in the context of competitive polyion exchange that has been observed in several heterostructure systems of practical interest. If these properties can be identified for a simple series of synthetic polyamines, it may be possible to predict how other polyelectrolytes will behave, and to contribute to developing predictive models of polyelectrolyte multilayer assembly.

To probe how the primary chemical structure of the polycations influences their capability to exchange from solution with PXV in a pre-existing multilayer structure, four different polycations were examined. LPEI is a hydrophilic, weak polyelectrolyte with secondary amine chemical functionality. Films of 25 layer pairs of PXV/PAA assembled at pH 4 on silicon substrates were immersed in 20 mmol solutions of PAMAM, LPEI, BPEI, or PAH at different pH values. Published data from multiple literature sources was used to determine the solution degree of ionization for each polyamine. LPEI has a pKa value of 5.5,[39, 40] BPEI has a pKa of 6.5,[38] PAH has a pKa value of 8.8,[26] and PAMAM has a pKa of 6.9 for the primary amine groups and 3.9 for the tertiary amine groups.[45] The overall degree of ionization for PAMAM dendrimer was defined as a weighted average of the ionization of the primary and tertiary amine groups at each pH value (64 primary groups and 60 tertiary groups). It is important to note that for simplicity the degree of ionization referred to here is that of the polyion in dilute aqueous solution at the stated pH. It has been demonstrated that the degree of ionization of weak polyelectrolytes is shifted as the polyion is incorporated into the LbL film; for example, the incorporation of polyacids with polyamines has been shown to lead to higher degrees of ionization of the acid groups, to levels well above that expected at the pH of interest.[26] It is also likely that the degree of ionizarion of polyamines within the film will be higher than solution as the groups titrate each other to form the polyelectrolyte complex. We have also observed this effect, as reported in the recent work with LPEI interdiffuion into PXV/PAA films.

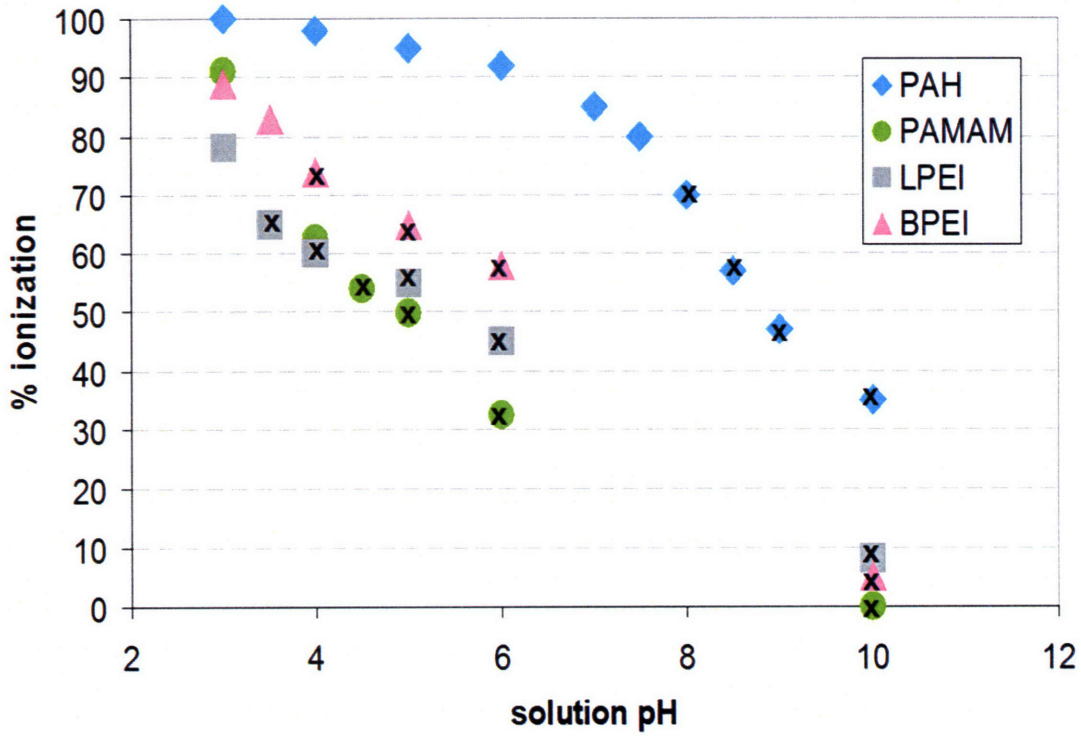

Figure 5-8: Degree of ionization of the various polycations in solution. Arrows represent the solutions which showed exchange with PXV in the $(PXV/PAA)_{25}$ multilayer. For each polycation there seems to be a critical degree of ionizaion above which exchange is not able to take place. In the case of PAMAM this critical degree of ionization is lower, likely due to PAMAM's geometry, which makes it more likely to deposit on a charged surface.

Each of the four polyamines is able to exchange with the PXV under the appropriate pH conditions. This result indicates that the interdiffusion and exchange processes do not require a specific chemical structure; indeed, although PAH is known to form very stable, linear LbL films, it exhibits interdiffusion at lower degrees of ionization and when presented with a driving force for exchange. Based on this observation, exchange must be related to a more general aspect of polyelectrolyte shape, size and ionization density. Importantly, this result confirms that exchange and diffusion can potentially impact any heterostructured LbL assembled film, or any LbL film which is exposed to a polymer solution after assembly.

It was possible to track the exchange and ejection of PXV out of the film by the disappearance of a peak around 1640 nm which corresponds to the aromatic carbon in the PXV chains and the appearance of peaks for the amine groups. Figure 5-9 shows the process for exposure of PXV/PAA films to solutions of PAH. The characteristic PXV peak at 1640 remains strong after exposure to pH

3, 4, and 6 solutions, but has nearly disappeared after exposure to the pH 10 solution. LPEI was able to exchange with PXV at pH 3.5 and above, and BPEI exchanged as pH 4 and above. In the case of PAMAM exchange occurred at pH 4.5 and above. For the PAH, exchange was observed at pH 8, 9, and 10 only. These results show that there is a critical degree of polycation ionization above this process does not occur, and PXV chains are not displaced by the weak polycation. When highly charged, the chains are more highly extended and therefore adsorb more readily to the surface which is terminated with polyanion. This is seen elsewhere in the LbL literature as "molecularly thin" adsorbed layers of highly charged polyelectrolytes.[24, 25] Highly charged polymers are also much more likely to become kinetically trapped at or near the surface of the film via ionic crosslinks; the mobility of the chains within the LbL bulk film would thus be further limited for the most highly charged polymers due to charge interactions as well as extended chain size. For PAH, LPEI and BPEI, this critical degree of ionization is ~70% ionization, and for PAMAM between 55% ionized.

Figure 5-8 tells us that partially charged polyamines are better able to diffuse through bulk LbL films than fully charged chains. The fully charged chains are much more likely to immediately adsorb to the LbL surface. Once the surface PAA molecules are satisfied, charge reversal will occur, and electrostatic repulsion is likely what keeps PAH chains from penetrating the multilayer. PAMAM dendrimer is known to be a "sticky" molecule due to the high density of charged groups confined to a small volume. At pH 3 and 4, all of the PAMAM's amine groups, tertiary and primary, are charged, but at pH 4.5 and above only the primary amines groups are charged. LPEI and BPEI are also more hydrophilic than the PAMAM and especially PAH. It seems to be a reasonable assumption that better solvated polymer chains will be able to more easily penetrate the LbL structure swollen in water. Hydrogen bonded systems as well as some of these weak polyelectrolyte systems, such as LPEI/PAA have been reported to show extremely thick per layer pair thickness over the pH regime at which we see interdiffusion to take place.[24, 46] Interdiffusion of the polymers most likely contributes to make these extremely thick films.

Post treatment of LbL films by exposure to solutions at different pH values has been known to create morphological changes in the films, such as the creation of pores.[47] Figure 5-9 shows that exposure of the PXV/PAA multilayer to the polycation solutions does change the degree of ionization of the carboxylic acid groups in the film, even in the cases for which no exchange takes place. Simply increasing PAA ionization is not sufficient to cause the replacement of PXV in favor of a polycation

which could form more ionic bonds with PAA. The polycation itself must also posses a certain degree of mobility that strongly charged chains do not.

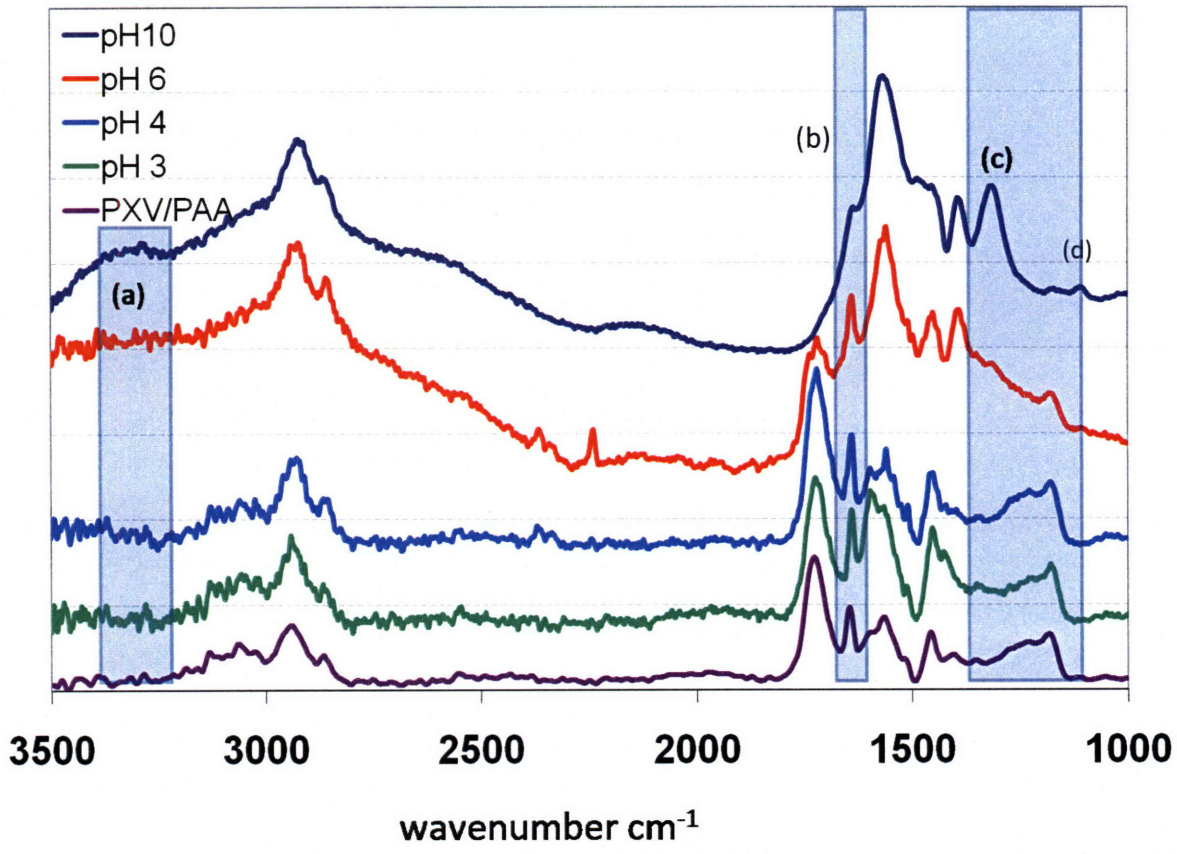

Figure 5-9: FTIR spectra of PXV/PAA multilayers after exposure to PAH solution at different pH values. For all of the pH values there is an increase in carboxylic acid ionization from the ~20% which is found in PXV/PAA films assembled at pH 4. In the pH 10 spectrum there is a new shoulder ~3300 nm (a), for primary amines, the aromatic carbon peak at peak at 1640 has significantly decreased (b), a peak for the primary amine around 1400 has appeared (c), and the aromatic amine peak at 1190 has nearly disappeared (d). PAH at pH 10 can exchange with PXV, but not at lower pH values.

Figure 5-10 shows the degree of ionization of the different multilayers assembled from pH 3 – 6, ranging from 30 – 45% at pH 3 to as high as 90% ionization at pH 6. In each of these films the percentage of ionized acid groups is significantly higher than that of the PXV/PAA multilayers as assembled at pH 4, about ~20%, and also higher than the degree of ionization of PAA in solution.[22] The carboxylic acid groups are much more readily deprotonated in the presence of 1°, 2°, or 3° amine groups rather than the bipyridine functionality of the PXV. These acid-base interactions are favored

over the PXV/PAA interactions. The charges of the carboxylic acid groups seem to be very labile and the degree of PAA ionization is extremely influenced by surrounding positive charge density.

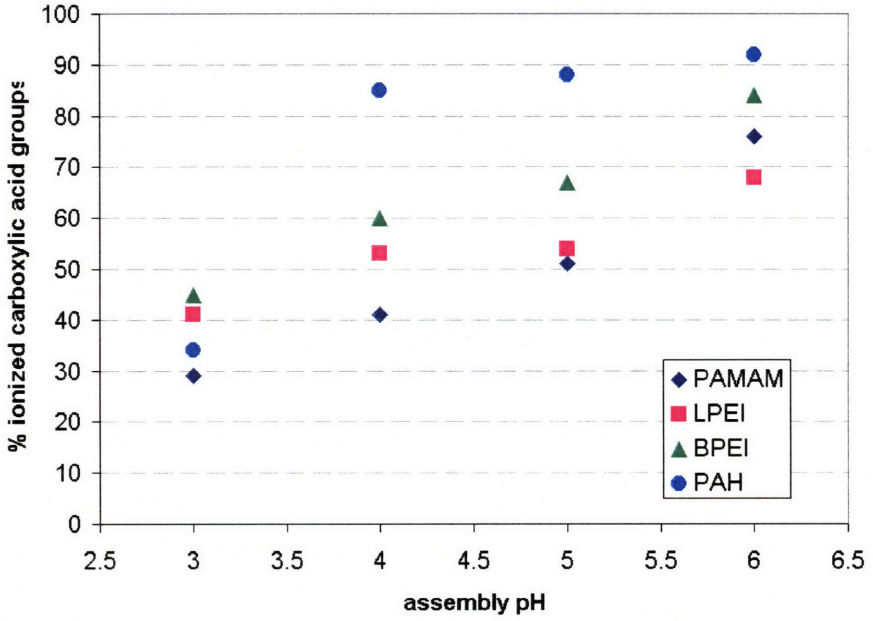

Figure 5-10: percentage of charged carboxylic acid groups in PAH/PAA, LPEI/PAA. BPEI/PAA. and PAMAM/PAA multilayer films.

In order to verify that the PXV/PAA films are not only incorporating the new polycations but also rejecting the PXV from the film structure UV-vis was performed on the solutions in which the PXV/PAA films were immersed. Figure 5-11 shows the spectra of BPEI solution, PXV solution, and the pH 3 and 4 BPEI solutions after exposure to the PXV/PAA films for 4 days. The spectrum of the pH 3 BPEI exchange solution shows features only of BPEI while spectrum of the pH 4 BPEI exchange solution is a composite of both PXV and BPEI spectra. This agrees with the FTIR data summarized in Figure 5-7; BPEI at pH 3 does not cause rejection of PXV from the LbL structure, but BPEI at pH 4 does.

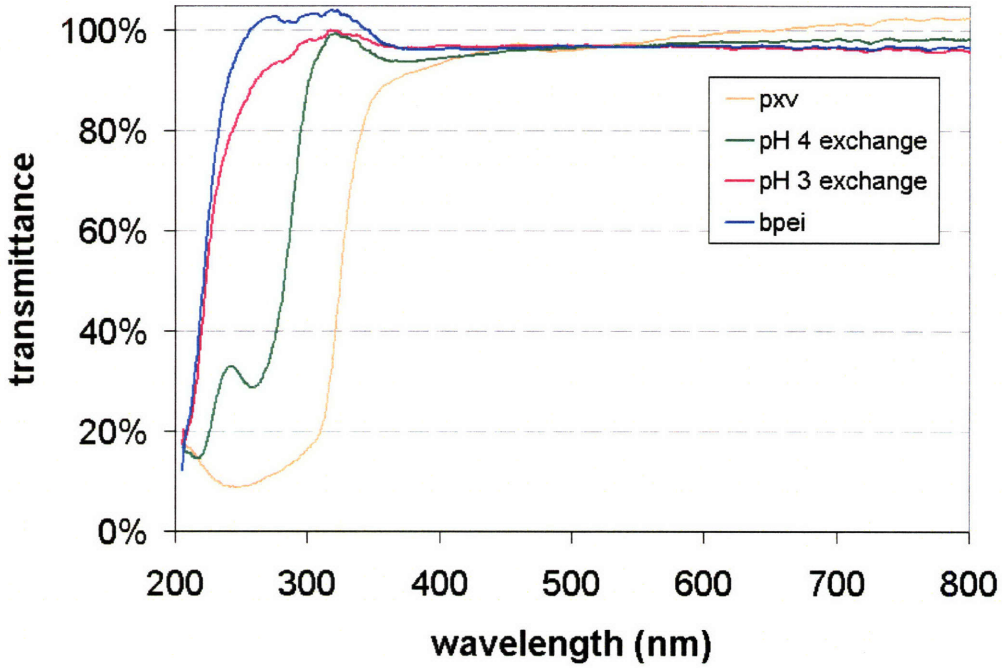

Figure 5-11: UV-vis of exchange solutions. Blue line is spectrum of 20 mmol BPEI solution, yellow line is spectra of aqueous PXV solution. The pink line is the UV-vis spectrum of the pH 3 BPEI solution after a PXV/PAA 25 layer pair film was immersed in the solution for 4 days; it shows the features of only BPEI. The green spectrum is of the pH 4 BPEI solution after 4 days of exposure to a PXV/PAA film. This spectrum shows the features of both PXV and BPEI.

These results point to some parameters that can be chosen in order to control the inner structure of LbL films, and more specifically heterostructures. Using non-diffusive polycations/conditions could be a general strategy for compartmentalizing film sections.

5.3.4 Film Compartmentalization

The complex interactions within our model heterostructure clearly do not allow its straightforward bottom-up assembly. LPEI from the ion conduction multilayer diffuses into the electrochromic PXV/PAA multilayer, it exchanges with and displaces PXV, and it changes the electrostatic crosslink density, leading to a dramatic decrease in film quality. To prevent this disruption, a blocking layer strategy was employed. In this strategy, layers of a third system - $(PAH/PAA)_n$ - were assembled in between the electrochromic PXV/PAA multilayer and the ion conductive LPEI/PAA multilayer. After the PXV/PAA base layer was assembled, 4 layers of PAH/PAA were assembled on top of the film. The film was then heated at 130°C for 1.5 hr to form covalent cross links between the carboxyl and amine groups in PAA/PAH.[22] Elsewhere, similar blocking layers have been reported,[18, 19] as well

as strategies to compartmentalize multilayers by using clay platelets.[20-22] After covalent crosslink formation, the LPEI/PAA multilayer was assembled onto the film. The resultant heterostructured film was optically clear and its rms roughness was only 1 nm. The heterostructure with the blocking layers is about 3.5 μm thick or 30 % thinner than the heterostructure assembled without blocking layers which is about 5.0 μm thick; LPEI/PAA assembled onto the blocking layer grows at the same linear rate as in isolation atop native silicon oxide, with 30 layer pairs assembled at pH 4 measuring ~1.3 μm. The PAH/PAA film is too thin to allow for LPEI to diffuse into it, and the PAH chains are extended at this pH, making the PAH/PAA layers even less permeable.

Heating an LbL assembled film can smooth the film surface. To determine whether the increase in the heterostructure film stability was due to the covalently crosslinked blocking layer or the simple effect of heat, the PXV/PAA base multilayer was assembled, then heated at 130°C for 1.5 hr, after which an LPEI/PAA multilayer was assembled onto the film. The heterostructure assembly was still disrupted; the film was optically opaque, and its rms roughness was 10 nm. Although simple heating did reduce the roughness of the heterostructure film, it did not provide the control over stability that is afforded by the blocking layer strategy.

Figure 5-12. (a) PXV/PAA and LPEI/PAA assembled at pH 4; due to LPEI diffusing into the bulk and displacing PXV the film has become extremely rough and is ~5.0 μm thick. (b) PXV/PAA assembled at pH 4, heated and then LPEI/PAA assembled at pH 4, which is smoother than without annealing but the haziness indicates disruption of film structure, and (c) PAA/PXV, crosslinked layers of PAH/PAA, and LPEI/PAA assembled at pH 4, yielding an optically clear and smooth film, ~3.5 μm thick.

Figure 5-12 depicts the heterostructure film quality that results from each assembly method. The film with blocking layers is clearly the only optically transparent film. Moreover, it is the thinnest film; the unblocked and unheated heterostructure film in (a) is approximately 5.0 μm thick, whereas the blocked heterostructure film in (c) is about 3.5 μm thick, 30% thinner than the disrupted structure. The growth is roughly linear in all cases, but only when a blocking layer strategy is used can smooth, laminar heterostructured films be produced.

To demonstrate that the blocking layer strategy prevents PXV displacement, we constructed our model heterostructure with a blocking layer atop an ITO substrate. The functional model heterostructure atop ITO was employed as the working electrode in an electrochemical cell as described elsewhere in our work,[10] and photographs were recorded of the electrochromism of PXV, as shown in Figure 5-13. The clear change in color from transparent to purple indicates that the underlying PXV/PAA layers are intact. The switching speed of the functional heterostructure is not measurably slowed by the presence of the blocking layer (compared to a PXV/PAA film assembled in isolation), indicating that the blocking layer does not impede small ion motion. The high ion conductivity of the thick LPEI/PAA multilayer also apparently avoids any negative impact on switching speed. This demonstration clearly shows that *working* functional heterostructures may be constructed by layer-by-layer assembly using a blocking layer strategy. Implementing this strategy eliminates the standing technical barriers to the creation of complex thin film devices containing three or more functional multilayers.

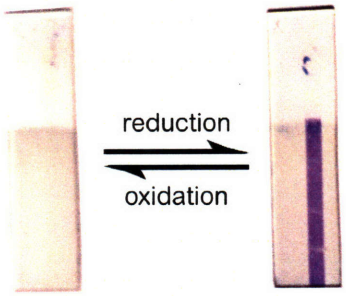

Figure 5-13. Redox switching of heterostructured film with crosslinked layers, indicating that PXV has not been displaced and that small ion motion has not been hindered by the crosllinked barrier layers.

5.4 Conclusions

The formation of functional heterostructured thin films by LbL assembly is often disrupted by complex interactions between polyelectrolytes. The mobility of polymer chains through the film is responsible for some types of heterostructure disruption, and the wholesale rejection of some heterostructure components is a possible outcome. This phenomenon shares its mechanism with the superlinear growth mode that is observed in some LbL assembled systems. In the early stages of its

development, LbL assembly was regarded as a surface-modification technique, where the bulk film was considered to be a glassy, inert solid. This perspective should be re-examined, because in many cases the entire film participates in the assembly process.

The disrupted assembly of our electrochrome/electrolyte system results from an exchange/displacement mechanism. Through FTIR spectroscopy we observed that LPEI from the ion conducting multilayer diffuses into the bulk of the electrochromic (PXV/PAA)n multilayer below it, exchanging with and eventually displacing PXV. We hypothesize that displacement occurs because PAA prefers interactions with LPEI over PXV. The ionization density of PAA is far greater when it is paired with LPEI than when it is paired with PXV. The ability of LPEI to "titrate" PAA and form additional electrostatic crosslinks with unpaired carboxylic acids in the bulk film may be related to the superlinear growth of the (LPEI/PAA)n system in isolation. The system grows superlinearly for more than fifteen layer pairs before it reaches a linear growth regime; typical LbL assembled systems only grow superlinearly for three layer pairs.23 This clear correlation between superlinear growth and atypical heterostructure assembly behavior illustrates that these two phenomena share the same underlying interdiffusion mechanism.

We also demonstrate that a number of weak polycations are capable of interdiffusion and exchange with a strong polycation, not just LPEI as shown in our previous work. This may have a number of implications for biological applications of LbL films, as this weak polycation class includes many proteins, polysaccharides, and other biologically derived macromolecules. Our second conclusion is that there is a critical ionization density of the polycation chains below which these weak polycations become able to interdiffuse into our model system and replace the strong polycation. This critical ionization is influenced by chain architecture.

Simple and effective strategies to overcome assembly disruption, such as the blocking layer used here, become obvious only after the mechanism of this disruption is understood. For example, an understanding of when certain polymers will exchange based on charge density can lead to appropriate materials selection.

Chapter 5 References

1. Zacharia, N. S.; DeLongchamp, D. M.; Modestino, M.; Hammond, P. T. Macromolecules 2007, 40, 1598-1603.
2. Decher, G.; Schlenoff, J. B. Multilayer Thin Films: Sequential Assembly of Nanocomposite Materials; Wiley-VCH: Weinheim, 2003.
3. Hammond, P.T. Adv. Mater. **2004**, 16, 1271-1293
4. Xie, A. F.; Granick, S.; Macromolecules **2002**, 35, 1805-1813.
5. Mermut, O.; Barrett, C. J.; J. Phys. Chem B **2003**, 107, 2525-2530.
6. Hübsch, E.; Fleith, G.; Fatisson, J.; Labbé, Voegel, J. C.; Schaaf, P.; Ball, V. Langmuir 2005, 21, 3664-3669.
7. Korneev, D.; Lvov, Y.; Decher, G.; Schmitt, J.; Yaradaikin, S. Physica B **1995**, 213/214, 954
8. Kellogg, G. J.; Mayes, A. M.; Stockton, W. B.; Ferreira, M.; Rubner, M. F.; Satija, S. K. Langmuir **1996**, 12, 5109.
9. Arys, X.; Laschewsky, A.; Jonas, A. M. Macromolecules **2001**, 34, 3318-3330.
10. Shiratorei, S. S.; Rubner, M.F. *Macromolecules* **1998**, *31*, 4309-4318.
11. DeLongchamp, D. M.; Kastantin, M.; Hammond, P. T. *Chem. Mater.*, **2003**, *15*, 1575-1586
12. Schoeler, B.; Poptoshev, E.; Caruso, F. *Macromolecules* **2003**, *36*, 5258-5264.
13. Lavalle, P.; Gergely, C.; Cuisinier, F. J. G.; Decher, G.; Schaaf, P.; Voegel, J. C.; *Macromolecules* **2002**, *35*, 4458-4465.
14. Lavalle, P; Picart, C.; Mutterer, J.; Gergely, C.; Reiss, H.; Voegel, J. C.; Senger, B.; Schaaf, P. *J. Phys. Chem B* **2004**, *108*, 635-648.
15. Hübsch, E.; Ball, V.; Senger, B.; Decher, G.; Voegel, J. C.; Schaaf, P. *Langmuir* **2004**, *20(5)*, 1980-1985.
16. Lavalle, P.; Vivet, V.; Jessel, N.; Decher, G.; Voegel, J. C.; Mesini, P.; Schaaf, P. *Macromolecules* **2004**, *37(3)*, 1159-1162.
17. Yoo, P. J.; Nam, K.; Qi, J.; Lee, S.; Park, J.; Belcher, A.; Hammond, P. T. *Nature Materials* **2006**, *5(3)*, 234-240.
18. Jomaa, H. W.; Schlenoff, J. B. *Langmuir* **2005**, *21(18)*, 8081-8084.
19. Garza, J.M.; Schaaf, P.; Muller, S.; Ball, V.; Stolz, J. F.; Voegel, J. C.; Lavalle, P. *Langmuir* **2004**, *20(17)*, 7298-7302.
20. Wood, K. C.; Chuang, H. F.; Batten, R. D.; Lynn, D. M.; Hammond, P. T. *submitted*, **2006**.
21. Glinel, K.; Laschewsky, A.; Jonas, A. M. *Macromolecules* **2001**, *34*, 5267-5274.
22. Struth, B.; Eckle, M.; Decher, G.; Oeser, R.; Simon, P.; Schubert, D. W.; Schmitt, J. *European Physical Journal E*, **2001**, *6*, 351-358.
23. Vuillaume, P. Y.; Glinel, K.; Jonas, Am M.; Laschesky, A.; Ladam, G.; Schaad, P.; Voegel, J. C.; Schaaf, P.; Decher, G.; Cuisinier, F. *Langmuir* **2000**, *16*, 1249-1255.
24. DeLongchamp, D. M.; Hammond, P. T. *Chem Mater.* **2003**, *15*, 1165-1173.
25. Harris, DeRose, Bruening. *J. Am. Chem. Soc.* **1999**, *121*, 1978-1979.
26. Choi, J.; Rubner, M. F. *Macromolecules* **2005**, *38*, 116-124.
27. Kharlampieva, E.; Sukishvili, S. A. Lamgmuir 2003, 19, 1235-1243.

28. Sukishvili, S. A.; Granick, S. *Macromolecules* **2002**, *35*, 301-310.
29. Voight, U.; Khrenov, V.; Thuer, K.; Hahn, M.; Jaeger, W.; von Klitzing, R. *J. Phys.: Condens. Matter* **2003**, *15*, S213-S218.Kolarik, L.; Furlong, D. N.; Joy, H.; Struijk, C.; Rowe, R. *Langmuir* **1999**, *15*, 8625.
31. Ball, V.; Hübsch, E.; Schweiss, R.; Voegel, J. C.; Schaaf, P.; Knoll, W. *Langmuir* **2005**, *21*, 8526-8531.
32. Schoeler, B.; Poptoshev, E.; Caruso, F. *Macromolecules* **2003**, *36*, 5258-5264.
33. Quinn, J. F.; Yeo, J. C.C.; Caruso, F. *Macromolecules* **2004**, *37*, 6537-6543
34. Debreczeny, M.; Ball, V.; Boulmedais, F.; Szalontai, B.; Voegel, J.C.; Schaaf, P.; *J. Phys. Chem. B*, **2003**, *107*, 12734
35. Johal, M. S.; Ozer, B. H.; Casson, J. L.; St. John, A.; Robinson, J. M.; Wang, H. L. *Langmuir* **2004**, *20*, 2792.
36. Sukhishvili, S. A.; Granick, S. *Langmuir* **2003**, *19(6)*, 1980-1983
37. Lutkenhaus, J. L.; Hrabak, K. D.; McEnnis, K.; Hammond, P. T. *Journal of the American Chemical Society* **2005**, *127 (49)*, 17228-17234.
38. Bloys van Treslong, C. J.; *Recueil, J. Royal Neth. Chem. Soc.* **1978**, 97, 13-21.
39. Weyts, K. F.; Goethals, E. J.; *Makromol. Chem., Rapid Commun.* **1989**, *10*, 299-302.
40. Smits, R. G.; Koper, G. J. M.; Mandel, M.; *J. Phys. Chem.* **1993**, *97*, 5745-5751.
41. Bromberg, L.; *J. Phys. Chem B* **1998**, *102*, 10736-10744.
42. Philippova, O. E.; Hourdet, D.; Andebert, R.; Khokhlov, A. R.; *Macromolecules* **1997**, *30*, 8278-8285.
43. Petrov, A.I.; Antipov, A., A.; Sukhorukov, G. B.; *Macromolecules* **2003**, *36*, 10079-10086.
44. Burke, S. E.; Barrett, C. J.; *Langmuir* **2003**, *19*, 3297-3303.
45. Tomalia, D. A.; Naylor, A. M.; Goddard, W. A. *Angewandte Chemie International Edition* **1990**, *29*, 138-175.
46. DeLongchamp, D. M.; Hammond, P. T. Langmuir 2004, 20(13), 5403 – 5411.
47. Mendelsohn, J. D.; Barrett, C. J.; Chan, V. V.; Pal, A. J.; Mayes, A. M.; Rubner, M. F. *Langmuir* **2000**, *16*, 5017.

Chapter 6
Encapsulasation of Micelles in LbL Films

6.1 Introduction

One of the possible applications for LbL films that has shown the most promise is drug delivery. LbL films are ideal for coating medical devices such as stents or implants, and could also be used to make patches or chips. LbL assemblies can modify surfaces in to make them more biocompatible, for instance to keep proteins or cells from attaching. This combined with drug delivery could be an important technological advance. Here we describe using a block copolymer in an LbL assembly in order to prolong drug release. Basic questions as to film formation using this new polymer architecture for LbL assembly are examined, as well as release of a model drug.

Several common strategies for using LbL films for drug delivery have been demonstrated. The first general area involves coating microparticles with an LbL film.[1, 2] The film can act as a diffusion barrier when coating a hydrophobic drug microparticle,[3] or hollow LbL microcapsules can be fabricated and loaded with water-soluble drug.[6, 7] These types LbL systems relies on diffusion of the drug through the LbL layer, which is often only slowed down by a matter of hours. Besides microparticles, integrating the drug into the fabrication of the LbL films is another approach. For example, LbL films are composed of drug and a degradable polymer, which then releases the drug as the film comes apart.[4, 5] The drawback to using the drug as one of the building blocks of the film is that it only includes a small class of drugs that are polyionic and water soluble. This method excludes drugs without the necessary functionality and water solubility, such as small, hydrophobic molecules. A solution to this limitation has been offered by the use of prodrugs to integrate hydrophobic molecules into the LbL assembly.[10] However, with this approach, drugs with no functional groups may not be used, and for drugs with multiple functional groups, the synthesis of the prodrug may require many steps. Another approach to incorporate hydrophobic drugs includes using porous multilayers to take up hydrophobic molecules and then release them in aqueous solution.[11]

A more broad approach for incorporating drug molecules that are not good candidates for LbL films is to use amphiphilic block copolymers. Amphiphilic block copolymers, which self-assemble in solution, can solubilize and encapsulate hydrophobic molecules within the hydrophobic core of the self-assembled structure. The only requirement is that the hydrophilic block is polyionic; thus, the hydrophobic block can be tuned to interact with the encapsulated hydrophobic drug for greater

encapsulation efficiency and for adjustment of release times. These block copolymers can be adsorbed onto substrates to form organized layers,[12] either by directly adsorbing unimers or aggregates such as micelles.[8, 9] Depending on the properties of the copolymer, these layers may be responsive to environmental stimuli such as change in ionic strength or pH. Biggs, et al, have reported adsorbed layers of weakly charged micelles which can "open" in response to change in pH,[13, 14] releasing encapsulated small molecules. Charged micelles have also been incorporated into LbL assemblies. Some of these micelles are stabilized through crosslinking prior to assembling in a LbL film,[15, 16] while others are directly incorporated into the film with no modification.[17, 18] The release times of representative hydrophobic molecules in these films were short, on the order of minutes to hours.

Linear-dendritic block copolymers have recently been shown to have potential as drug delivery agents.[19-21] Our group has recently synthesized a dendritic-linear-dendritic block copolymer,[22] using hydrophilic poly(amidoamine) (PAMAM) dendritic blocks, and a hydrophobic poly(propylene oxide) (PPO) linear block. The linear block forms the hydrophobic interior of the micelle, with the positively charged dendrons on the outside. It has been shown previously that they form micelles in solution and have a significantly higher encapsulation capacity for a model hydrophobic bactericide, triclosan, over pluronic micelles. In this paper we demonstrate the use of these micelles as a building block for LbL films, providing a matrix for the incorporation of hydrophobic drug into ionically crosslinked LbL assemblies. The micelles remain intact within the LbL films, providing hydrophobic microenvironments. Drug release lasts over a period of weeks in an active form, providing the possibility for the film to be utilized as an antibacterial coating for implants.

6.2 Experimental Details

Materials: Poly(acrylic acid) (PAA) (M_w ~ 20,000, 40% aqueous solution) and linear poly(ethyleneimine) (LPEI) (M_w ~ 250,000) were obtained from Polysciences. Poly(sodium 4-strenesulfonate) (PSS) (M_w ~ 70,000), pyrene (sublimed, 99%), and 5-chloro-2-(2,4-dichlorophenoxy)phenol (triclosan, ≥97.0% purity) were purchased from Sigma-Aldrich and used as received. Quartz slides were obtained from Chemglass.

Synthesis of Poly(propylene oxide)-Poly(amidoamine): The amphiphilic ABA linear-dendritic block copolymer was previously synthesized.[22] Briefly, the synthesis begins with poly(propylene glycol) bis(2-aminopropyl ether) (PPO). The poly(amidoamine) (PAMAM) blocks are synthesized

from the amine ends of the PPO with alternating reaction steps of the first reaction, Michael addition with methyl acrylate, and the second reaction, exhaustive amidation with ethylenediamine. Generation 4.0 PPO-PAMAM block copolymers with 32 amine ends present on each dendritic block were synthesized. The synthesis of the block copolymer was confirmed through ^{1}H-NMR and FTIR.

Drug Loading: An oil/water emulsion technique was utilized to load a model hydrophobic drug, triclosan, into preformed PPO-PAMAM micelles. Triclosan, dissolved in dichloromethane, was added dropwise to an aqueous solution of PPO-PAMAM. The emulsion was vigorously stirred and left open overnight for the dichloromethane to evaporate. The final concentrations of the PPO-PAMAM and triclosan in aqueous solution were 19 mg/ml and 5 mg/ml, respectively. The solution obtained was centrifuged at 4500 rpm for 10 minutes. Any undissolved triclosan was removed with a 0.45 μm PTFE syringe filter. To quantify the amount of drug in solution for subsequent studies, the solution was analyzed by an Agilent 8453 UV-Visible Spectrometer System (Palo Alto, CA). The characteristic absorbance of triclosan was measured at 281 nm. For concentrated solutions of triclosan encapsulated by PPO-PAMAM micelles, the solution was diluted with methanol in a 1:9 ratio. A calibration curve applicable in the 0-100 μg/ml range for triclosan in 1:9 water:methanol mixtures was used to determine the concentration ($Y = 60.90*X - 1.22$, $r^2 = .9973$).

LbL Film Formation: Lbl films were assembled on quartz substrates approximately 0.5 cm by 1.5 cm in size. The quartz substrate was dipped into a PPO-PAMAM aqueous solution (1.9 mg/ml, with or without drug encapsulated) adjusted to pH 5.5 with dilute HCl for 10 minutes and then subsequently rinsed off in three water baths for 0.5, 1.0, and 1.0 minutes, respectively. Next, the substrate was dipped into an aqueous solution of PAA adjusted to pH 5.0 with dilute HCl (20 mM based on repeat unit) for 10 minutes. The substrate was rinsed off in three water baths for 0.5, 1.0, and 1.0 minutes, respectively. The dipping process was repeated until the number of layer pairs desired was achieved. For LbL films containing pyrene, PPO-PAMAM aqueous solutions were incubated with 10^{-7} M pyrene overnight before being used for film formation.

LbL Film Characterization: Film thickness was measured with a Tencor P10 profilometer. For film fluorescence studies, the LbL films were formed on a quartz substrate, and a FluoroMax-2 Spectrometer (Horiba Jobin Yvon, Longjumeau, France) was used to obtain emission spectra. The emission spectra were recorded over a range of 355 nm to 500 nm with an excitation wavelength of 333 nm. For detection of triclosan deposited in the LbL films on a quartz substrate, an Agilent 8453 UV-Visible Spectrometer System was used.

TGA: LbL films were deposited onto polypropylene substrates. Films composed of PAA and PPO-PAMAM with or without triclosan were fabricated up to 150 layer pairs. The films were peeled from the substrate, and then heated at a rate of 5° per minute, from room temperature to 115°, held at an isotherm for 30 minutes in order to evaporate any residual water in the film, then heated to 700°C.

GISAXS: Grazing Incidence Small Angle X-ray Scattering (GISAXS). GISAXS experiments were performed at the G1 beamline at the Cornell High Energy Synchrotron Source (CHESS). The wavelength of the incident beam was 1.239Å and a 2-D area detector was used for data collection.[24]

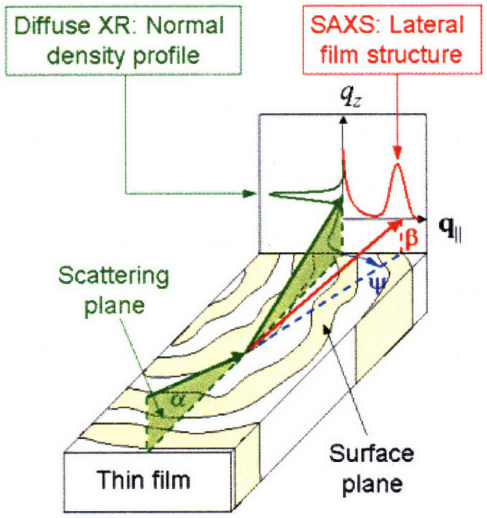

Figure 6-1: Geometry of the GI-SAX experiment, which allows for structural investigation normal to the substrate. http://staff.chess.cornell.edu/~smilgies/gisaxs/GISAXS.php

Drug Release Studies: LbL films on silicon substrates composed of PAA and PPO-PAMAM encapsulating triclosan were placed into vials of phosphate buffered saline (PBS) at pH 7.4 and 37 °C. To maintain sink conditions, the films were moved to fresh vials of PBS at appropriate time points. The PBS solutions were analyzed with UV-Vis. A calibration curve of triclosan in PBS from 0-9 μg/ml was used to calculate the concentration of the solution and the amount of triclosan released ($Y = 105.76*X - 0.0599$, $R^2 = .99$).

Kirby Bauer Test: A standard Kirby Bauer test was performed using *Staphylococcus Aureus* (*S. Aureus*).[27] Cation-adjusted Mueller Hinton broth was inoculated with *S. Aureus* and cultured overnight. The culture was diluted to a concentration where with UV-Vis, the O.D. was 0.1 at 600 nm. The culture was then grown for an additional 4 hours, and then plated onto agar plates

containing cation-adjusted Mueller Hinton broth. LbL films of PAA and PPO-PAMAM with or without triclosan on 3 mm by 3 mm silicon substrates were placed onto the plate. The plates were incubated at 37 °C overnight. A zone of inhibition (ZOI) was measured for each sample and was calculated as:

$$ZOI = \frac{Outer\ Diameter\ of\ Inhibition - Diameter\ of\ Substrate}{2}$$

6.3 Results and Discussion

Formation and Characterization of Micelle-Containing LbL Films. LbL films were produced containing amphiphilic linear-dendritic block copolymer micelles. The linear-dendritic block copolymer is composed of a hydrophobic block of poly(propylene oxide) (PPO) and is flanked by two hydrophilic dendritic PAMAM blocks. Generation 4.0 PPO-PAMAM linear-dendritic block copolymers, with 32 amine ends on each block, were used as the counter-polyelectrolyte to PAA. The films contain hydrophobic domains that could potentially be used as coatings to deliver hydrophobic drugs or to encapsulate hydrophobic molecules that otherwise could not be incorporated into an LbL film due to insolubility in water or a low charge density. For preliminary studies, the micelles were used to encapsulate a hydrophobic bactericide, triclosan. It has a log P (octanol-water) of 4.76 and a water solubility of 10^{-2} mg/ml. As shown in a previous article, the loading efficiency of triclosan into PPO-PAMAM micelles is significantly higher (85 w/w%) compared to the loading efficiency of F127 (42 w/w%), a pluronic with similar PPO block length and CMC value.[22]

The LbL films were fabricated on either quartz or silicon surfaces, with the positively charged PPO-PAMAM deposited first from an aqueous solution and then PAA. Both polyionic solutions were adjusted approximately pH 5.5. Films formed in a linear fashion from 4 layer pairs up to 25 layer pairs (Figure 6-1). On average, a layer pair was 80 nm thick. Film growth was also corroborated by measuring the UV-Vis absorbance of the triclosan incorporated into the film as a function of the number of layer pairs in the film. As shown in Figure 6-2, triclosan was integrated into the films linearly up to 25 layer pairs. Although the growth curve for larger numbers of layer pairs is not shown, superlinear growth was observed above 25 layer pairs until 40 layer pairs. This suggests that interdiffusion may play a role in the film formation; with the micelles likely diffusing through the bulk film.

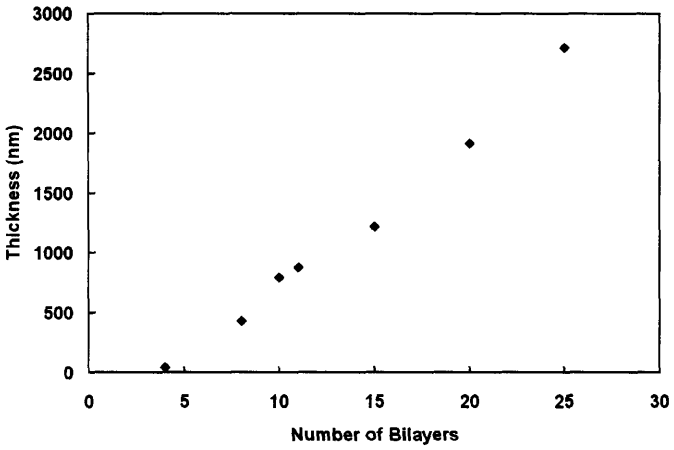

Figure 6-2: Growth curve of PAA and PPO-PAMAM encapsulating triclosan.

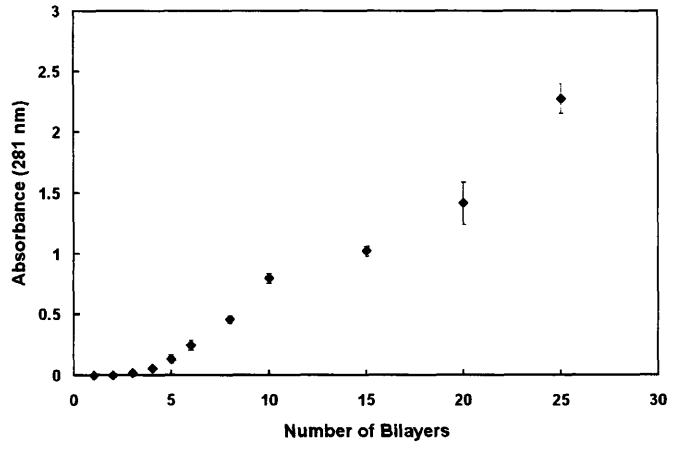

Figure 6-3: UV-vis measurements of triclosan at a characteristic wavelength of 281 nm at varying number of layer pairs in a LbL film.

In order to answer the question of whether or not the micelles retain their structure within the film or spread apart upon adsorption, additional film characterization was performed with micelles in which pyrene was encapsulated. PPO-PAMAM micelles were equilibrated in an aqueous solution with 10^{-7} M pyrene. The LbL films were fabricated with the PPO-PAMAM micelles encapsulating pyrene on quartz substrates. The fluorescence emission spectra of the films were measured and the maximum emission at 393 nm was recorded. Similar to the thickness and UV-Vis measurements, there was a linear relationship between the number of layer pairs in the film and the fluorescence

emission of the pyrene in the film (Figure 3) – although with the nonlinear induction period lasting upto 10 layer pairs, once again indicating perhaps some degree of micelle mobility within the film.

Additionally, the fluorescence emission spectrum can elucidate the environment that the pyrene is in by examining the vibronic band intensities.[23] The ratio of the emission intensity at 383 nm to 373 nm (III/I) is indicative of the type of solvent-solute interactions of pyrene and its environment. In more hydrophobic environments, the ratio is higher. In LbL films of PPO-PAMAM and PAA, the III/I ratio of pyrene was 0.91, while the III/I ratio of pyrene in an aqueous PPO-PAMAM solution above the critical micelle concentration was 0.85. The III/I ratio indicates that pyrene is in a hydrophobic environment.

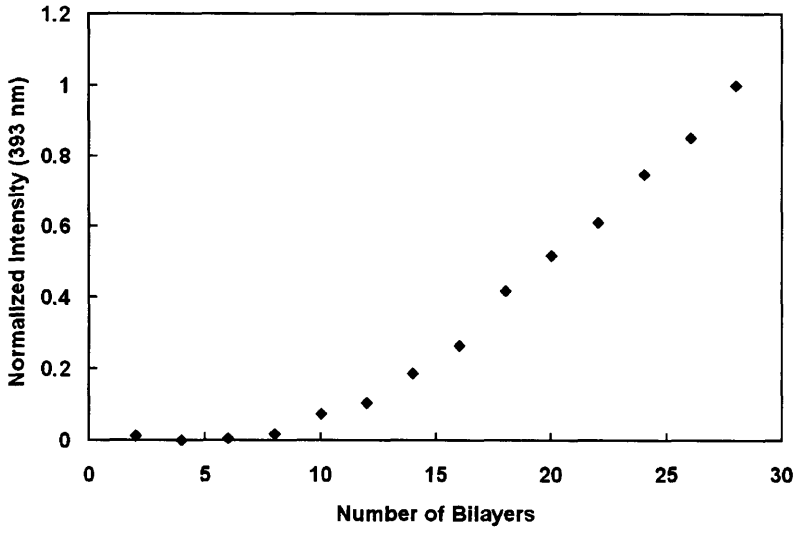

Figure 6-4: Intensity of pyrene at 393 nm in PPO-PAMAM containing LbL films.

To further confirm the presence of micelles in the LbL films, GI-SAXS was performed on LbL films composed of PPO-PAMAM and PAA. The films contained either empty micelles or micelles encapsulating triclosan. From the GI-SAXS data, it was established that there was regular spacing of ~10 nm in the direction parallel to the film and normal to the film. Previous experiments from dynamic light scattering had determined the hydrodynamic diameter of generation 4.0 PPO-PAMAM micelles as 17 nm in pH 5.5 water, and static light scattering experiments revealed that the micelles have a diameter of gyration of 15 nm. TEM measurements performed on micelles in a dry state

sitting on a flat surface also showed micelles approximately the same order of magnitude.[22] These measurements are of the same order of magnitude as the spacing seen in the LbL films.

In order to determine whether the spacing was due to individual PPO-PAMAM unimers versus PPO-PAMAM micelles, volume fraction calculations were experimentally determined. A generation 4.0 PPO-PAMAM unimer was simulated with molecular dynamics and was equilibrated in water. The equilibrated diameter of the unimer was approximately 4 nm. TGA measurements were completed on LbL films of PAA and generation 4.0 PPO-PAMAM with or without triclosan. By comparing the TGA data of the LbL films to TGA data of bulk PAA, generation 4.0 PPO-PAMAM, and triclosan, calculations established that the film was composed of 22% (w/w) PAA, 57% (w/w) PPO-PAMAM, and 20% (w/w) triclosan. For this system, PAA is a much smaller constituent of the films than when compared to the other weak polycation/PAA films discussed in chapter 2. In combination with the GISAXS data, this suggests a structure of loosely packed micelles wrapped by PAA chains. The GISAXS data indicates that the films are more ordered parallel to the substrate as opposed to normal to the substrate. The micelles likely pack relatively well in each adsorption step, but the mobility of them within the film structure keeps them from ordering vertically as well. Figure 6-5 shows a schematic of the proposed film structure.

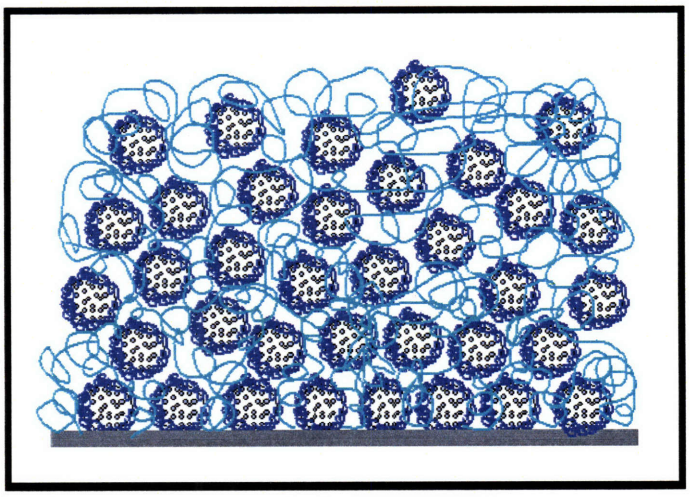

Figure 6-5: Proposed structure of PPO-PAMAM micelle containing films. Micelle packing becomes more disordered vertically.

Drug Release and Efficacy.

Drug release experiments were performed on the LbL film to determine the length scales of drug release. LbL films (10 layer pairs) on silicon substrates were placed in PBS solutions at 37 °C. Sink conditions were maintained by changing the solutions before the concentration of triclosan in the PBS was too high. The half-life of release was approximately 77 hours, with release lasting up to 20 days. The release curve indicates that the mechanism of release is diffusion through the film. FTIR of the samples before and after release show the PPO-PAMAM remaining in the film. GI-SAXS further indicates that the same spacing is maintained after drug release.

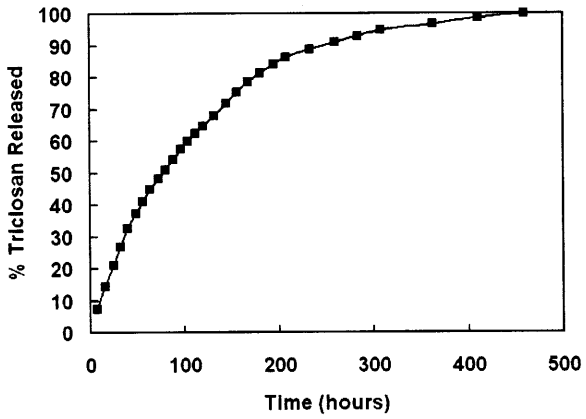

Figure 6-6: Percentage of triclosan released with time. After 10 days about 90% of the drug was released.

A Kirby Bauer assay was completed to determine the efficacy of the released triclosan. LbL films (10 layer pairs) of PAA and PPO-PAMAM with and without triclosan on silicon substrates were tested against *Staphylococcus Aureus*. As the films are incubated with the bacterial agar plates, the drug diffuses out and leaves a circular area free of bacteria called the zone of inhibition (ZOI). The ZOI for the film containing drug was 14.6±0.3 mm while there was no ZOI of the film without drug. As a control, a disk containing 10 μg of gentamycin was also tested, resulting in a ZOI of 7.7 mm.

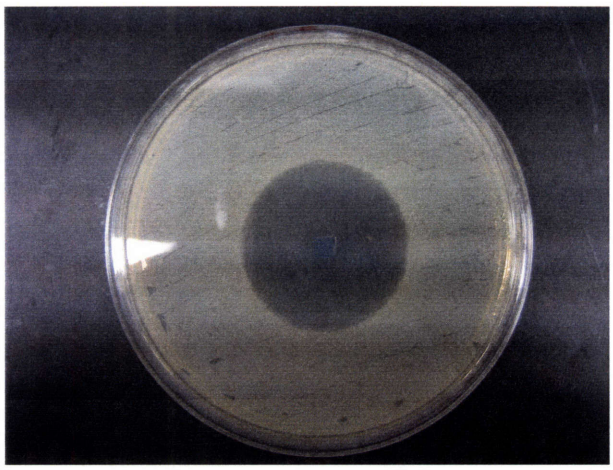

Figure 6-7: Agar plate of *S. Aureus* growth inhibited by release of triclosan from a 10 bilayer LbL film of PPO-PAMAM micelles encapsulating triclosan and PAA.

6.4 Conclusion

An LbL film was fabricated incorporating micelles composed of a novel amphiphilic linear-dendritic block copolymer. Although it may be less synthetically costly to incorporate charged linear-linear block copolymer micelles into an LbL film as shown in other groups' past studies[12, 25, 26] drug encapsulation is superior in the case of PPO-PAMAM micelles encapsulating triclosan[17] due to the linear-dendritic architecture.

The formation of the PPO-PAMAM/Triclosan/PAA film was shown to be linear after the initial first 4 layer pairs. GISAXS, fluorescence measurements, and film composition measurements confirmed the presence of micelles within the multilayer films. These micelles are smaller in the film than in solution, due to complexation with negatively charged carboxylic acid groups. Data also suggest that the micelles have some degree of mobility within the LbL assembly. These films grow in a manner similar to the PAMAM/PAA films discussed in chapter 2.

Additionally, *in vitro* tests indicated that the films created are functional. Drug release studies show that there is prolonged release of drug from the film over a period of several weeks. Due to the versatility of the LbL method, the drug release time can be tuned by either changing the amount of drug encapsulated within the micelles or by changing the number of layer pairs, thereby controlling the total amount of drug within the film. Kirby Bauer tests demonstrate that the drug released is still

active. The results presented demonstrate the applicability of obtaining hydrophobic domains within an LbL film by incorporating charged micelles in order to deliver hydrophobic drugs. This could potentially be applied as a coating to biomedical devices such as stents or catheters.

Chapter 6 References

1. Shchukin, D. G.; Patel, A. A.; Sukhorukov, G. B.; Lvov, Y. *J. Am. Chem. Soc.* **2004**, *126*, 3374-3375.
2. Dejugnat, C.; Halozan, D.; Sukhorukov, G. B. *Macromolecular Rapid Communications* **2005**, *26*, *(12)*, 961-967.
3. Vázquez, E.; Dewitt, D. M.; Hammond, P. T.; Lynn, D. M. J. Am. Chem. Soc. 2002, 124, 13992-13993.
4. Wood, K. C.; Boedicker, J. Q.; Lynn, D. M.; Hammon, P. T. *Langmuir* **2005**, *21(4)*, 1603-1609.
5. Thierry, B.; Kujawa, P.; Tkaczyk, C.; Winnik, F. M.; Bilodeau, L.; Tabrizian, M. Journal of the American Chemical Society 2005, 127, (6), 1626-1627.
6. Berg, M. C.; Zhai, L.; Cohen, R. E.; Rubner, M. F. Biomacromolecules 2006, 7, (1), 357-364.
7. Zhang, L. F.; Eisenberg, A. Science 1995, 268, (5218), 1728-1731.
8. Webber, G. B.; Wanless, E. J.; Butun, V.; Armes, S. P.; Biggs, S. Nano Letters 2002, 2, (11), 1307-1313.
9. Webber, G. B.; Wanless, E. J.; Armes, S. P.; Tang, Y. Q.; Li, Y. T.; Biggs, S. Advanced Materials 2004, 16, (20), 1794.
10. Emoto, K.; Iijima, M.; Nagasaki, Y.; Kataoka, K. J. Am. Chem. Soc. 2000, 122, 2653-2654.
11. Emoto, K.; Nagasaki, Y.; Kataoka, K. Langmuir 2000, 16, 5738-5742.
12. Ma, N.; Zhang, H.; Song, B.; Wang, Z.; Zhang, X. Chemistry of Materials 2005, 17, (20), 5065-5069.
13. Ma, N.; Wang, Y.; Wang, Z.; Zhang, X. Langmuir 2006, 22, (8), 3906-3909.
14. Gitsov, I., Linear-dendritic block copolymers. Synthesis and characterization. In Advances in Dendritic Macromolecules, Newkome, G. R., Ed. Elsevier Science: Amsterdam, 2002; Vol. 5, pp 45-87.
15. Grinstaff, M. W. Chemistry - A European Journal 2002, 8, (13), 2838-2846.
16. Fréchet, J. M. J. Journal of Polymer Science Part A: Polymer Chemistry 2003, 41, (23), 3713-3725.
17. Nguyen, P. M.; Hammond, P. Langmuir 2006, 22, (18), 7825-7832.
18. Kalyanasundaram, K.; Thomas, J. J. Am. Chem. Soc. 1977, 99, 2039.
19. Gitsov, I., Linear-dendritic block copolymers. Synthesis and characterization. In *Advances in Dendritic Macromolecules*, Newkome, G. R., Ed. Elsevier Science: Amsterdam, 2002; Vol. 5, pp 45-87.
20. Grinstaff, M. W. *Chemistry - A European Journal* **2002,** 8, (13), 2838-2846.
21. Fréchet, J. M. J. *Journal of Polymer Science Part A: Polymer Chemistry* **2003,** 41, (23), 3713-3725.
22. Nguyen, P. M.; Hammond, P. *Langmuir* **2006,** 22, (18), 7825-7832.
23. Kalyanasundaram, K.; Thomas, J. *J. Am. Chem. Soc.* **1977,** 99, 2039.

24. Busch, P.; Rauscher, M.; Smilgies, D.-M.; Posselt, D.; Papadakis, C. M., *Journal of Applied Crystallography* **2006,** 39, (3), 433-442.

25. Qi, B.; Tong, X.; Zhao, Y. *Macromolecules* **2006,** *39, (17),* 5714-5719.

26. Cho, J.; Hong, J.; Char, K.; Caruso, F. *J. Amer. Chem. Soc.* **2006,** *128, (30),* 9935-9942.

27. Bauer, A. W.; Kirby, W. M. M.; Sherris, J. C.; Turck, M. *Am. J. Clin. Pathol.* **1966,** 45, 493-496.

Chapter 7

Drug Delivery and Freestanding Films with Prussian Blue

7.1 Introduction

As described previously, the incoporation of inorganic nanoparticles is a well established way to add new functionalities to LbL films. In addition to the synthesis of neutral metal nanoparticles within the film's structure, it is possible to adsorb nanoparticles which are charged, either inherently or by surface modifications. One such example is iron hexacyanoferrate, commonly known as Prussian Blue, a compound that is well known for its electrochromic,[23] electrochemical,[24] and magnetic properties.[25] PB can be synthesized in the form of polydisperse, anionic nanoparticles (median size 4-5 nm) which are stable in aqueous solution,[27] and incorporated into LbL films. These films showed electrochrmoic properties with a large contrast between clear and colored states, meaning that nearly all, if not all, of the PB was electrochemically accessible. PB exhibits a number of stable oxidation states known colloquially as Prussian White (PW), Prussian Blue (PB), Berlin Green (BG), and Prussian Brown (PX), in order of increasing oxidation state. These states are all negatively charged with the exception of PX, which is neutral.[26] Applying a potential of +1.5V (compared to SCE) switches these materials between the PB (negative) and PX (neutral) states.[26]

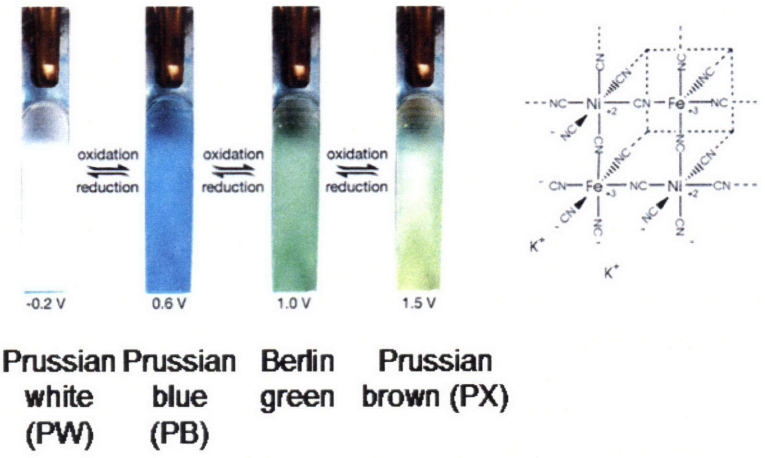

Figure 7-1: Stable oxidation states of iron hexacyanoferrate as well as the structure of its unit cell.

As films assembled with PB nanoparticles and LPEI are held together electrostatically, oxidizing the PB nanoparticles leads to first the swelling of the film, based on repulsion of the like charged LPEI chains, and eventually dissolution of the film. Based on this idea, two different applications were developed. First, encapsulation and delivery of a charged drug within LbL films containing PB, and then the formation of free-standing LbL assemblies. Schematics of these strategies are shown in figure 7.2. For the drug release, holding the assembly in a controlled manner at the Prussian brown state causes the film to slowly dissolve and therefore release. To make free-standing films an electrochemically inactive LbL film is assembled onto the PB layers. Then when the film is held at 1.5 V the PB/LPEI part swells and detaches from the substrate, releasing the entire LbL structure in one piece.

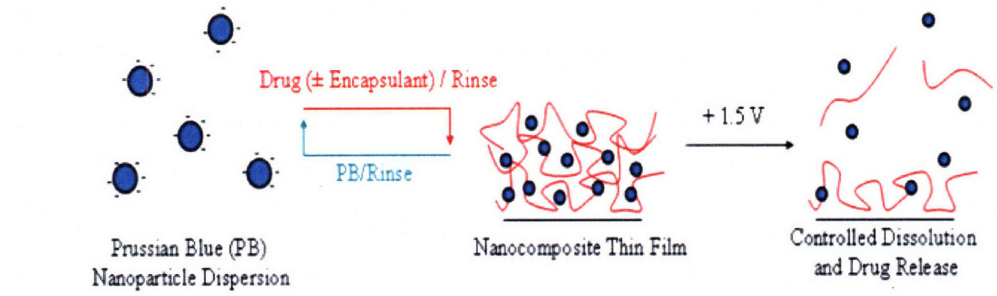

(a)

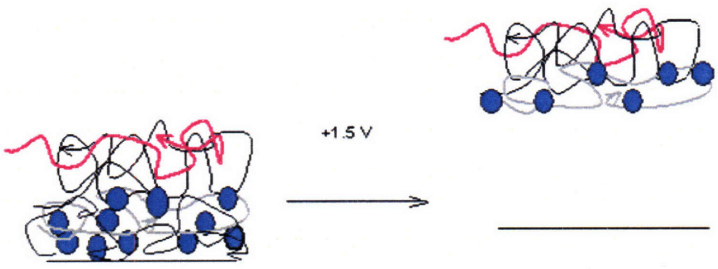

(b)

Figure 7-2: Schematics for (a) drug delivery stategy and (b) film liftoff.

7.2 Experimental Details

Dextran sulfate sodium salt (M_n = 8000) was obtained from Sigma-Aldrich (St. Louis, MO). ^{14}C-dextran sulfate sodium salt (100 µCi, 1.5 mCi/g, M_n = 8000) was obtained from American

Radiolabeled Chemicals, Inc (St. Louis, MO). Radiolabeled and corresponding unlabeled polymers were chosen with similar molecular weights and polydispersities in order to mimic the behavior of the unlabeled species as closely as possible. LPEI (M_n = 25000), and PAA (M_n = 90000) was received from Polysciences, Inc. PAH (M_n = 70000), $FeCl_2$, potassium ferricyanide, and KCl were purchased from Aldrich. All materials and solvents were used as received without further purification.

Synthesis of PB nanoparticles proceeded as follows. Briefly, 35 mL of 10 mM aqueous $FeCl_2$ (Aldrich) was added dropwise to an equivalent volume of 50 mM potassium ferricyanide (Aldrich) and 50 mM KCl, agitated for 1 min, and filtered continuously with deionized water (with magnetic stirring) against a 3000 Da MWCO regenerated cellulose membrane. Permeate solutions (containing ten or more equivalent volumes) were yellow, suggesting that only the excess potassium ferricyanide along with a trivial amount of PB may have passed through the membrane. The retentate solution was collected, pH adjusted to 4 by addition of potassium hydrogen phthalate buffer, and used immediately in LbL assembly.[27]

LbL films were assembled on conducting ITO-coated glass substrates (Delta Technologies, 0.7 cm × 5 cm, 6 Ω/square) for profilometry, deconstruction, and drug release studies. ITO-glass substrates were cleaned via ultrasonication in dicholormethane, acetone, methanol, and deionized water for 15 min each, followed by a 5 min oxygen plasma etch (Harrick PCD 32G) to ensure that the surfaces were clean and abundant in hydroxyl groups. Dextran sulfate, LPEI, PAA, and PAH dipping solutions were prepared at concentrations of 10 mM with respect to the polymer repeat unit, in acetate buffer (100 mM, pH 5.1) for the dextran sulfate and deionized water (pH 4 by addition of HCl) for the other polyelectrolytes. Deionized water used to prepare all solutions was obtained using a Milli-Q Plus (Bedford, MA) at 18.2 MΩ.

LbL films were constructed as follows according to the alternate dipping method using an automated Carl Zeiss HMS Series Programmable Slide Stainer.[8] Briefly, pretreated substrates were submerged in a polycationic dipping solution for 10 minutes followed by a cascade rinse cycle consisting of three deionized water rinsing baths (15, 30, and 45 seconds, respectively). Substrates were then submerged in a polyanionic solution (or PB dispersion) for 10 minutes followed by the same cascade rinsing cycle, and the entire process was repeated as desired to construct (LPEI/PB) films with desired numbers of layer pairs. Tetralayer films containing LPEI/dextran sulfate/LPEI/PB were constructed using the same general protocol; however, in this case, the PB dipping step alternated with a dextran sulfate dipping step (10 min with cascade rinse cycle). Following

deposition, films were immediately removed from the final rinsing bath and dried thoroughly under a stream of dry nitrogen gas. Film thickness and deconstruction experiments on conducting ITO-glass substrates were conducted using a Tencor P10 profilometer by scoring the film and profiling the score. A tip force of 5 mg was used to avoid penetrating the underlying ITO film.

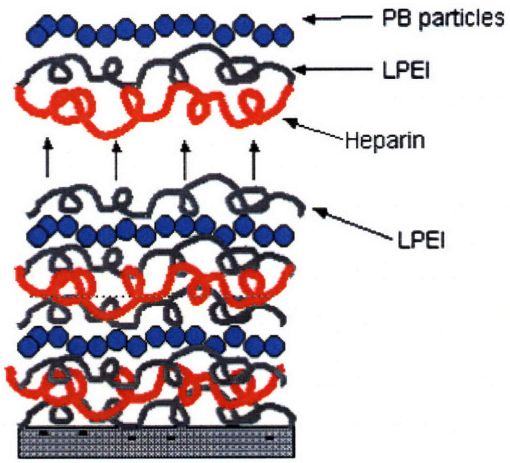

Figure 7-3:tetralayer structure including PB nanoparticles and drug

Electrochemical deconstruction and film liftoff studies were performed using an EG&G 263 A potentiostat/galvanostat. The electrolyte was a 10 mM KCl solution. Approximately 0.3 cm^2 was used, the reference electrode was a K-type saturated calomel electrode, and the counter electrode was a piece of Pt foil (2.5 cm × 2.5 cm).

For drug release experiments, films were formed using a radiolabeled ^{14}C-dextran sulfate sodium salt (100 µCi, 1.5 µCi/mg) dipping solution at a concentration of 4 µCi/mL. The LBL deposition procedure was then performed as described above. Following deposition, ^{14}C-dextran sulfate labeled films were immersed in 100 mL of 10 mM KCl, and electrochemical deconstruction was performed by applying square wave potentials, also as described above. In all cases, films were first immersed for 10 min prior to application of potential, and no passive release was observed. A 1 mL sample was extracted at indicated time points and analyzed for radioactive ^{14}C content by adding 5 mL of ScintiSafe Plus 50% (Fisher Scientific, Atlanta, GA) prior to measurement. Raw data (disintegrations per minute per mL, DPM/mL) were converted to micrograms per mL (µg/mL) of ^{14}C-dextran sulfate

using the conversion factor 2.2 x 10^6 DPM = 1 μCi = 0.67 mg ^{14}C-dextran sulfate. Finally, the total dextran sulfate release from a single film was calculated according to the following equation:

$$M_i = C_i \times V_i + (1mL)\sum_{j=1}^{i-1} C_j \qquad (1)$$

where M_i (μg) is the total cumulative mass released from the film as of measurement i, C_i (μg/mL) is the concentration of sample i, V_i (mL) is the total volume of the deconstruction bath prior to measurement i, and $(1mL)\sum_{j=1}^{i-1} C_j$ is the total mass in previously extracted samples.

Cell viability assays were performed in triplicate using the following protocol. All materials, buffers, and reagents were sterilized prior to use. Cell culture reagents were purchased from Invitrogen Corporation (Carlsbad, CA) and MTT viability assay kits were obtained from American Type Culture Collection (Manassas, VA). Focus HCC cells were grown in 96-well plates at an initial seeding density of 5000 cells/well in 150 μL/well of growth medium (90% modified Eagle's medium supplemented with 10% fetal bovine serum, 100 units/mL penicillin, and 100 μg/mL streptomycin, 0.1 mM non-essential amino acids, 1 mM sodium pyruvate, and 2 mM L-glutamine). HeLa cells were grown in 96-well plates at an initial seeding density of 10000 cells/well in 150 μL/well of growth medium (90% modified Eagle's medium supplemented with 10% fetal bovine serum, 100 units/mL penicillin, and 100 μg/mL streptomycin, 0.1 mM non-essential amino acids, 1 mM sodium pyruvate, and 2 mM L-glutamine). Cos-7 cells were grown in 96-well plates at an initial seeding density of 15000 cells/well in 150 μL/well of growth medium (90% Dulbecco's modified Eagle's medium supplemented with 10% fetal bovine serum, 100 units/mL penicillin, and 100 μg/mL streptomycin). After seeding, cells were allowed to attach and proliferate for 24 h in an incubator (37° C, 5% CO_2). A sterile, 10X concentrated PBS buffer solution was added to an aqueous suspension of PB nanoparticles to yield a final solution containing 1.125 mg/mL PB, 137 mM NaCl, 2.7 mM KCl, and 10 mM Na_2HPO_4 at pH 7.4. Growth media were removed from cells and replaced with the above suspension of PB particles diluted in Opti-MEM (Invitrogen) at concentrations ranging from 0 mg/mL to 1.0 mg/mL PB. In parallel, cells were also incubated with carrier solutions alone (Opti-MEM plus an equivalent concentration of PBS without PB particles) to account for toxicity associated with the carrier solution only. Cells were incubated with the solutions for 4 h, after which solutions were removed and replaced with growth media. After 72 h, cell metabolic activity was assayed using the MTT cell proliferation assay kit (ATCC, Manassas, VA). Initially, a

10 μL aliquot of MTT assay reagent was added to each well. After incubating for two hours, 100 μL of detergent reagent was added. The plate was then covered and left in the dark for 4 h, after which optical absorbance was measured at 570 nm using a SpectraMax 190 microplate reader (Molecular Devices, Sunnyvale, CA). Background (media plus MTT assay reagent plus detergent reagent with no cells present) was subtracted from the value of each well, and all values were normalized to the value of control (untreated) cells. In similar fashion, the toxicity of an equivalent amount of PBS buffer in Opti-MEM (with no PB) was calculated. Values reported in Figure 5 represent the normalized viability of PB-treated cells divided by the normalized viability of cells treated with equivalent amounts of pure PBS (to account for the toxicity of PBS itself).

7.3 Drug Delivery

7.3.1 Background

Recently, great interest has centered on the development of 'smart' controlled release systems capable of administering drugs in response to external stimuli such as electric or magnetic fields for use in applications such as controlled release implants ('pharmacy-on-a-chip').[1-3] Toward these goals, microfabricated devices have been developed which make use of micrometer-scale pumps, channels, and wells to deliver drugs on demand.[1-5] However, while these technologies have resulted in encouraging new treatment possibilities, several challenges still remain. For example, the direct integration into non-planar, functional or structural implants such as arterial stents, medical sutures, and bone prostheses is challenging, as photolithographic and micromachining techniques are primarily developed for planar, silicon-based substrates.[6] Further, the multi-step processing of these devices can be both time consuming and expensive.[7] Here, we demonstrate for the first time the fabrication of ultrathin films made from nontoxic, FDA-approved materials which can undergo remotely controlled dissolution to release precise quantities of drugs in response to a small applied voltage (+1.5V). These nanoscale systems can be used to conformally coat surfaces of virtually any shape, size, or chemical composition, and represent a new class of versatile, responsive drug delivery systems.

Electroactive thin films are constructed using the layer-by-layer (LbL) directed self-assembly technique, which utilizes the alternating adsorption of materials containing complementary charged or functional groups onto a solid substrate to form thin films.[8] This method can be used to create highly

tunable, conformal thin films with nanometer-scale control over film composition and structure. The only criteria for inclusion in an LbL thin film is that the species of interest either possess, or that it be encapsulated in a 'carrier' species (i.e., nanoparticle, micelle, dendrimer, etc.) that possesses the desired complementary functional group. Thus, a wide range of components including polymers, proteins, nucleic acids, small molecules, and nanoparticles have been incorporated into these assemblies, which can further be constructed in a range of interesting geometries and patterns.[9, 10] As a result of this versatility, LbL thin films have been used in a variety of drug delivery applications, most notably as coatings that can release drugs passively[11-13] or in response to environmental changes such as pH or ionic strength.[14-22]

Here, we demonstrate that by applying a low voltage to PB nanoparticle-based LbL thin films, and thus changing the PB oxidation state from negative to zero-valent, we can induce repulsion of adjacent, like-charged layers, rapid film destabilization, and controlled release of the film's components. We believe that this destabilization is based on the loss of electroneutrality occurring within the film following the PB to PX transition, resulting in the repulsion of adjacent, like-charged layers. Destabilization is associated with swelling and then release of the film's components into solution, and we quantify this controlled release using a model, radiolabeled drug (14C-dextran sulfate). We further show that this release is well-controlled; that is, removal of the oxidizing potential results in restabilization of the remaining film. Finally, as a measure of biocompatibility we demonstrate that PB particles exhibit no measurable toxicity on a panel of mammalian cell lines at concentrations up to 1.0 mg/mL. Together, this technology represents a new robust, inexpensive, and versatile platform for the fabrication of nanostructured, field-activated (remote-controlled) drug delivery systems.

7.3.2 Results and Discussion

In order to encapsulate durg within the PB films a glass substrate coated with a conducting film of indium tin oxide (ITO) is first dipped in a solution containing a cationic drug or drug-containing 'carrier' species, then rinsed in deionized water. Next, the substrate is dipped into an aqueous PB solution at pH 4 and rinsed again in deionized water. The process is repeated to build up a multilayer nanocomposite film with desired properties. Controlled film deconstruction occurs upon the application of an electrochemical potential of +1.5 V, "switching" PB to the neutral PX state and releasing the encapsulated species. Removing the potential reduces the particles back to the anionic

PB state, allowing one the ability to switch the assembly back and forth between stable and unstable states.

Figure 7.1 depicts the structure of 'soluble' PB, $KFe^{III}[Fe^{II}(CN)_6]$. Potassium inclusions in this form of PB can dissociate in aqueous solutions, resulting in a net negative charge on the particle surface which renders nanoparticles stable in solution. PB nanoparticles are formed via the room temperature, aqueous-phase reaction that occurs upon the addition of a molar excess of potassium ferricyanide to iron(II) chloride (see Methods). This synthesis and purification procedure yielded dark blue, aqueous suspensions that were stable in the absence of sonication or chemical stabilizers.

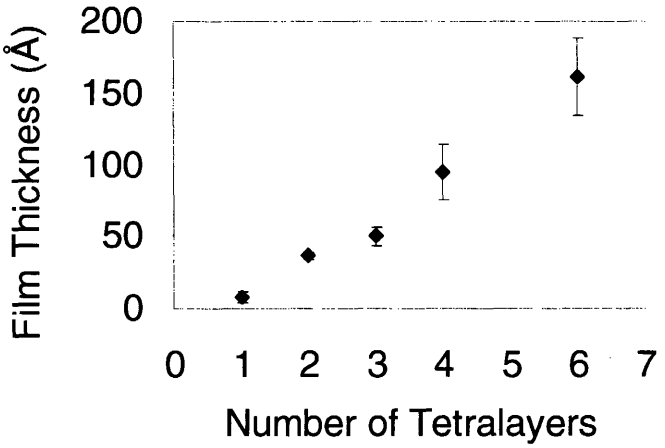

Figure 7.4: Total film thickness (Å) versus number of deposited tetralayers for the $(PB/LPEI/DS/LPEI)_6$ system as determined by profilometry. Measurements were performed at five predetermined spots on the surface of the films. Error bars represent one standard deviation.

Figure 7.4 shows the linear build-up of the tetralayer system containing LPEI/dextran sulfate/LPEI/PB used in this study (measured by profilometry). Tetralayer systems, rather than traditional layer pair systems, were used in order to encapsulate and release ^{14}C-dextran sulfate, our negatively charged model drug species. The thickness of an average tetralayer was 2.3 ± 0.3 nm. (This value reflects the average of five data points taken at various positions on the surface of the film.) Films were observed to grow linearly in thickness with increasing numbers of layers. The linear growth behavior observed in these systems may have important implications for the controlled delivery of precise quantities of drugs, as the thickness (and mass) of a given layer can be precisely predicted with no dependence on the thickness of the underlying film, resulting in facile control over drug payloads.

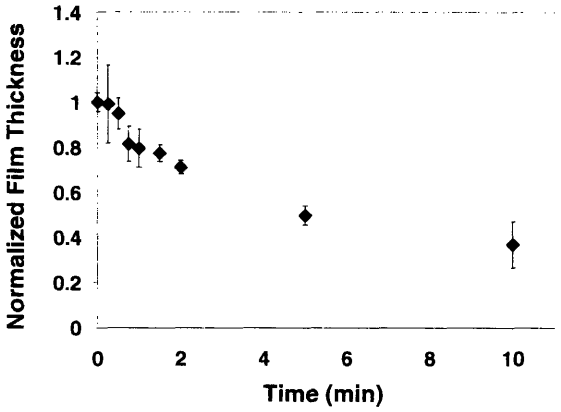

(a)

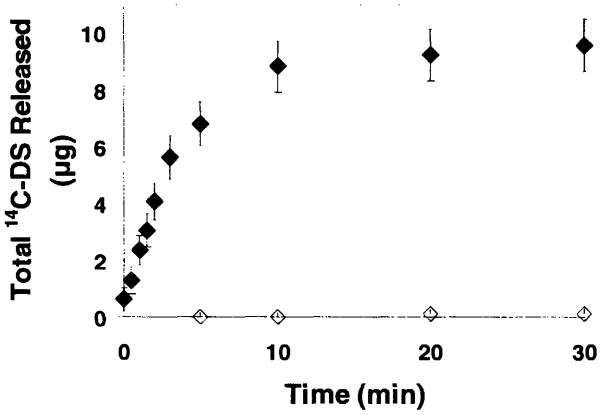

(b)

Figure 7.5. Applying a constant potential of +1.5 V results in deconstruction and drug release from (PB/LPEI/^{14}C-dextran sulfate/LPEI)$_{30}$ systems. (a) Total film thickness versus time with constant potential held at +1.5 V. Error bars represent one standard deviation of the measured thickness values at five predetermined locations on the surface of the film. As such, error bars provide an indication of the surface roughness of films (standard deviation of multiple thickness measurements taken at a single location was less than 10 Å). (b) ^{14}C-Dextran sulfate release versus time with potential held constant at +1.5 V (closed diamonds) or no applied potential (open diamonds; error bars are small). All error bars represent one standard deviation in measured values.

Figure 7.5 shows the deconstruction and drug release behavior of 30 tetralayer LPEI/^{14}C-dextran sulfate/LPEI/PB systems under the influence of an applied voltage held constant at +1.5V. Film thickness was observed to decline rapidly during the first 5-10 minutes, reaching 30-40% of original film thickness by 10 minutes (see Figure 2(a)). Thereafter, thickness decreased only subtly to a value

of around 20% of the original film thickness after 30 minutes (data not shown). Corresponding measurements of ^{14}C-dextran sulfate release (Figure 2(b)) show that all of the observed drug release also occurred during the first ten minutes. It appears on the basis of this data, as well as analogous deconstruction behavior observed in PB/LPEI systems (see Figure S1, Supplemental Materials), that PB-containing films are quickly destabilized by the applied potential, resulting in rapid film deconstruction. To verify that release occurs only in the presence of an applied potential, we soaked films in a solution identical to those used in the deconstruction experiments (10 mM KCl) and observed no significant drug release (Figure 2(b)).

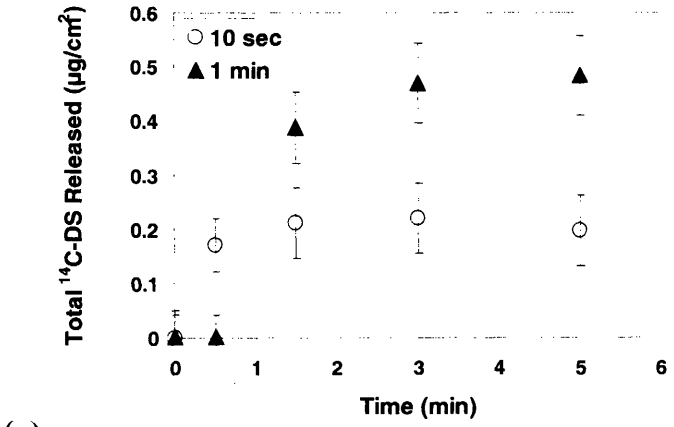

(a)

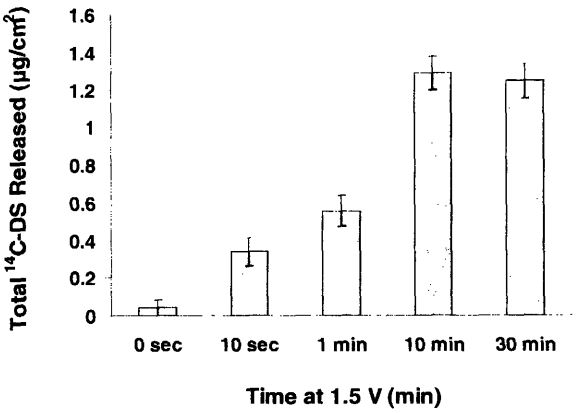

(b)

Figure 7.5. Examining the kinetics of film deconstruction in response to an applied potential of +1.5 V in (PB/LPEI/^{14}C-dextran sulfate/LPEI)$_{30}$ systems. (a) ^{14}C-Dextran sulfate release after applying potential for 10 s and 1 min intervals. (b) Total ^{14}C-dextran sulfate release from equivalent samples

held at the oxidizing potential for varying times. In all cases, error bars indicate one standard deviation.

To more closely examine the kinetics of film deconstruction, we measured drug release from representative 30 tetralayer LPEI/14C-dextran sulfate/LPEI/PB systems under the influence of a square wave potential of +1.5V for varying amounts of time. All films used in these studies were deposited onto identical 2.45 cm2, ITO-coated glass substrates from the same dipping solutions in order to ensure uniform thickness and drug loading. Figure 7-5(a) shows the release due to 10 s and 1 min square wave intervals at +1.5 V. Application of the oxidizing potential for very short intervals (10 s) is not sufficient to significantly destabilize the film, likely because diffusion of polyelectrolytes out of the destabilized structure is the rate-limiting process (PB redox switching times are less than 1 s).27 Thus, only a relatively small amount of 14C-dextran sulfate was released. A longer interval (1 min) at the oxidizing potential results in significantly greater total drug release. Further, in both cases the drug release was observed to stop shortly after removing the potential, suggesting that films can become restabilized. In Figure 7-5(b) the drug release in response to differing time intervals at +1.5V is shown. Films release significantly more drug following 10 min and 30 min intervals than shorter 10 s or 1 min intervals, an indication of the reversible nature of film destabilization. Further, 10 min and 30 min intervals result in similar quantities of drug release with similar kinetics (data not shown), suggesting that all of the available drug was released within the first 10 min. This is in agreement with the data in Figure 2(b), which shows that ~10 min at a 1.5 V potential is sufficient to achieve complete release. From this data, we can conclude the following: (1) the process of destabilization can be reversed by removing the oxidizing potential so long as this occurs prior to complete film deconstruction; (2) diffusion of the film's components out of the destabilized film structure is a rate-limiting step; and (3) deconstruction and release from 30 tetralayer systems is completed in fewer than 10 min when held at constant potential.

An interesting phenomenon that we observed in all cases is that film thickness decreased by only ~80%, leaving behind a fraction of the film on the substrate surface even after holding the oxidizing potential constant for long amounts of time (e.g., 1-2 h). We hypothesize that the remaining material is composed of oxidized hydrophobic PX particles which aggregate at the substrate-liquid interface. To characterize this material, we used atomic force microscopy (AFM) and UV-Visible spectroscopy (UV-Vis) (Figure 7-6). Figures 7-6(a), 7-6(b), and 7-6(c) show AFM images of a (LPEI/14C-dextran sulfate/LPEI/PB)15 film (PB is the outermost surface layer) taken after application of the oxidizing potential of +1.5V for 0, 1.5, and 10 min, respectively. Initially, the film surface exhibits small,

regular surface features that likely reflect a monolayer of nanoparticles on the film surface. Following degradation, the film surface becomes rougher, and larger, agglomerated particles become visible. This data supports the hypothesis that oxidized hydrophobic PX particles aggregate at the substrate surface following degradation. Further, the observed changes in surface morphology parallel the changes in film thickness and drug release with time; in all cases, the majority of the observed deconstruction occurs during the first 2-3 minutes following application of the oxidizing potential. To gain a quantitative measure of PB depletion from the film during deconstruction, we used UV-Vis spectroscopy. Figure 7-6(d) shows transmission through films at 530 nm before and after deconstruction. Although transmission increases following deconstruction, it never fully reaches 100%, suggesting that while some PB is lost into the surrounding solution, most of it remains on the substrate surface. The fact that absorbance decreases by only ~10% during deconstruction, whereas film thickness decreases by about 70% over this same time period, suggests that the majority of the material released during the film deconstruction is LPEI and dextran sulfate, not PB, which largely remains in the film assembly. This further suggests that the surface morphology observed via AFM owes to the presence of insoluble or aggregated PB particles on the film surface. The fact that the drug and carrier species are selectively released from the film while the PB component is retained may be advantageous in drug delivery applications, as it may help to prevent undesired tissue accumulation of PB.

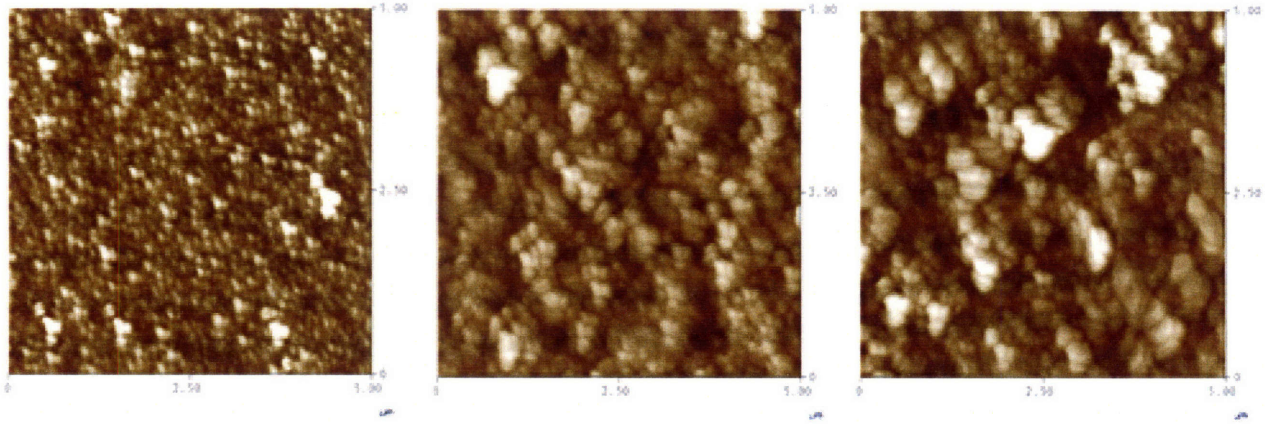

(a) **(b)** **(c)**

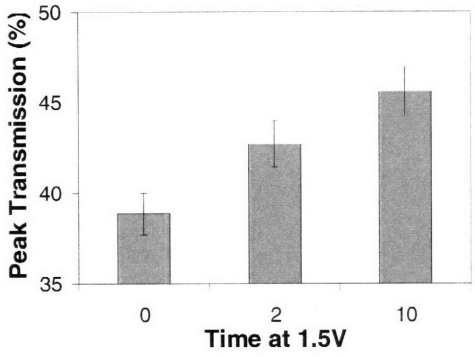

(d)

Figure 7.6. Morphological and optical analysis of film deconstruction. Height-mode AFM images showing the surface of (LPEI/^{14}C-dextran sulfate/LPEI/PB)$_{15}$ films after (a) 0 min, (b) 1.5 min, and (c) 10 min at the oxidizing potential of +1.5V. Each image depicts a representative 5 μm × 5 μm area on the film surface (Z-range, height scale, 100 nm). (d) Plot of peak transmission at 530 nm (via UV-Visible Spectroscopy) following 0, 2, and 10 min of constant voltage at the oxidizing potential of +1.5V (background subtracted).

Finally, as a measure of the biocompatibility of PB nanoparticles, we measured their toxicity on a panel of mammalian cell lines, including hepatocellular carcinoma (HCC), ovarian cancer (HeLa), and kidney fibroblast (Cos-7) cells, using a conventional MTT assay. The MTT assay measures the effect of added substances on cell growth and metabolism, and is commonly used as an *in vitro* measure of toxicity.[28] Interestingly, PB particles caused no observable toxicity at all concentrations tested (up to 1.0 mg/mL) (Figure 5). These findings are not surprising, as PB is known to cause no adverse health effects in humans and was approved by the US FDA in 2003 for the treatment of radiation contamination and heavy metal poisoning.[29]

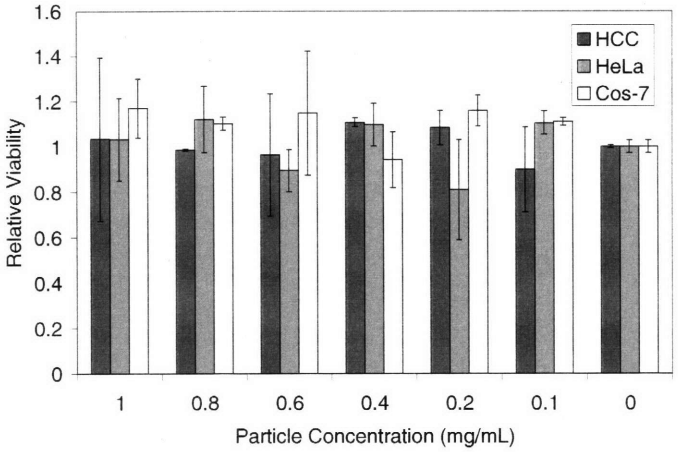

Figure 7.7. MTT assay for cellular toxicity indicates that PB nanoparticles exhibit no toxicity on three different cell lines at concentrations up to 1.0 mg/mL. Error bars represent one standard deviation.

7.3.3 Conclusions

We have demonstrated a new approach for constructing nanostructured thin films capable of releasing precise quantities of chemicals on demand in response to small electrochemical potentials. Further, we have shown that the films are stable enough to release a fraction of their contents, then restabilize upon removal of the applied potential. The LbL technique is sufficiently general to allow for the incorporation of chemicals of any structure (small molecules, macromolecules, charged and uncharged species, etc.) into these systems, alone or in conjunction with a 'carrier' species.[8-10] As a simple proof of principle, we have studied the (LPEI/dextran sulfate/LPEI/PB) system, in which the model chemical species of interest (dextran sulfate) is alternately deposited (in conjunction with a 'carrier' species, LPEI) with the electroactive component, PB. Similar model drug species that are currently under study include heparin sulfate and a range of charged proteins.[17, 30] Finally, we have outlined a mechanistic hypothesis to explain the deconstruction process occurring in these systems, whereby an electrochemical signal oxidizes the nanoparticles to the PX state, resulting in loss of particle charge and destabilization of the film through self-repulsion of the polycation species. We expect that these electroactive controlled release thin films may find interesting applications in fields including drug delivery, tissue engineering, medical diagnostics, analytical chemistry, and chemical detection. Further, using the various thin film patterning techniques developed in recent years, we

suggest that these materials may eventually be arrayed to produce multi-drug or multi-dose 'smart' devices.[1]

7.4 Free-standing Film Formation

While one of the advantages of LbL assembly is how easily a wide range of substrates can be coated, for certain applications it may be desirable to use free-standing films. One method for creating such structures is to coat microparticles with an LbL assembly and then dissolve the core, leaving a haollow microcapsule. One application for these is to load drug into the hollow center and then use the diffusion process as a strategy for drug delivery. Other methods include assembling the film on a hydrophobic substrate and then peeling it off (although for this the films must be quite thick; on the order or microns) or using a sacrificial layer or substrate. Examples of this second technique include assembling the film on glass and then using HF to dissolve the glass substrate, or assembling a layer onto a hydrogen bonded sacrificial layer, and then exposing the structure to pH conditions under which the sacrificial layer dissolves. The use of sacrificial layers allows for much thinner free-standing LbL assemblies; on the order of hundreds of nanometers, but the necessary harsh solvents or salt/pH conditions are not always desirable. Our strategy of employing a sacrificial layer allows for film release over a wide range of pH and ionic strength conditions, and allows for precise control of the timing of film liftoff.

For our system we chose layers of PAA/PAH to be deposited onto the PB/LPEI multilayer. This particular polyion pair was chosen because it had previously been shown to support the growth of cells. The films were first soaked overnight in 1 mol KCl solution in order to demonstrate stability in the presence of salt, as high ionic strength has been known to dissolve LbL assemblies. For the film liftoff, the samples were held at +1.5 V as described in the experimental details section. Figure 7-8 (a) shows that the films are indeed stable in a KCl solution with no applied voltage. Figure 7-8 (b) shows the same film after having been held at +1.5 V for approximately 1 hour; it can be clearly seen that the the film has begun to peel off of the substrate. In order to more cleanly remove a portion of the film, a small square was cut on a sample using a razor blade. When this sample was held at +1.5 V the small square lifted off in entirety. Figure 7-9 shows both the sample after the small square was lifted off and the small square which had been collected onto a glass slide. When the film lifts off into the electrolyte solution it does not crumple, and can be transferred onto another substrate as a smooth film.

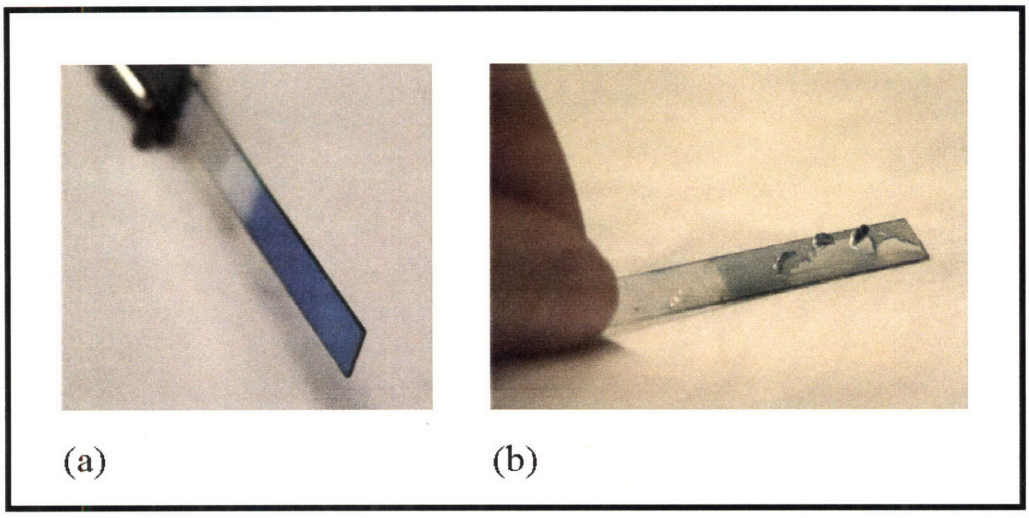

Figure 7-8: (a) LPEI/PB + PAH/PAA film after soaking overnight in 1 mol KCl solution; film is stable after exposure to salt at 0V (b) same film after Being held at +1.5 V for approximately 1 hour; film has lifted off the substrate.

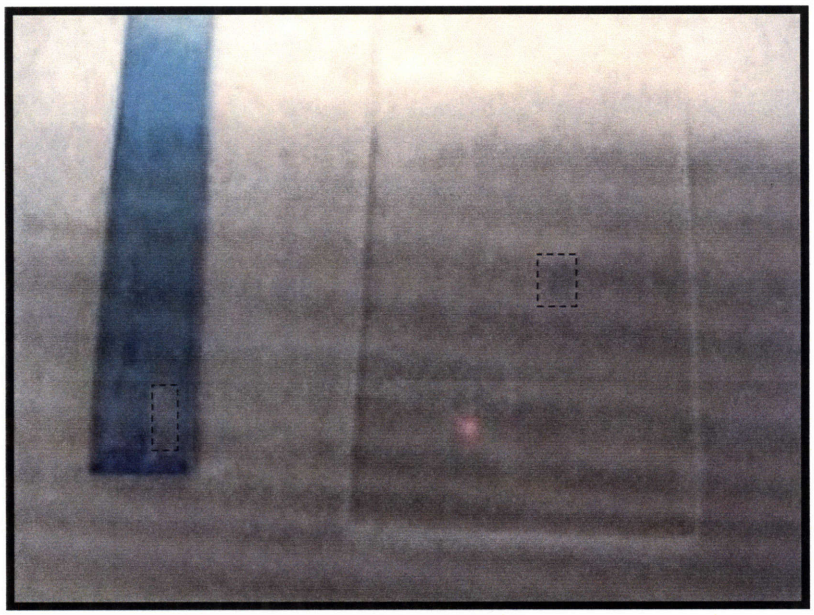

Figure 7-9: Lefthand figure shows the LPEI/PB + PAH/PAA substrate from which a small square has been removed, and the righthand image shows that square after being collected onto a glass microscope slide.

Since the system that was chosen supports cell growth, one possible application could be to transfer cells from one substrate to another, or a type of negative cell patterning (or indeed in general thin film patterning), achieved by removing sections from a substrate.

Chapter 7 References

1. LaVan, D.; McGuire, T.; Langer, R. *Nat Biotechnol.* **2003** *21*, 1184-1191.
2. Santini, J.; Richards, A.; Scheidt, R.; Cima, M.; Langer, R. *Angew Chem Int Ed* **2000**, *39*, 2396-2407.
3. Santini, J.; Cima, M.; Langer, R. A. *Nature* **1999**, *397*, 335-338.
4. Razzacki, S.Z.; Thwar, P.K.; Yang, M.; Ugaz, V.M.; Burns, M.A. *Adv Drug Deliv Rev* **2004**, *56*, 185-198.
5. Staples, M.; Daniel, K., Cima, M.J. ; Langer, R. *Pharm Res* **2006**, *23*, 847-863.
6. Reed, M. et al. *J Pharm Sci* **1998**, *87*, 1387-1394.
7. Duffy, D.; McDonald, J.; Schueller, O.; Whitesides, G. *Anal. Chem.* **1998**, *70*, 4947-4984.
8. Decher, G. *Science* **1997**, *277*, 1232-1237.
9. Hammond, P. T. *Colloid Interface Sci* **2000**, *4*, 430-432.
10. Hammond, P. T. *Adv. Mater.* **2004**, *16*, 1271-1293.
11. Caruso, F.; Schuler, C. *Langmuir* **2000**, *16*, 9595-9603.
12. Shi, X.; Caruso, F. *Langmuir* **2000**, *17*, 2036-2042.
13. Sukhorukov, G. B.; Brumen, M.; Donath, E.; Mohwald, H. *J Phys Chem B* **1999**, *103*, 6434-6440.
14. Jewell, C., Zhang, J., Fredin, N. & Lynn, D. *J. Control Release* **2005**, *106*, 214-223.
15. Vazquez, E., DeWitt, D., Hammond, P. T.; Lynn, D. *J. Am. Chem. Soc.* **2002**, *124*, 13992-13993.
16. Wood, K. C.; Boedicker, J.; Lynn, D.; Hammond, P. T. *Langmuir* **2005**, *21*, 1603-1609.
17. Wood, K. C.; Chuang, H.; Batten, R.; Lynn, D.; Hammond, P. T. *Proc Natl Acad Sci USA* **2006**, *103*, 10207-10212.
18. Zhang, J.; Chua, L.; Lynn, D. M. *Langmuir* **2004**, *20*, 8015-8021.
19. Chung, A.; Rubner, M. F. *Langmuir* **2002**, *18*, 1176-1183.
20. Hiller, J.; Rubner, M. F. *Macromolecules* **2003**, *36*, 4078-4083.
21. Ma, Y.; Dong, W. F.; Hempenius, M.A.; Mohwald, H.; Vancso, G.J. *Nat. Mater.* **2006**, *5*, 724-729.
22. Schuler, C.; Caruso, F. *Biomacromolecules* **2001**, *2*, 921-926.
23. Mortimer, R. *Chem. Soc. Rev.* **1993**, *26*, 147-156.
24. Karyakin, A.; Gltelmacher, O.; Karyakin, E. *Anal. Chem.* **1995**, *67*, 2419-2423.
25. Mingotaud, C.; Lafuente, C.; Amiell, J.; Delhaes, P. *Langmuir* **1999**, *15*, 289-292.
26. Neff, V. *J. Electrochem. Soc.* **1978**, *125*, 886-887.
27. DeLongchamp, D. M.; Hammond, P. T. *Adv. Func. Mater.* **2004**, *14*, 224-232.
28. Hansen, M.; Nielsen, S.; Berg, K. *J Immunol Methods* **1989**, *119*, 203-210.
29. Pearce, J. *Food Chem Toxicol* **1994**, *32*, 577-582.
30. Wood, K. C.; MacDonald, M.; Smith, R.; Chuang, H.; Hammond, P. T. unpublished data **2006**.

Chapter 8
Summary and Future Work

8.1 Summary and Conclusions

Polyelectrolyte multilayers have been a topic increasingly studied in the last decade or so. Beginning with Iler's work in the 60's,[1] but not fully appreciated until the 90's starting with Decher,[2] the direction of the complexation between oppositely charged polyelectrolytes onto a surface in order to create a film can be a powerful tool. LbL films can incorporate inorganic species such as quantum dots or nanoparticles or biological macromolecules such as proteins or even viruses. Their proposed applications range from thin coatings to modify surface properties such as wettability to stand alone devices such as photovoltaic cells or sensors. As these proposed applications become more complex and use a wider variety of materials, greater understanding of film structure is necessary.

LbL films are highly sensitive to small perturbations of assembly parameters – including (but not limited to) dipping time, rinsing steps, charge density of the polyelectrolytes used. Method of deposition can also lead to significant differences in film properties. These structures are kinetically trapped, and post-processing such as annealing or exposure to solution of a different pH than the assembly conditions[3,4] can lead to new structures. Secondary interactions such as hydrophobic interactions or hydrogen bonding can further complicate the matter. Furthermore, weak polyelectrolytes are strongly influenced by local variation in charge density. This means that when brought into close proximity, weak polyelectrolytes will redistribute and change their charge densities in order to minimize their free energy.[5]

Although LbL films have long been understood to not be precisely stratified, "layer-by-layer" structures, it has only more recently become clear that in certain systems the entire film participates in the assembly process due to diffusion of polymer chains throughout the bulk film. These diffusion has been proposed to be the cause for such phenomena as extended, nonlinear growth,[6,7] disruption of LbL heterostructures,[8] and exchange of polymer chains within LbL films.[9,10] Understanding of what factors influence a polyelectrolyte's mobility within a particular polyelectrolyte multilayer can help to predict when diffusion might become a dominating process in LbL assembly.

Polymer chemical functionality, hydrophobicity, and molecular architecture can all be expected to influence LbL film assembly. The complexation between two oppositely charged polyelectrolytes is

not just ion pair formation between plus and minus charges, but chemical interactions between different functional groups. Differences in the enthalpy of complexation[11] will cause certain polyelectrolyte pairs to form preferentially and other differences in film structures. When using weak acids and bases, relative basicity or acidity will change the complexes formed. Hydrophobicity, or how well the polymer is solvated in solution will effect chain mobility and the driving force for those polymer chains to adsorb onto a surface. Electrostatically bound LbL films are composed of ionic crosslinks as well as physical entanglements, which the size and shape of the specific polyelectrolytes should effect.[12]

In this thesis a series of polyelectrolyte multilayers containing PAA and a polyamine were examined. The four polyamines used were LPEI, BPEI, G4 PAMAM dendrimer, PAH. These four polycations were chosen because they each have similar chemical functionality but vary in other properties such as molecular geometry or hydrophobicity. The multilayers were probed in order to determine the influence of the polycation structure and relative basicity of amine groups on the overall properties of the polyelectrolyte multilayers.

In Chapter 2, basic film properties such as film thickness, chemical functional group availability, and relative composition of the LbL films were measured. The various systems showed thickest film growth when both polyelectrolytes were partially charged, and PAA within all of the films was more charged than when observed alone as cast films. PAH containing multilayers were the most ionized, and PAMAM containing multilayers the least ionized.

PAMAM containing films are much thicker than the other films, anunexpected result given that the diameter of the fully extended dendrimer in solution is ~5 – 7 nm, much shorter than the average end-to-end distance of the other polycations. We attribute this to the fact that many of the dendrimer's amine groups are difficult for the PAA chains to access due to their close proximity to each other, causing PAMAM/PAA films to have a large number of free carboxylic acid groups. These neutral –COOH groups will be able to lie close to one another and hydrogen bond. The hydrogen bonding interactions therefore are able to stabilize the LbL film's interior ctructure. Evidence for hydrogen bonding in these films can be seen in the FTIR spectra of PAMAM/PAA and pH 3 and 4, by the doublet around 1710, the peak for neutral carboxylic acid groups. PAH/PAA films are the thinnest over the pH assembly range studied because PAH is strongly charged. These films have strongly charged carboxylic acid groups.

Chapter 3 looks at deposition of LbL films using an automated spraying system, in order to speed up the process as well as deposit films onto substrates not well suited to the dipping technique, such as textiles. Spraying (at least by our process, as different groups using other parameters report different results) results in thinner films, and at very low number of bilayers (<2) gives better coverage and smaller "island" growth than the dipping technique.

Films misted onto Nucleopore membranes were then exposed to organic vapor (of a half mustard gas, chloroethyl ethyl sulfide, or CEES) to determine which system would act as the best diffusion barrier. Preliminary testing gives us the result that PAH/PAA films are the best diffusion barrier and that PAMAM/PAA films are the worst. This correlates roughly with the fact that PAH/PAA films are the thinnest and most ionic crosslinked, and that the PAMAM/PAA films have by far the highest per bilayer thickness, suggestion an "open" film structure. Therefore diffusivity of CEES is highest in the PAMAM containing films and lowest in the PAH containing films. The solubility of CEES vapor in the multilayers was found to follow the opposite trend; PAH containing films had the highest solubility and PAMAM containing films the least. CEES is a polar molecule, and was seen to be most soluble in the most highly ionized films.

Chapter 4 looks at synthesis of metal nanoparticles within LbL films. Many groups have reported metal NPs within LbL films, usually formed by exposing a film to a metal malt solution and then to a reducing agent. Our method was different in that metal NPs were first formed in PAMAM dendrimers, which were then used to assembly multilayer films. Metal NP synthesis within LbL films as reported by Crooks, et al suggests that the interior amine groups and amide linkages are used to coordinate metal ions. Our FTIR data from Chapter two suggests that the PAMAM interior groups are not utilized in ionic crosslinks within the LbL films; therefore films assembled with PAMAM-NP hybrids should be expected to have similar properties to PAMAM/PAA films. Our method gives us the possibility of added several different types of nanoparticles into a film in a known ratio – either by using different dendrimer-NP solutions or utilizing the –COOH groups of the PAA chains after film assembly. We showed that Pd nanoparticles synthesized within PAMAM dendrimers and then assembled into LbL films can used for the catalysis of hydrogenation of allyl alcohol.

Chapter 5 provides an example of how LbL heterostructures can be disrupted by diffusion. It was demonstrated by optical microscopy, FTIR, and UV-vis spectroscopy that when LPEI/PAA was assembled onto a pre-existing PXV/PAA multilayer the result is an opaque disrupted film that has expelled the PXV content. The PXV polymer used was of high molecular weight, meaning that the

driving force for this process is not simply entropic benefits of releasing smaller molecules into solution, but preferential complexation between LPE and PAA. FTIR also shows that LPEI/PAA multilayers are more ionically crosslinked than PXV/PAA multilayers.

In order to explain which of LPEI's properties explains this film disruption, the other polyamines were tested for this, at a variety of pH conditions. It was seen that all four polycations are able to undergo this exchange process with PXV under some circumstances; when the solution pH is such that the polycation is only partially charged. For example, PAH does not show this exchange at all over the pH range of 3 – 6, but does at pH 10. It seems that the more extended, charged chains are too "sticky" to move through the multilayer structure, but rather immediately adsorb. PAMAM shows a similar trend; at or above pH 5 it is able to exchange with PXV. When fully charged, the dendrimer is not mobile throughout the film structure. Using this information, we were able to prevent diffusion of LPEI into the PXV/PAA by introducing several layers of PAH/PAA (assembled at pH 4) in between the two systems. The PAH did not diffuse into the PXV/PAA multilayer and do to its thin and stretched out nature, further prevented LPEI diffusion.

Chapters 6 and 7 examine new strategies for drug delivery using LbL assemblies. In Chapter 6 the encapsulation of micelles within LbL films using dendritic-linear-dendritic block copolymers was investigated. Micelles monolayer adsorption onto surfaces has been considered for drug encapsulation and creation of responsive films. Micelles have also been incorporated into LbL structures in a few instances, stabilized either solely by electrostatics[13, 14] or by chemical crosslinking.[15, 16] Drug delivery with these systems was shown to be very short; on the order of minutes or hours. PAMAM-PPO block copolymers have been developed by our group for encapsulation of hydrophobic drug and drug delivery in solution. We took hydrophobic drug containing micelles formed by these systems and incorporated them into LbL structures with PAA. UV-vis and GI-sax confirmed that their micellar structure remained intact without any need for chemical crosslinking. GI-sax also suggested that the micelles were well ordered parallel to the substrate, but less so perpendicularly. Given that these films were assembled at pH 5 and the outer portion of the micelles are PAMAM dendrons, we explain this by the mobility of PAMAM within a LbL structure at those assembly conditions. The drug delivery from our films last over a period of days, and was improved compared to the drug release of these micelles in solution.[17]

Chapter 7 described the use creation of electrochemically responsive LbL films using LPEI and Prussian Blue (PB) nanoparticles. PB nanoparticles are a negatively charged dispersion as

synthesized, and exhibit a number of stable redox states. One of these is an electrically neutral state. When the particles are held at this state, the then unshielded positive charges of the LPEI chains repel each other causing the film to swell and then deconstruct. We were able to demonstrate incorporation of drug into these films and then delivery of this drug upon film deconstruction.

Another proposed usage for the PB system is the creation of free-standing LbL structures. When another LbL film is assembled onto a PB/LPEI film, when the PB particles are held at a neutral state the PB/LPEI film detaches from the substrate but remains attached to the other LbL assembly, creating a free-standing film in solution. We had success at causing film liftoff using PAH/PAA and PAH/sulfonated polystyrene (SPS) systems, which we know do not diffuse into the underlying multilayer.

8.2 Suggestions for Future Work.

While the work presented here has attempted to explain how different polycations geometries can alter the properties of multilayers, many questions remain. Although the polycations examined all contained amine groups, the relative basicity of primary, secondary, and the tertiary amine groups will play some role in the complexation with the polyanion. Again, because of the different types of amine groups in each polycations, the charge density at each of the pH values which was considered, which no doubt also plays some role in the film properties. The third factor that needs to be considered is the hydrophobicity of the polycations. The hydrophobicity of the PAH backbone is likely the major factor as to why it exhibits little mobility within LbL constructs. All of these properties of the different weak polyelectrolytes contribute to the resulting LbL assembly properties. Further investigation to deconvolute these would prove valuable. Using hyperbranched PEI, or dendrimers of higher generation could further explain the effect of molecular architecture.

In terms of polycation mobility within multilayers, a general set of properties that could predict this behavior would be of great use. In this work, polymer hydrophilicity and partial charge (i.e. more coiled rather than more extended conformations) have been shown to be more mobile. We have seen PXV be replaced by a number of polycations. PXV is a hydrophobic polymer which (given lower degrees of PAA ionization) does not seem to form a very strong complex with PAA. A more quantitative study of enthalpies of complexation might prove as a predictor to when this behavior will occur – then we could predict if LPEI would replace PAH or BPEI. Again, degree of branching seems

as though it should affect polymer mobility, as it does change viscosity and other solution state behaviors, so it would be interesting to try these experiments with higher generation dendrimers. Other works correlate diffusion in LbL films to non-linear, or extended super-linear (that is, extended beyond the first 3-5 bilayers) growth. It would be interesting to investigate if all of the systems reported as super-linearly growing could exchange in certain situations, and if all those systems which can exchange show super-linear growth.

The PB drug delivery system still needs development to be truly interesting. The films do show a small degree of passive release, which would ideally be eliminated. Although the system is responsive in that the release can be stopped and started again, a materials system that degraded over a longer time span would be of greater interest. Likely using a more hydrophobic polycation than LPEI would extend film degradation time. For the freestanding film work, functionalizing the freestanding film would allow us then to release sections of film coated with drug or protein. This in combination with some of the patterning techniques already developed in our group could pave the way for selective release of multiple side-by-side components.

LbL assemblies are simple to produce and versatile in the type of materials which can be incorporated into them, and for these reasons are potentially interesting for any number of applications. Subtle differences in film assembly, however, can result in vastly different films. Many of these parameters have been studied in depth, but some questions still remain. As our understanding of the complexity of LbL internal structure increases, so does our understanding of how materials selection can affect the film properties. This work has served to examine several different weak polyelectrolyte systems. A number of properties were observed and attributed to differences in molecular geometry or charge density, and some of these differences were used to design LbL structures for use in various applications.

Chapter 8 References

1. R. K. Iler, *J. Colloid Interface Sci.* **1966**, *21*, 569.
2. G. Decher, J. D. Hong, *Makromol. Chem. Macromol. Symp.* **1991**, *46*, 321.
3. Hiller, J.; Rubner, M. F. *Macromolecules* **2003**, *36(11)*, 4078-4083.
4. Mendelsohn, J. D.; Barrett, C. J.; Chan, V. V.; Pal, A. J.; Mayes, A.M.; Rubner, M. F. *Langmuir* **2000**, *16(11)*, 5017-5023.
5. Choi, J.; Rubner, M. F. *Macromolecules* **2005**, *38*, 116-124.
6. Picart, C.; Mutterer, J.; Richert, L.; Luo, Y.; Prestwich, G. D.; Schaaf, P.; Voegel, J. C.; Lavalle, *P. Proc. Nat. Acad. Sci. U. S. A.* **2002**, *99(20)*, 12531-12535.
7. Porcel, C.; Lavalle, P.; Ball, V.; Decher, G.; Senger, B.; Voegel, J.C.; Schaaf, P. *Langmuir* **2006**, *22*, 4376-4383.
8. Zacharia, N. S.; DeLongchamp, D. M.; Modestino, M.; Hammond, P. T. *Macromolecules*, **2007**, ASAP.
9. Jomaa, H. W.; Schlenoff, J. B. *Langmuir* **2005**, *21(18)*, 8081-8084.
10. Lavalle, P.; Vivet, V.; Jessel, N. Decher, G.; Voegel, J.C.; Mesini, P. J.; Schaaf, P. *Macromolecules* **2004**, *37(3)*, 1159-1162.
11. Laugel, N.; Betscha, C.; Winterhalter, M.; Voegel, J. C.; Schaaf, P.; Ball, V. *J. Phys. Chem. B* **2006**, *110*, 19443-19449.
12. Porcel, C.; Lavalle, P.; Decher, G.; Senger, B.; Voegel, J.C.; Schaaf, P. *Langmuir* **2007**, *23*, 1898-1904.
13. Ma, N.; Zhang, H.; Song, B.; Wang, Z.; Zhang, X. *Chemistry of Materials* **2005,** 17, (20), 5065-5069.
14. Ma, N.; Wang, Y.; Wang, Z.; Zhang, X. *Langmuir* **2006,** 22, (8), 3906-3909.
15. Emoto, K.; Iijima, M.; Nagasaki, Y.; Kataoka, K. *J. Am. Chem. Soc.* **2000,** 122, 2653-2654.
16. Emoto, K.; Nagasaki, Y.; Kataoka, K. *Langmuir* **2000,** 16, 5738-5742.
17. Nguyen, P. M.; Hammond, P. *Langmuir* **2006,** 22, (18), 7825-7832.

Appendix A
Molecular weight determination of PXV.

The molecular weight of poly(hexyl viologen) was determined by two methods; end group analysis using a Varian Mercury 300 MHz Nuclear Magnetic Resonance Spectrometer, and static light scattering (SLS).

A 1H NMR spectrum of the polymer in a deuterated water (D2O) solution was recorded (Figure A-1).

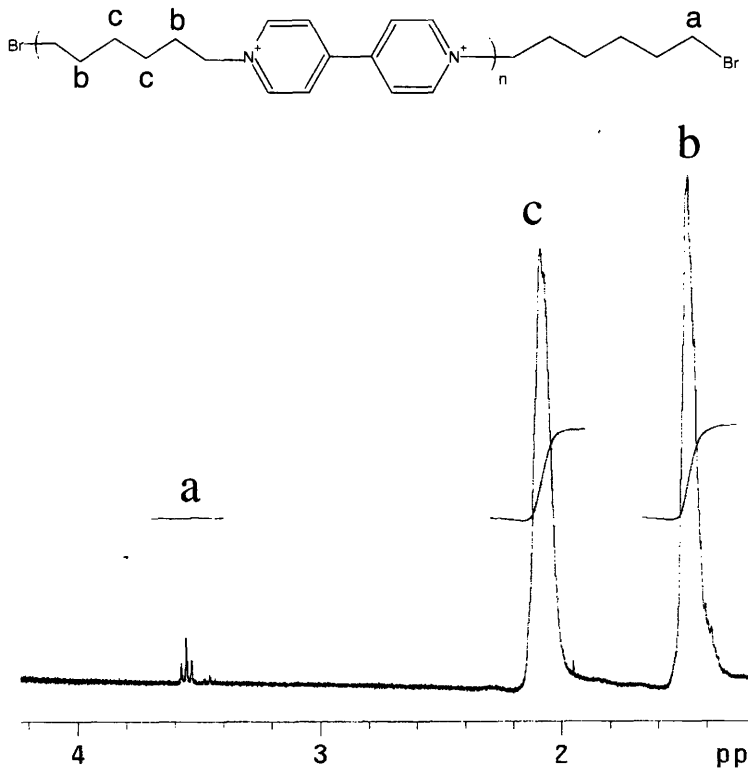

Figure A - 1. ^{1}H NMR Spectrum of Poly(hexyl viologen) in D_2O.

The degree of polymerization was obtained from the peak a corresponding to the two ($-CH_2Br$) end groups of the polymer, and the peaks b and c corresponding to the ($-CH_2-$) groups b and c of the polymer. The polymerization degree was calculated as half ration between the sum integrals

of the peaks b and c, over the integral of peak a. The obtained degree of polymerization was 1218, which corresponds to a polymer molecular weight of 292200 g/mol.

Figure A – 2 shows the Zimm plot for the light scattering. As estimate of 150,000 g/mol was determined for the molecular weight of PXV.

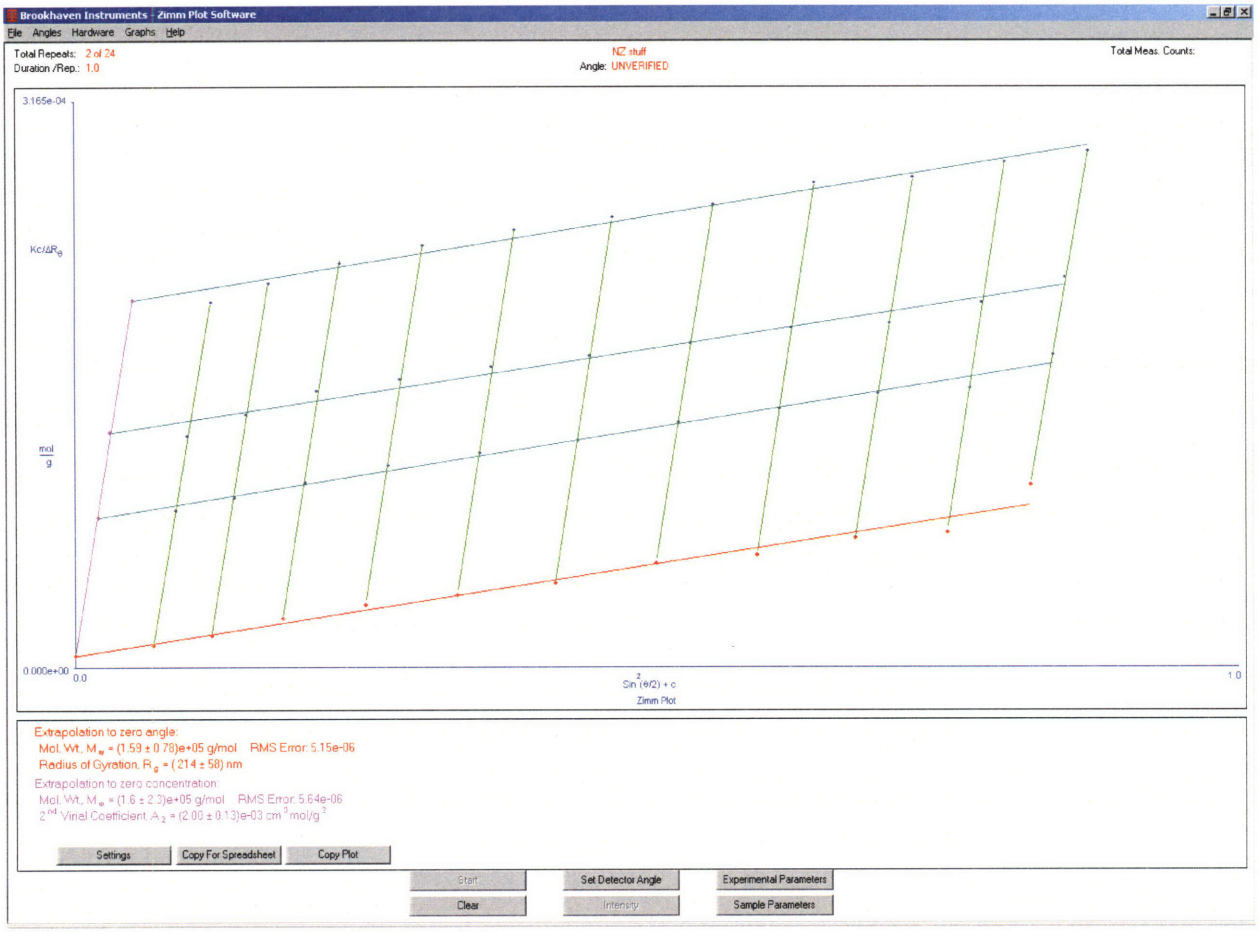

Figure A - 2: Zimm plot of SLS MW determination of PXV. Concentration range = 20-50 mg/ml, and dn/dc = -.1 (based on 2 points).